Instituto Universitário de Lisboa

Department of Information Science and Technology

Transmission of 5G signals in multicore fibers impaired by inter-core crosstalk

André Filipe Simões da Silva Marques

Dissertation presented in partial fulfillment of the Requirements for the Degree of

Master in Telecommunications and Computer Engineering

Supervisor

Prof. Dr. João Rebola, Assistant Professor

ISCTE-IUL

Co-Supervisor

Prof. Dr. Adolfo Cartaxo, Full Professor

ISCTE-IUL

October 2018

Resumo

A capacidade de dados exigida pelo surgimento do 5G levou a mudanças na arquitetura das redes sem fios passando a incluir fibras multinúcleo (MCFs, acrónimo anglo-saxónico de multicore fibers) no fronthaul. No entanto, a transmissão de sinais nas MCFs é degradada pela interferência entre núcleos (ICXT, acrónimo anglo-saxónico de intercore crosstalk). Neste trabalho, o impacto da ICXT sobre o desempenho na transmissão de sinais CPRI (acrónimo anglo-saxónico de Common Public Radio Interface) numa rede de acesso 5G com detecção direta, suportada por MCFs homogéneas com um acoplamento reduzido entre núcleos, é estudado através de simulação numérica. A taxa de erros de bit (BER, acrónimo anglo-saxónico de bit error rate), a análise de padrões de olho, a penalidade de potência e a indisponibilidade são utilizadas como métricas para avaliar o impacto da ICXT no desempenho do sistema, considerando dois modelos para a polarização dos sinais. Os resultados numéricos são obtidos através da combinação de simulação de Monte Carlo com um método semi-analítico para avaliar a BER.

Para uma penalidade de potência de 1 dB, para sinais CPRI com FEC (acrónimo anglo-saxónico de forward-error correction), devido ao aumento do walkoff da MCF de 1 ps/km para 50 ps/km, a tolerância dos sinais CPRI relativamente à ICXT aumenta 1.4 dB. No entanto, para níveis de interferência que levam a uma penalidade de potência de 1 dB, o sistema está praticamente indisponível. Para alcançar uma probabilidade de indisponibilidade de 10^{-5} usando sinais com FEC, são necessários níveis de interferência muito mais reduzidos, abaixo de -27.8 dB e -24.8 dB, para sinais de polarização única e dupla, respectivamente. Este trabalho demonstra que é essencial estudar a indisponibilidade em vez da penalidade de potência de 1 dB para garantir a qualidade do serviço em sistemas de comunicação óptica com detecção direta suportados por MCFs homogéneas com um acoplamento reduzido entre núcleos onde a ICXT domina a degradação do desempenho.

Palavras-chave: CPRI, fibra multinúcleo, fronthaul 5G, indisponibilidade, interferência entre núcleos, penalidade de potência, redes sem fios 5G, taxa de erros de bit.

Abstract

The data capacity demanded by the emergence of 5G lead to changes in the wireless network architecture with proposals including multicore fibers (MCFs) in the fronthaul. However, the transmission of signals in MCFs is impaired by intercore crosstalk (ICXT). In this work, the impact of ICXT on the transmission performance of Common Public Radio Interface (CPRI) signals in a 5G network fronthaul supported by homogeneous weakly-coupled MCFs with direct detection is studied by numerical simulation. Bit error rate (BER), eye-patterns analysis, power penalty and outage probability are used as metrics to assess the ICXT impact on the system performance, considering two models for the signals polarizations. The results are obtained by combining Monte Carlo simulation and a semi-analytical method to assess numerically the BER.

For 1 dB power penalty, with forward error correction (FEC) CPRI signals, due to the increase of the MCF walkoff from 1 ps/km to 50 ps/km, an improvement of the tolerance of CPRI signals to ICXT of 1.4 dB is observed. However, for crosstalk levels that lead to 1 dB power penalty, the system is unavailable with very high outage probability. To reach a reasonable outage probability of 10^{-5} for FEC signals, much lower crosstalk levels, below -27.8 dB, and -24.8 dB, for single and dual polarization signals, respectively, are required. Hence, this work shows that it is essential to study the outage probability instead of the 1 dB power penalty to guarantee quality of service in direct-detection optical communication systems supported by weakly-coupled homogeneous MCFs and impaired by ICXT.

Keywords: 5G fronthaul, 5G wireless networks, bit error rate, common public radio interface, intercore crosstalk, multicore fiber, outage probability, power penalty.

Acknowledgements

Firstly, I would like to express my sincere thanks to my supervisors, Professor João Rebola and Professor Adolfo Cartaxo, for all the availability and support during the realization of this project. I would also like to thank Bruno Pinheiro for helping me at the beginning of the dissertation and to Instituto de Telecomunicações (IT)-IUL, for providing access to their installations and the material support.

I want to thank my family for all their unconditional support, for letting me make my own decisions and for all the trust they always had in me.

I also want to thank my friends André, Daniel, João, Pedro, e Valter who accompanied me since the beginning of my academic journey and to Carolina, Catarina, Miriam and Rodrigo for the motivation and help they gave me during the dissertation.

Finally, I want to thank my girlfriend, Inês, specially for all the support, motivation and patience over the last months.

Contents

List of Figures

List of Tables

List of Acronyms

1G	**F**irst **G**eneration
2G	**S**econd **G**eneration
3G	**T**hird **G**eneration
4G	**F**ourth **G**eneration
5G	**F**ifth **G**eneration
BBU	**B**ase **B**and **U**nit
BER	**B**it **E**rror **R**ate
BS	**B**ase **S**tation
CO	**C**entral **O**ffice
CPRI	**C**ommon **P**ublic **R**adio **I**nterface
C-RAN	**C**loud-**R**adio **A**ccess **N**etwork
DCM	**D**iscrete **C**hanges **M**model
DRoF	**D**igital **R**adio **o**ver **F**iber
E-UTRA	**E**volved **U**MTS **T**errestrial **R**adio **A**ccess
FEC	**F**orward **E**rror **C**orrection
F-CRAN	**F**og **C**loud **R**adio **A**ccess **N**etwork
GSM	**G**lobal **S**ystem for **M**obile communications
HDLC	**H**igh-level **D**ata **L**ink **C**ontrol
H-CRAN	**H**eterogeneous **C**loud **R**adio **A**ccess **N**etwork
ICXT	**I**ntercore **C**rosstalk
IoT	**I**nternet of **T**hings
IQ	**I**n-phase **Q**uadrature
ISI	**I**ntersymbol **I**nterference
LTE	**L**ong **T**erm **E**volution

MC	**M**onte **C**arlo
MCF	**M**ulticore **F**iber
MIMO	**M**ultiple **I**n **M**ultiple **O**ut
NEP	**N**oise **E**quivalent **P**ower
NRZ	**N**on-**R**eturn to **Z**ero
OCT	**O**uter **C**ladding **T**hickness
OFDM	**O**rthogonal **F**requency **D**ivision **M**ultiplexing
OFDMA	**O**rthogonal **F**requency **D**ivision **M**ultiplexing **A**ccess
OOK	**O**n-**O**ff **K**eying
PIN	**P**ositive **I**ntrinsic **N**egative
PMD	**P**olarization **M**ode **D**ispersion
PMP	**P**hase-**M**atching **P**oints
RAN	**R**adio **A**ccess **N**etwork
RE	**R**adio **E**quipment
REC	**R**adio **E**quipment **C**ontrol
RoF	**R**adio **o**ver **F**iber
RPS	**R**andom **P**hase **S**hift
RRH	**R**emote **R**adio **H**ead
RU	**R**adio **U**nit
SCF	**S**ingle **C**ore **F**iber
SDM	**S**pace **D**ivision **M**ultiplexing
SMF	**S**ingle **M**ode **F**iber
SPM	**S**elf-**P**hase **M**odulation
UMTS	**U**niversal **M**obile **T**elecommunications **S**ystem
WDM	**W**avelength **D**ivision **M**ultiplexing

List of Symbols

A	number of antennas per sector
a_k	Signal amplitude level
B_{CPRI}	Fronthaul radio channel bandwidth with CPRI signals
$B_{e,n}$	Rlectrical noise bandwidth of optical receiver
b_s	Number of bits per sample
c	Speed of light in vacuum
d_{mn}	MCF walkoff parameter
D_λ	Dispersion parameter
$\mathcal{F}^{-1}\{\ \}$	Inverse Fourier transform
$F(\omega)$	ICXT transfer function
f	Lowpass equivalent frequency
f_{3dB}	-3 dB cutoff frequency
$F_{a,b}(\omega)$	ICXT transfer function for dual polarization model
F_i	Optimized decision threshold
f_s	Sampling rate
h	Planck constant
$H_e(f)$	Amplitude transfer function of the electrical filter
$i_{PIN}(t)$	PIN photo-current
K_{nm}	Discrete coupling coefficient between cores n and m
$\overline{K}_{nm}$	Average discrete coupling coefficient between cores m and n
L	Fiber length
L_{max}	Maximum fiber length
$m_{j,k,i}$	Mean of the current at the input of the decision circuit
N_b	Number of generated OOK bits per MCF realization

$n_c(t)$	Thermal noise
N_i	Number of interfering cores
N_{MCF}	Number of MCF realizations
N_p	Number of PMPs
$p(t)$	Pulse shape
P_c	Transmitted signal average power
$\overline{p}_i$	Receiver sensitivity
q	Charge of the electron
R_b	bit rate
$R_c b$	Radio channel bandwidth
R_λ	PIN responsivity
$S_c(f)$	Power spectral density of the thermal noise
$s_c(t)$	OOK signal at the optical transmitter output
$s_{ICXT}(t)$	Interfering signal at the output of core m in the two polarization
$s_m(t)$	Interfering CPRI signal
$s_{m,x}(t)$	Interfering CPRI signal in polarization x
$s_{m,y}(t)$	Interfering CPRI signal in polarization y
S_{mn}	MCF skew parameter
$s_n(t)$	Interfered CPRI signal
$s_{n,x}(t)$	Interfered CPRI signal in polarization x
$s_{n,y}(t)$	Interfered CPRI signal in polarization y
$s_{SMF}(t)$	Interfered CPRI signal at the output of core n
$s_{XT,x}(t)$	ICXT signal in polarization x
$s_{XT,y}(t)$	ICXT signal in polarization y
T_b	Bit period
t_k	Sampling instant at the decisio circuit input
t_{opt}	Optimum sampling time
T_s	Symbol time
X_c	Crosstalk level
$X_{c,max}$	Maximum tolerable crosstalk level per each core
z_k	Longitudinal coordinate of k-th center point between consecutive PMPs

α	Attenuation coefficient
β_0	Phase constant
β_1	Inverse of group velocity
β_2	Group velocity dispersion parameter
$\beta_n(\omega)$	Intrinsic propagation constant of core n
$\overline{\beta}_m$	Average of propagation constants in core m for both polarizations
$\overline{\beta}_n$	Average of propagation constants in core n for both polarizations
ΔD_{mn}	Difference of the dispersion parameter between cores m and n
$\Delta\beta_{0,mn}$	Difference of propagation constants of cores m and n at zero frequency
$\Delta\overline{\beta}_{mn}$	Difference of the average intrinsic propagation constants between cores m and n
ζ	Uniformly distributed random variable between 0 and L/N_p
η	Quantum efficiency of the photodetector
σ_c^2	Noise power of the thermal noise after electrical filtering
$\sigma_{j,k,i}$	Standard deviation of the current at the input of the decision circuit
ϕ_k	k-th RPS associated with the k-th PMP
ω	Lowpass equivalent angular frequency
λ	Carrier wavelength

Chapter 1

Introduction

In this work, the impact of intercore crosstalk (ICXT) arising from the coupling between cores in weakly-coupled multicore fibers (MCFs) on the transmission performance of common public radio interface (CPRI) signals in 5G networks fronthauls with direct detection is assessed by numerical simulation. The results are obtained using as metrics to analyze the system performance, the bit error rate (BER), the ICXT impact on the eye-patterns, the 1 dB power penalty and the outage probability.

1.1 Motivation and scope

Along the years, since the 1980s, mobile communications have evolved to meet users requirements, and about every 10 years, a new generation of mobile communications has been developed and implemented [1]. Since then, four generations of mobile communications have emerged, ranging from simple analog radio signals to the ability of supporting mobile applications with multimedia contents with sufficient speed, bandwidth and coverage to meet users needs and take advantage of the network capacities [1], [2]. Nowadays, a fifth generation (5G) is being developed with the aim of improving the existing fourth generation (4G) features and supporting the growing number of devices connected to the network through a wireless connection with a data rate that can be 1000 times superior to 4G

[3], [4]. Hence, 5G networks have to fulfill very demanding requirements such as higher system capacity, higher data rate, massive device connectivity, reduced latency, energy saving and cost reduction [5]. Fig. 1.1 depicts the main differences between 4G and 5G, comparing latency, data traffic per month, peak data rate, available spectrum and connection density. It is possible to observe that in 5G, latency is expected to be 10 times lower, data traffic per month more than 5 times higher, peak data rate 20 times higher, available spectrum 10 times higher and connection density 10 times higher than in the 4G implementation.

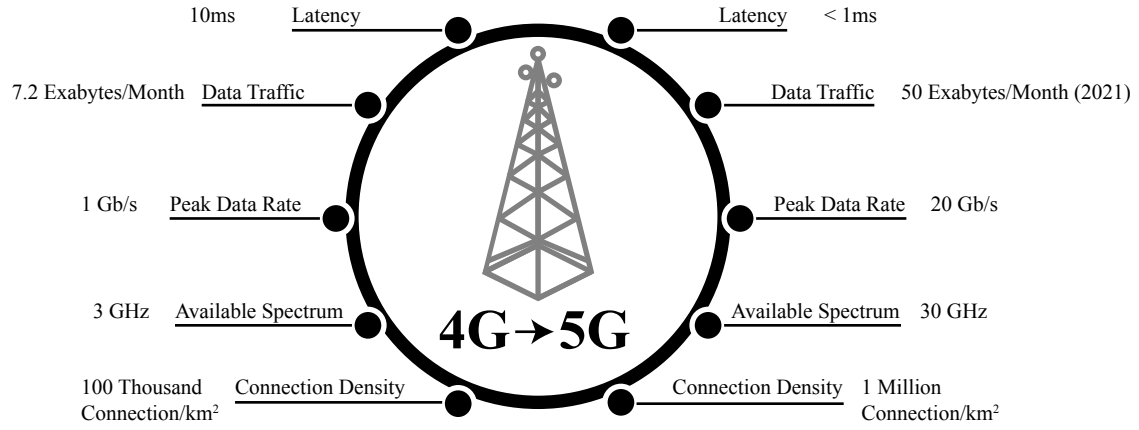

FIGURE 1.1: Latency, data traffic, peak data rate, available spectrum and connection density of 5G in comparison with 4G [6].

The 5G requirements could be implemented in the existing Radio Access Networks (RANs) by increasing the number of base stations (BSs), however it would not be efficient in terms of inter-cell interference and cost effectiveness. Therefore, alternative access network architectures have been proposed [7]. In 4G, the conventional macro BS architecture, where the Base Band Unit (BBU) and the radio unit (RU) were together at the base of a tower or a building have been replaced by the distributed BS architecture, where the BS is physically separated in BBU and Remote Radio Head (RRH). Then, in 5G, distributed architecture gave rise to the centralized RAN architecture, where the BBUs are moved to a central office (CO) that aggregates the BBUs in a BBU pool. The centralized RAN architecture has three variants, the Cloud-RAN (C-RAN), the Heterogeneous C-RAN (H-CRAN)

and the Fog C-RAN (F-CRAN), being C-RAN the most consensual, and consequently the most used, due to its energy efficiency, higher network capacity and cost reduction [2], [8].

In C-RAN, the geographical separation of the BBUs, placed at the BBU pool, from the RRHs at the cell site, creates a new transmission segment called fronthaul [7], [9]. One way to cope with the high data transmission efficiency and capacity of the fronthaul is to consider optical fiber-based solutions such as radio over fiber or digital radio over fiber (D-RoF). Since single-core fibers will fail in a near future to achieve the required capacity in the 5G fronthaul. MCFs, by exploiting space division multiplexing (SDM), have been proposed as a way to reach the demanded capacity for short-haul links with radio-over-fiber and also for fiber access networks, or datacenters interconnections [10], [11], [12]. In this work, a 5G fronthaul with direct detection transmitting On-Off keying (OOK) CPRI signals is considered. Different proposals have been made to the fronthaul configuration using MCFs: a) using two MCFs in the fronthaul for duplex transmission, one for the upstream direction and the other for the downstream direction; b) only one MCF is used for duplex transmission, the upper half cores are used for upstream transmission and the lower half for downstream transmission [10], [13]; c) one MCF is used for the fronthaul duplex transmission, where transmission directions are set in order that adjacent cores transmit in opposite directions, a technique known as propagation direction interleaving, which reduces ICXT impact on the system performance [14]. In this work, homogeneous weakly-coupled MCFs are considered, since in these fibers, all the cores have the same propagation constant, and, hence, each core can be treated as an individual waveguide with low interference from neighboring cores [15]. Homogeneous weakly-coupled MCFs allows to share receiver resources between cores and avoids the complexity of using digital signal processing at the receiver, such as MIMO processing.

However, the signal transmission through weakly-coupled MCFs has the problem of ICXT, since the signals transmission through the different cores causes interferences between them. This interference is stronger in adjacent cores than

in non-adjacent cores and is distributed along the MCF. Several works have investigated the ICXT effect on the performance over the last years, for a better understanding of its impact and to find ways of suppressing it [16], [17], [18], [19], [20], [21], [22]. The ICXT depends on several fiber parameters such as core refractive index, core pitch, transmission distance, wavelength, cladding diameter, bending radius and clad thickness [23]. The study of ICXT has also shown that its impact on the performance fluctuates randomly over short or long periods of time [21], [22]. In short periods of time, the ICXT leads to a random variation of the Q-factor and can be quantified by the degradation of the optical signal to noise ratio required to maintain the BER or by the degradation of the receiver sensitivity in unamplified transmission systems. Over long periods of time, the ICXT can be analyzed using the outage probability as a performance metric [21], [24].

1.2 Objectives

In this dissertation, the main goal is to study the signal transmission in 5G network fronthauls with weakly-coupled MCFs impaired by ICXT. This is done by considering two different models proposed in the literature for the ICXT, the discrete changes models (DCMs) with single and dual polarization signals [18], [25]. The performance of 5G fronthaul is obtained numerically through the combination of Monte Carlo (MC) simulation to assess the signal distortion and ICXT impact on the performance, with a semi-analytical method for noise evaluation. The performance metrics used for this assessment are the analysis of the eye-pattern, BER, power penalty and outage probability. For a better understanding of the results, the BER is analyzed as a function of the MCF realizations and as a function of the ICXT level. The results obtained in a Matlab^{TM} software are tested for different CPRI bit rates and for the maximum fiber length proposed for the 5G fronthaul, in order to obtain results similar to those expected in a real life scenario. The main objectives of this work are:

- understand the 5G signals characteristics, and how they can be transmitted through the fronthaul;
- analyze the proposed fronthaul architectures with MCFs;
- implement the signal transmission in a 5G fronthaul network with MCFs impaired by ICXT;
- assess the ICXT behavior and impact in the transmission of CPRI signals on the 5G fronthaul through the BER, eye-pattern, power penalty and outage probability analysis, for the single and dual polarization DCMs;

1.3 Dissertation organization

This work is organized as follows. In chapter 2, the fundamental concepts of 5G fronthauls supported by MCFs are presented. A particular emphasis in the 5G wireless networks evolution until the establishment of the Cloud-Radio Access Network, the use of MCFs in opposition to SCFs for deployment of the 5G fronthaul and the Common Public Radio Interface is given. In Chapter 3, the 5G fronthaul system model supported by MCFs and impaired by ICXT is presented: the optical transmitter, the MCF with single and dual polarization models to address the impact of ICXT, and the optical receiver and the electrical filter are modeled and characterized. The electrical noise at the receiver electrical circuit is characterized and the method to assess the BER in a system impaired by ICXT is also described. The validation is performed through the BER assessment in a back-to-back configuration and with a dispersive SCF without ICXT. In Chapter 4, the impact of the ICXT on the performance of CPRI signals transmission in 5G fronthauls supported by MCFs is assessed and discussed for the single and dual polarization DCMs. Firstly, the ICXT impact is studied per MCF realization through the BER assessment and eye-patterns observation, for different CPRI signals bit rates, ICXT levels, number of MCF realizations and MCF walkoffs. Then, the power penalty and the outage probability of the 5G fronthaul supported by

MCFs is studied and discussed. Finally, in Chapter 5, final conclusions and possible future work are presented.

1.4 Dissertation main contributions

This dissertation presents the following contributions:

- study of the proposed 5G fronthaul networks supported by MCFs;
- implementation of 5G signal transmission in a fronthaul with dispersive MCFs impaired by ICXT;
- development of a numerical method to assess the BER in presence of distortion caused by ICXT and noise from the electrical receiver by combining MC simulation with a semi-analytical method;
- assessment of the BER, in case of CPRI signals transmission impaired by ICXT, with and without Forward Error Correction (FEC), and the implications of different target BERs on the obtained results;
- effect of the ICXT on the received eye-patterns, for different MCFs walkoffs;
- comparison of the ICXT impact for single and dual polarization system models, for small and high MCF walkoffs;
- power penalty and outage probability innovative results for single and dual polarization models;
- conclusion that the outage probability is a very important metric to analyze the ICXT impact on the system performance.

The work performed in this dissertation has originated the following publications:

- A. Marques, J. Rebola, and A. Cartaxo, "Transmission of CPRI signals along weakly-coupled multicore fibers for support of 5G networks," Int. Conf. Transp. Opt. Netw. (ICTON), paper We.B2.7, Bucharest, Romania, Jul. 2018.

- J. Rebola, A. Cartaxo, and A. Marques, "10 Gbps CPRI signals transmission impaired by intercore crosstalk in 5G fronthauls with multicore fibers", submitted to Springer Photon. Netw. Commun. (PNET), in Jul. 2018.

- J. Rebola, A. Cartaxo, T. Alves, and A. Marques, "Outage Probability due to Intercore Crosstalk in Multicore Fiber Links with Direct-Detection", submitted to IEEE Photon. Technol. Lett. (PTL), in Oct. 2018.

- J. Rebola, A. Cartaxo, T. Alves, and A. Marques, "5G fronthauls with multicore fibers: CPRI signals performance degradation induced by intercore crosstalk", accepted for publication in SPIE Photonics West 2019, Feb. 2019.

Chapter 2

5G fronthauls supported by MCFs: fundamental concepts

In this chapter, the review of the literature and the fundamental concepts considered relevant to this work are going to be presented. Section 2.1 provides a brief description of 5G wireless networks. Then, in section 2.2, the C-RAN architecture is characterized. Section 2.3 describes the main properties of optical fibers and section 2.4 puts a particular emphasis on the MCFs. Then, in section 2.5, the application of MCFs in the C-RAN architecture for 5G fronthauls is discussed. Finally, the CPRI standard for digital optical transmission through the 5G fronthaul is described in section 2.6.

2.1 5G wireless networks

The technological revolution has opened the door to the first methods of long-distance telecommunications based on electricity. One of the best known cases was when Giugliemo Marconi set the groundwork for wireless communications by transmitting the letter "S" in Morse code over a distance of 3 km through electromagnetic waves. Based on this transmission and through the study of the theory related to the electromagnetism, the first steps were taken, for that, which today, is known as the global architecture of mobile communications [3].

By 1980, it was common to use analog signals in mobile wireless telecommunications networks to transfer voice data, known as 1G (first generation) networks. A decade later, developments in the area of telecommunications allowed the emergence of 2G networks with digital signals, with more fast, secure and reliable transmissions [2]. The third evolution of mobile technology came around the year 2000. The main added value of the third generation is to support multimedia applications for the services offered by the internet, which was acquiring a global importance. Ten years later, the 4G technology has been developed, and improved 3G systems, by giving them more speed, more bandwidth and better network coverage, in the context of a society increasingly consuming online multimedia content [1], [3]. In a natural evolution of this process, the development of the fifth generation, 5G networks, is being initiated, which in addition of improving the service already offered by 4G, paves a way for supporting the growing number of devices connected to the network and their increasing demand for capacity through a wireless connection [3]. Fig. 2.1 illustrates the evolution of the different generations of mobile technology along the year, as well as the main innovations introduced in each generation. While on 4G the network is an IP-based network where the IP protocol is used to send and receive messages, in 5G there are IoT (Internet of Things [26]) networks that connect physical devices, vehicles, home appliances, and other items embedded with electronics, software and sensors [26].

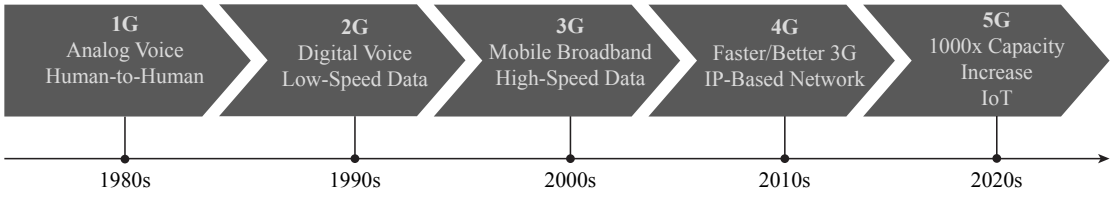

FIGURE 2.1: Mobile technology evolution from 1G to 5G [27].

The developments that are being seen in society lead to a path where more and more devices are connected to the network through wireless connections. Taking into account this phenomenon, which encompasses services such as e-banking, e-learning, e-health, or even the increasingly real prospect of cars without drivers, 5G will have to meet a series of challenges, like inter-cell interference or traffic management, that will lead to a transformation of the actual networks [28]. But

these are not the only challenges, as the high complexity and battery life of the devices connected to the network will require high scalability and flexibility [4].

One of the main concerns will be the amount of data transmitted, since this is one of the main motivations to move to 5G. Several types of data rates, among them the aggregate data rate, the edge data rate and also the peak data rate should be defined for 5G networks [4]. The aggregate data rate refers to the total traffic that can be transmitted over the network measured in bits/area. When compared to 4G networks, it is expected to grow up to 1000 times higher [4], [29]. Secondly, the edge data rate refers to the amount of data that, in the worst case, the user expects to receive. It is expected that this value will vary between 100 Mbps and 1 Gbps [4]. Achieving these values will be a challenge, since the current 4G networks can only offer 1 Mbps to about 5% of users. Finally, there is the peak data rate that refers to the maximum amount of data that a user can obtain from the network. Normally, the peak data rate values are a marketing issue on the part of the operators, and they are not usually fully reached. In the case of 5G, in comparison to 4G, the peak data rate is expected to be 20 times higher [4].

Besides transmission capacity, another challenges presented to 5G networks are the latency and reliability of the network [30]. The current latency of the 4G is around 15 ms [4], but taking into account all the 5G requirements, it is expected that the goal latency of the networks will be about 1 ms [4], [31]. Regarding the reliability, it is expected to be around 99.99% [4]. The costs that will be associated with all the improvements inherent to 5G should also be taken into account.

In addition to all these changes, the type of transmitted signal may also change. The suggestion taken as the most feasible is based on OFDM (Orthogonal Frequency Division Multiplexing) and OFDMA (Orthogonal Frequency-Division Multiple Access) [5], as this is the dominant signal format with respect to high-speed wireless communications corresponding to the standards required to meet 4G long term evolution (LTE) standards and wireless communications [4], [29]. However, although the spectral efficiency of OFDM is satisfactory, it can still be improved and several alternative signal formats have already been suggested for 5G transmission. Among the suggestions proposed are filterbank multicarrier, time-frequency

packing, nonorthogonal signaling, generalized frequency division multiplexing and single carrier or tunable OFDM [4].

2.2 Cloud-Radio Access Network

In existing RANs, the conventional macro BSs consist in two functional elements that are located at the base of a tower or in a building. These elements are the RU, whose functions are amplification, frequency conversion, carrier modulation/demodulation, digital-to-analog or analog-to-digital conversion and filtering radio signals and the BBUs, whose functions are baseband signal processing, management and control of the BS and interfacing the radio network controller. The required improvements to the 5G transmission, which could be achieved by increasing the number of BSs, are too expensive and increase the inter-cell interference [7]. Thus, to reduce costs, reduce energy consumption, improve spectral efficiency and still allow the introduction of new services, new architecture proposals have been made [7], [31], [32]. The new architectures are based on a distributed BS architecture where the traditional BS is physically separated in BBU and RRHs [32], [33]. RRHs, which are now located at the antenna mast, are radio frequency transmitters/receivers that help in frequency conversion and in analog-to-digital and digital-to-analog conversion. The BBU-RRH connection is usually made using optical fiber, although it can be replaced by coaxial cable [7]. The connection of the RRHs to the antennas is made using short coaxial cables. From the distributed architecture arises a new architecture, that presents a new network configuration, where the BBUs are moved from the ground of the antenna site to a CO or point of centralization, where the BBUs are put together in a BBU pool. This pool aggregates BS control functions at the CO, that now works as a BS, and the RRHs can be placed at rooftops or lampposts [7]. This architecture is known as the centralized architecture [7].

In the architecture proposals for centralized BS architecture are the C-RAN, the H-CRAN and the F-RAN. The C-RAN architecture consists in a large number of RRHs with low power and low cost, that are highly distributed in the network.

The BBUs, that are all together in a BBU pool, work as high-performance processors with real-time virtualization, and management technologies that aggregate all BSs resources and manages a large number of RRHs [7]. The advantage of having a BBU pool is that it supports the dynamic allocation of the resources, but also lowers the costs and simplifies the design of the RRHs, making them more efficient. The connection between the RRHs and the BBU pool located at the CO originates a high speed and low latency transmission segment named as fronthaul [7], [9]. The H-CRANs have practically the same architecture than the C-RANs with the addition of high power nodes that have the centralized control and signaling functions of the fronthaul, that now is only used for data transmission [7]. This architecture has the advantage of extending the network coverage and decrease the amount of information in the fronthaul, but has the disadvantages of being more expensive and higher latency than the C-RAN. F-RAN is implemented by using the H-CRAN architecture with the addition of developing the traditional RRH into a fog-computing-based access point, that are RRHs with caching capabilities, cooperative signal processing, and radio resource management functionalities. This architecture has the advantages of having less latency and lower requirements for BBU pool and fronthaul, when compared with C-RAN but the disadvantages of having more interference and limited caching. C-RAN ends up being the most utilized network architecture since it has advantages such as energy efficiency, increased network capacity, adaptability to non-uniform traffic, smart internet traffic offload and cost reduction [2], [8].

Fig. 2.2 illustrates the C-RAN architecture, showing the geographical separation between the BBUs pool and the RRHs. From Fig. 2.2, it is possible to observe two connectivity segments, named backhaul and fronthaul. The backhaul connects the BSs (located at the CO) to the core network via an IP/MPLS based network. The fronthaul is defined as the segment that connects the BBUs and the RRHs, using analog or digital signals, usually through an optical fiber.

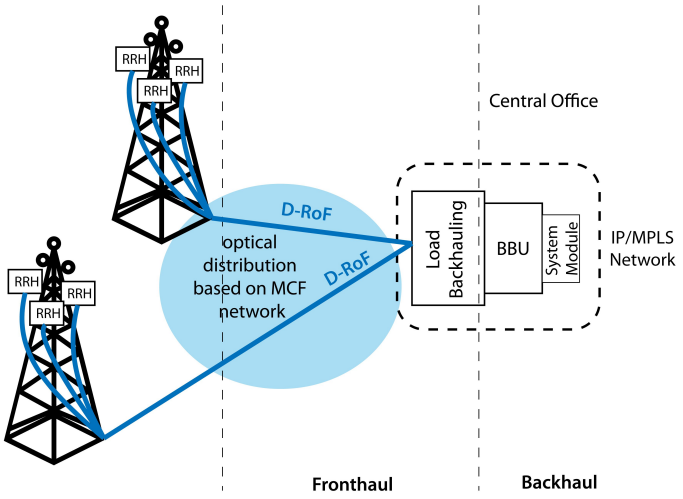

FIGURE 2.2: C-RAN architecture with fronthaul supported by MCFs.

C-RANs have a set of challenges to accomplish in order to meet the 5G networks requirements. Among them, there are the high capacity of the 5G optical fronthaul, the interconnection between the various BBUs inside the BBU pool, and the introduction of virtualization technology inside the CO. Regarding the first challenge, the link between BBU and RRH needs to carry high bandwidth data in real time. So, this link must have a capacity of tens of terabits (see section 2.6) with very tight criteria with regard to latency. Regarding the ability to receive/transmit data, the joint processing of the various BBUs is required in order to achieve the desired high spectral efficiency. To reduce system interference, multi-point processing algorithms must be developed, which should use the information in the uplink and downlink directions between the BSs. Furthermore, it will be necessary to ensure the security of the connections between the various BBUs, so that in case of failure, it guarantees the reliability of the network and allows it to recover. Finally, there is the base station virtualization technology that will be crucial for grouping or distributing virtual BSs. The main challenges of this technology will be the implementation of algorithms of real-time processing, virtualization of the baseband processing or the dynamic processing of the allocation of the cells in the system [32].

2.3 Optical fibers

Fiber-optic communication is a technology that uses pulses of light to transfer information from one point to another through an optical fiber medium. An optical fiber is a dielectric and cylindrical waveguide made of low loss materials. The core of the waveguide has a higher refractive index than the cladding of the fiber, so that, the light is guided along the fiber through total internal reflection [34]. The use of optical fibers for telecommunications is related to the several advantages that they present. Among them, there are the large system bandwidth, the small dimension and weight of the fiber, fiber flexibility, low transmission loss, potential low cost, reliability of the system and ease of maintenance [34].

In communication networks, there are two dominant fiber types, single mode and multimode fibers. In these fibers, there is a central core, where the pure silica is doped and provides a light-guiding region, confining the electromagnetic field to the core. The most common fiber is the fiber whose core is smaller, around 10 μm, which is known as single-mode fiber (SMF) [35]. The other type of fiber, has a larger and more doped core. This feature leads to an higher number of modes propagated inside the fiber. For this reason, this type of fiber is known as multimode fiber [35]. The multimode fiber allows coupling in a simpler way, which is its main advantage over SMF. However, due to the different propagation velocities of the different modes the dispersion in multimode fibers is much severe than in single mode fibers, which limits the transmission distance and the bit rate achieved with these fibers. Hence, the most utilized fibers are the single mode fibers [34], which are the ones considered in this work.

When a signal is transmitted through an optical fiber, it is necessary to take into account the transmission effects that may affect the system performance, such as attenuation, dispersion and non-linear effects. The attenuation in the fiber is due mainly to two mechanisms, the Rayleigh scattering and the material absorption. The Rayleigh scattering depends on the wavelength and reduces proportionally to its fourth power. The material absorption can be divided in intrinsic absorption and extrinsic absorption and is caused by the dopant materials that are

used in order to increase the fiber refractive index [34]. The typical attenuation coefficient is 0.2 dB/km, for a wavelength of $\lambda = 1550$ nm, for standard SMFs [34], [35], [36].

In SMFs there are, essentially, two types of dispersion mechanisms, the chromatic dispersion, that results from the contribution of material and waveguide dispersions, and the polarization-mode dispersion (PMD). The material dispersion arises from the dependence of the refractive index of the fiber material on wavelength. The waveguide dispersion is a consequence of the reduction of the mean refractive index and respective increase of the phase velocity. The PMD is caused by the residual birefringence of the fiber resulting from stresses that bending produce on the fibers and from its imperfect geometry [35]. This type of dispersion leads to broadening of optical pulses due to random variations in the birefringence of an optical fiber along its length [34]. In optical fibers, the dispersion leads to the overlap between the transmitted symbols, which will lead to bit errors [35], [36]. Comparing chromatic dispersion and PMD, it is possible to say that chromatic dispersion is deterministic, linear, not affected by the environment and its typical value is $D_\lambda = 17$ ps/(nm·km) for $\lambda = 1550$ nm, for a standard SMF. On the other hand, PMD is stochastic, affected by the environment and has a typical value of $D_{PMD} < 0.1$ ps/$\sqrt{\text{km}}$ for recent fibers [34]. In this work, PMD is not considered and its study is left for future work.

Finally, there are the non-linear effects that arise from the modification of the properties of the physical medium, caused by the electric field of the light propagated in the fiber. There are two fundamental mechanisms to generate the nonlinear effects, the Kerr effect, where the refractive index is affected by the light intensity, and the inelastic scattering, that originates the Raman and Brillouin scatterings [34], [35]. The Kerr effect originates self-phase modulation (SPM) in single wavelength transmission, which originates chirp on the pulses. This chirp increases the spectral width of the pulse and the normal positive dispersion of the fiber broadens the pulse as it propagates along the fiber and causes an increased ISI at the receiver; the non-linear effect of cross-phase modulation is generated by the same physical mechanism than SPM, but in a WDM environment; and, finally,

the four-wave mixing, where two or more incident light waves produce additional wavelengths, that when mixing with the ones that already exists, originate new waves [35]. In this work, the non-linear effects are not considered, since the fiber length considered in this work is the typical one of an access network.

2.4 Multicore fibers

The use of single-core fibers and their exploitation to the extreme of their capacities can lead to the so-called capacity crunch [15]. The maximum capacity reported in SCFs is around 100 Tbps [17]. One way of overcoming this crunch is through SDM, which can be made using a bundle of SCFs, few-mode fibers and a fiber that can have multiple cores inside a single cladding, known as MCF [35]. In MCFs, the idea of incorporating multiple cores in a single fiber, allows obtaining several independent channels within the fiber cross section [37]. The use of MCFs in SDM was first proposed in 1979, but due to the cost-effectiveness for the user, they were not commercialized [35]. However, nowadays, due to the foreseen capacity crunch, MCFs are once again seen as a compelling solution. In order to keep up with the increase in capacity achieved through SDM and not having to deal with the different speeds of propagation of each mode, the MCF are knowing a huge development. In MCFs, through SDM, the increased capacity is attained by sending different signals through different fiber cores [38]. Several works dealing with MCFs have already reached capacities such as 10 Pbps·km for a 100 km MCF, 100 Pbps·km for a 7000 km MCF or even 1 Ebps·km for a 8000 km MCF [15]. The number of cores inside the fiber can range typically from 7 to 31 cores [17], [39]. This number is dependent on the core diameter, the core pitch, that is the distance between two neighboring cores, and the outer cladding thickness (OCT), the minimum distance between the center of the outer cores and the cladding-coating interface [39]. In Fig. 2.3 the differences between the cross-sections of a SCF and of a MCF, as well as several MCF physical parameters such as core diameter (d_c), cladding diameter (d_{cl}) core pitch (Λ) and OCT (d_{OCT}) are presented. In SCFs, the core diameter, usually, is around 9 μm and the cladding

diameter is around 125 μm. In MCFs, the core diameter dimension is similar to the SCF core diameter, and the cladding diameter, which can be thicker in order to support an higher core density, can vary around 200-300 μm. The core pitch can be above or below 30 μm, depending on the MCF type and the OCT is around 20 μm [40], [41].

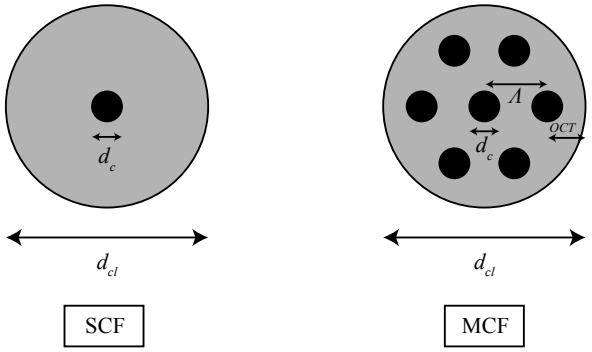

FIGURE 2.3: Cross section of single core fiber and multicore fiber with seven cores in an hexagonal arrangement.

The MCFs can be divided into two categories, the weakly-coupled MCFs and strongly-coupled MCFs [15]. In weakly-coupled MCFs, each core can be used as an individual waveguide with sufficiently low interference between signals in neighboring cores. In this type of fiber, it is necessary to take into account the ICXT between adjacent cores, since part of the optical power inserted in a core is coupled with the neighboring cores during the propagation [15]. In weakly-coupled MCFs, the coupling coefficient is typically $\kappa < 0.1$ m^{-1}, and the core pitch is $\Lambda > 30$ μm [15]. On the other hand, in strongly-coupled MCFs, the ICXT between cores is introduced intentionally by decreasing the distance between cores and increasing the cores density. In theory, these fibers support several modes and can be considered a form of multimode fibers. Strongly-coupled MCFs have a coupling coefficient of $\kappa > 0.1$ m^{-1} and a core pitch of $\Lambda < 30$ μm [15]. In addition, MCFs can be classified as homogeneous, quasi-homogeneous and heterogeneous [37]. In homogeneous MCFs, when the cores have similar properties and, if no bending induced perturbations are considered, all cores have the same propagation constant. In these fibers, ICXT is dominated by the core pitch. Quasi-homogeneous MCFs result from the variations of fiber properties due to fabrication, which even if the cores are intended to have the same properties, the fabrication procedure causes

fluctuations in the cores propagation constants. Finally, heterogeneous MCFs have intentionally different propagation constants between each cores, in order to mitigate the coupling between electric fields. These fibers have higher complexity since they use digital signal processing at the receiver, such as MIMO processing [15]. In this work, homogeneous weakly-coupled MCFs are considered.

With the use of MCFs, the problem of ICXT arises, since the transmission of the signal through the various cores of the fiber causes interference between the signals transmitted in both cores. [15]. The ICXT, i.e., power coupling between cores, is much stronger between adjacent cores than between non-adjacent cores, and its generation is distributed along the MCF [16], [18]. Furthermore, the ICXT has a random time varying frequency dependence, which may cause the random appearance of high levels of ICXT in short periods of time [19], [21]. Hence, the ICXT may affect severely the signal quality, particularly for MCFs with a large number of adjacent cores and long path lengths.

With the aim of understanding and mitigating the impact of ICXT on the MCF system performance, the characterization and suppression of ICXT in weakly-coupled MCFs has been investigated over the last years. The dependence of the mean ICXT power on MCF parameters (such as core refractive index and radius, bend and twisting, core pitch), dual polarization and wavelength have been reported [16], [25], [42]. The evolution of the random fluctuation of ICXT along the time has been investigated, and a model that provides the stochastic description of that evolution has been proposed and validated [21], [22]. In order to achieve high capacity and long distance transmission, ICXT suppression has become one of the focus in weakly-coupled MCF research [16], [17]. In this direction, new structures of MCF [16] and techniques for reduction of the ICXT impact, for example, using signals transmitted in opposite directions on adjacent cores of the MCF [17], have been proposed. As a consequence of the random evolution of ICXT along the time, two ICXT effects, should be considered when evaluating the MCF transmission system performance [24]. For an analysis over short periods of time, the Q-factor varies randomly [43]; this effect is quantified by the degradation of the optical signal to noise ratio required for the same BER in line-amplified transmission systems

[24]; or by the degradation of the receiver sensitivity in amplifier-less transmission systems. On the other hand, for an analysis over long periods of time, high levels of ICXT occurring in short time intervals appear and cause outage periods of system operation [21], [24].

2.5 C-RAN fronthaul supported by MCF

The introduction of MCFs instead of using conventional fibers, in order to increase capacity and meet the requirements demanded in the 5G fronthaul has been proposed in several works [13], [44].

Fig. 2.4 illustrates three possible configurations for the 5G fronthaul with MCFs [14]. In all three configurations, it is assumed that a single channel (wavelength) is transmitted in a single core. WDM solutions can be also envisioned, however, with higher cost. The wavelengths used for the downstream transmission, λ_D, are the same, which means that the transmitters for the downstream direction have equal characteristics. The same idea is considered for the upstream transmission in the upstream wavelength λ_U. This wavelength is provided by the central office from a continuous-wave laser through transmission in a single dedicated MCF core and is distributed to the upstream transmitters [10], for connecting the MCFs to external equipment, MCF connectors are assumed (which are not depicted in Fig. 2.4). These assumptions simplify the 5G network implementation and reduce its cost.

Fig. 2.4 a) shows the configuration where, to guarantee duplex-transmission, one MCF is used for each transmission direction. Fig. 2.4 b) depicts the 5G fronthaul configuration that utilizes only one MCF to ensure duplex transmission: the upper cores are used for upstream transmission and the lower cores are used for downstream transmission. This configuration is the one proposed in [10], [13]. Fig. 2.4 c) illustrates a 5G fronthaul ICXT-"aware" configuration using one MCF, as it explores the fact that transmitting signals in opposite directions in adjacent cores reduces the ICXT effect [17]. Hence, in this configuration, the transmission directions in adjacent cores are set interchangeably in opposite directions. Even

though, with this configuration, when many cores are used for transmission, the same transmission direction is employed in some adjacent cores.

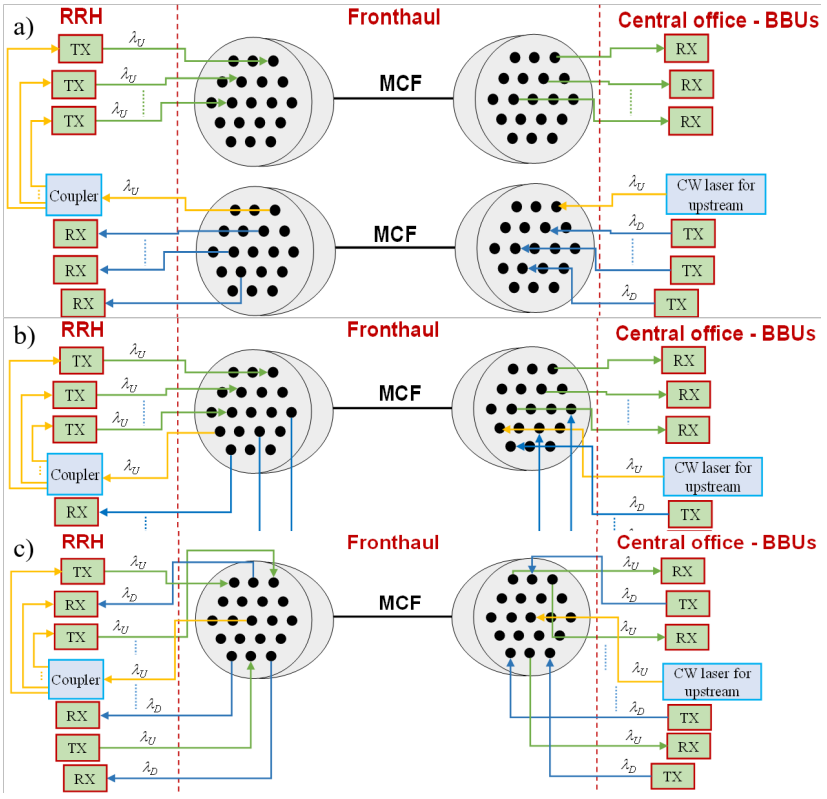

FIGURE 2.4: Different configurations for the 5G fronthaul with MCFs. a) Two MCFs are used in the fronthaul for duplex transmission: one for upstream and other for downstream. b) One MCF is used in the fronthaul for duplex-transmission: the upper half cores are used for upstream and the lower half cores for the downstream. This is the solution proposed in [10], [13]. c) One MCF is used in the fronthaul for duplex-transmission: transmission directions are set in order that adjacent cores transmit in opposite directions in order to minimize ICXT [17]. In all three configurations, a single core is used to transmit a CW laser from the central office to the RRHs in order to provide the wavelength for the upstream direction. U: upstream wavelength; D: downstream wavelength; RX: receiver; TX: Transmitter.

The connection in the fronthaul, can be made via Radio over Fiber (RoF) or D-RoF [13], [44]. RoF is the transmission of a radiofrequency signal from the CO to the RRHs through optical fiber, using wireless communications to establish the connection between the antenna and the user [45], [46]. In the first case, the CO (with a BBU pool) is connected to the RRHs through multicore fibers with $2N + 1$ (N cores for the downlink transmission/N cores for uplink transmission) [10]. In this case, the spatial diversity presented in the CO has several advantages:

each sector within a given BS can be configured independently through a certain MCF, the allocation of resources can be implemented electronically allowing carrier aggregation and the existence of MIMO, and, finally, the number of MIMO transceivers of a given sector can be implemented dynamically and independently in the respective CO [10]. RoF has other advantages, such as, having a simple configuration, allowing high bandwidth, being immune to electromagnetic interference, low attenuation, being able to be used in flexible and high capacity networks and still be able to be used regardless the type of modulation chosen [45], [46]. On the other hand, this analogue solution presents the disadvantages of suffering intermodular distortions caused by the microwave and optical components, and nonlinearities associated, and also the fiber optic attenuation reduces the reach in these connections [45].

In turn, in the DRoF connection there is an electronic switch and the downlink and uplink transmission from/for is done through a pool of virtual BBUs where each of them is controlled by software in order to serve a given antenna site. Here, each BBU, linked to a specific core of a given MCF, can be configured to allocate different capabilities dynamically [10]. DRoF has the advantages of having a simplified BBU architecture, the cost of the network is lower (low-cost digital receivers and transmitters), and is capable of maintaining the reach of the fiber access network [45]. In this work, DRoF transmission is the chosen one for the C-RAN 5G fronthaul, considering the standard protocol for digital transmission in these connections, the CPRI.

2.6 Common Public Radio Interface

The CPRI results from the cooperation of the telecommunications industry to create a standard that would serve as the base station interface between Radio Equipment Control (REC), which in a 5G fronthaul corresponds to the BBUs, and Radio Equipment (RE), which corresponds to the RRHs. RE and REC can also be called nodes. The REC is responsible for the radio functions of the digital baseband domain along the fiber, while the RE deals with the radiofrequency functions.

The CPRI standard definition is based on Universal Mobile Telecommunications System (UMTS), WiMAX, Evolved UMTS Terrestrial Radio Access (E-UTRA) and GSM, and can support other types of radio standards [47].

In this norm, the focus is the layers that depend on the hardware (layer 1 and layer 2), since they guarantee an independent evolution of the technology, avoiding the need to make significant changes in the network equipment. Fig. 2.5 shows an overview of CPRI protocol, where layers 1 and 2 and their information flows (User Plane data, Control and Management Plane data, and Synchronization Plane data) are represented [47].

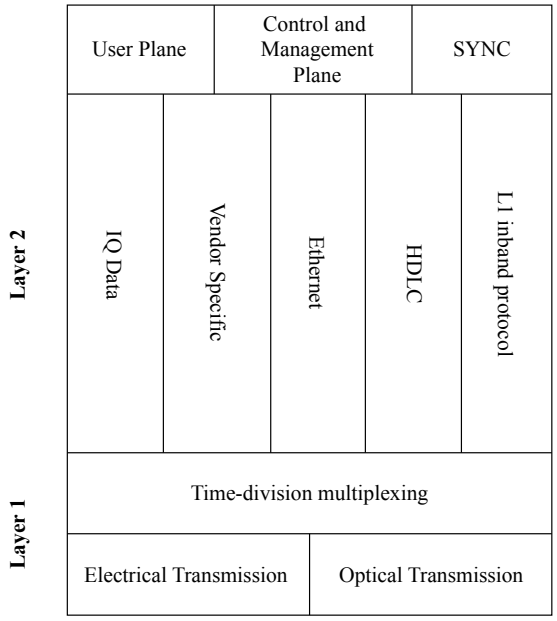

FIGURE 2.5: CPRI protocol overview [47]

Layer 1 is responsible for defining the electrical and optical interfaces characteristics, sets time-division multiplexing used for different data flows, and low-level signaling. In this layer, the I/Q data of the different carriers is transmitted using a time division multiplexer to an electric or optical transmission line [47]. Layer 2 defines media access control and flow and data protection related to the control and management of information flows and supports network flexibility and scalability [47]. According to Fig. 2.5, it can be seen that layer 2 is composed of the following elements:

- User plane: data that must be transferred from the base station to the mobile station or from the mobile station to the base station;

- Control plane: control data flow used for call processing and multimedia transmission;
- Management plane: information to manage the operation, administration and maintenance of the CPRI connection and the nodes;
- Sync: data flow that transfers synchronization and timing information of the nodes;
- IQ data: User plane information of digital baseband signals;
- Vendor specific: additional time slots for vendor-specific information;
- High-level Data Link Control (HDLC) and Ethernet: Layer 2 protocols, multiplexed with IQ data, which are used in control and management data;
- L1 inband protocol: information related to the connection that is directly transmitted on the physical layer.

The CPRI signals are composed by basic frames. A basic frame contains 16 words, depending its size on the chosen binary bit rate to be used [48], [49]. Before the physical transmission of each word, they pass through an encoding process according to the Ethernet standard 802.3 of the IEEE. The first word is for control and the remaining 15 used for the user plane data that transports the data in phase and quadrature. The junction of 256 basic frames originates a hyperframe, whose beginning is composed of synchronization bytes for control. The remaining control words can be used for the L1 inband protocol, maintenance of the physical layer connection, loss of signal, loss of frame and delay calibration or accuracy [49], [50]. The CPRI bit rate options, for the most recent version of the protocol are presented in Table 2.1.

TABLE 2.1: CPRI bit rates specified in version 7.0 [47].

Bit Rate option	Bit rate	Line Coding
1	614.4 Mbit/s	8B/10B (1 x 491.52 x 10/8 Mbit/s)
2	1228.8 Mbit/s	8B/10B (2 x 491.52 x 10/8 Mbit/s)
3	2457.6 Mbit/s	8B/10B (4 x 491.52 x 10/8 Mbit/s)
4	3072.0 Mbit/s	8B/10B (5 x 491.52 x 10/8 Mbit/s)
5	4915.2 Mbit/s	8B/10B (8 x 491.52 x 10/8 Mbit/s)
6	6144.0 Mbit/s	8B/10B (10 x 491.52 x 10/8 Mbit/s)
7	9830.4 Mbit/s	8B/10B (16 x 491.52 x 10/8 Mbit/s)
7A	8110.08 Mbit/s	64B/66B (16 x 491.52 x 66/64 Mbit/s)
8	10137.6 Mbit/s	64B/66B (20 x 491.52 x 66/64 Mbit/s)
9	12165.12 Mbit/s	64B/66B (24 x 491.52 x 66/64 Mbit/s)
10	24330.24 Mbit/s	64B/66B (48 x 491.52 x 66/64 Mbit/s)

In Table 2.1, the CPRI bit rates options and their respective line coding are presented. The bit rates are ordered from lowest to highest, with exception to bit rate option 7 and 7A, where the line coding changes from 8B/10B, where no FEC is considered, to 64B/66B, where FEC is considered. Before the IQ line coding process the CPRI basic signal capacity is 30.72 MSample/s×16 bit/Sample = 491.52 Mbit/s [51], which takes as a reference the bit rate referring to an I or Q component of a 20 MHz LTE component carrier [51]. To accommodate a specific number of LTE component carriers on the CPRI signal and reach a desired CPRI bit rate, it is necessary to multiply the CPRI basic signal capacity by 10/8 or 66/64, depending on the line coding and by a factor that is twice the number of LTE component carriers to reach the desired bit rate. For example, the bit rate option 8 is reached by $20 \times 491.52 \times 66/64$ Mbit/s=10137.6 Mbit/s.

Table 2.2 shows the time domain IQ data fronthaul capacities (bit rates without line coding) needed to support various radio frequency bandwidths and numbers of antenna ports in 5G wireless networks as defined by 3GPP [52].

TABLE 2.2: Required fronthaul capacity in 5G wireless network [51].

Number of antenna ports	Radio channel bandwidth			
	10 MHz	20 MHz	200 MHz	1 GHz
2	1 Gbps	2 Gbps	20 Gbps	100 Gbps
8	4 Gbps	8 Gbps	80 Gbps	400 Gbps
64	32 Gbps	64 Gbps	640 Gbps	3200 Gbps
256	128 Gbps	256 Gbps	2560 Gbps	12800 Gbps

The values of Table 2.2 are approximate data rates and are obtained using [52]

$$B_{CPRI} = A \cdot f_s \cdot \frac{R_{cb}}{20 \times 10^6} \cdot b_s \cdot 2 \cdot (16/15) \tag{2.1}$$

where A is the number of antennas per sector, f_s is the sampling rate per 20 MHz radio bandwidth (30.72 MSamples/s), R_{cb} is the radio channel bandwidth, b_s the number of bits per sample (16 for LTE), factor 2 corresponds to the separate processing of I and Q data and 15/16 is a factor corresponding to the additional overhead information. Using Eq. 2.1, $B_{CPRI} = 2 \cdot 15.36 \times 10^6 \cdot 15 \cdot 2 \cdot (16/15) \approx 1$ Gbps which is an example of a value presented in Table 2.2, for 2 antenna ports and a radio channel bandwidth of 10 MHz, is in agreement with Table. 2.2.

Chapter 3

5G fronthaul system model

In this chapter, the system model for the 5G fronthaul supported by MCFs and impaired by ICXT is presented: optical transmitter (section 3.2), MCF (single and dual polarization models, section 3.3), optical receiver composed by the photodetector and the electrical filter (section 3.4). The noise at the receiver electrical circuit is characterized in section 3.5 and the decision circuit, where the bit error probability is estimated, is also described in section 3.6. Then, the BER assessment in presence of electrical noise is performed, and the receiver sensitivity, the transmitted optical power, and fiber dispersion and attenuation on the signal transmission in single core fiber transmission (without ICXT) are studied for the purpose of simulation and numerical results validation.

3.1 5G fronthaul with MCF model

In Fig. 3.1, the 5G fronthaul model supported by MCF used in this work is depicted. The link under study is composed by the optical transmitters, a representation of the MCF, which considers a test core and single interfering core, and single or dual polarization transmitted signals, and the direct-detection optical receiver that includes the PIN photodetector, the electrical filter and the decision circuit. All the components presented in Fig. 3.1 are described in the following subsections.

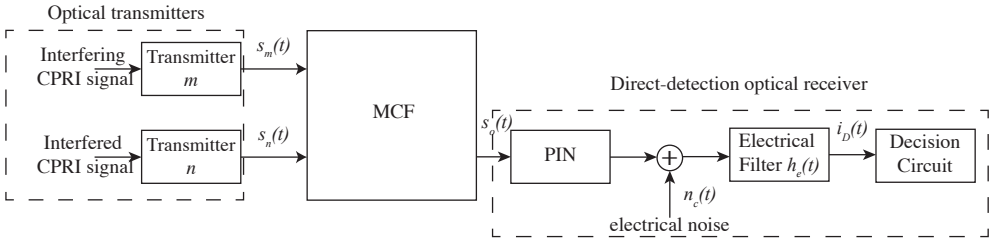

FIGURE 3.1: Simulated 5G fronthaul with MCF system model

3.2 Optical transmitter

Ideal chirpless and optical transmitters are considered in this work. They convert the electrical binary bits sequence obtained from a deBruijn sequence [53], from the electrical to the optical domain, without introducing signal distortion and considering an ideal extinction ratio. As can be seen in Fig. 3.1, two optical transmitters are considered, one for the interfering core, core m, and one for the interfered core, core n. Each transmitter generates an OOK signal with rectangular NRZ pulse shape, with the same CPRI bit rate. It is assumed that the bits transitions in the two cores at the MCF input are aligned in time.

The OOK modulation is chosen because of its inherent simplicity, and it is the one used in the CPRI protocol to transmit the I/Q data, since it allows the possibility of using direct detection at the optical receiver. To obtain the bit sequence, sequences with the maximum length of $2^{N_b}-1$ bits are generated, where N_b represents the length of the offset register used to generate the sequence. In this way, a deBruijn sequence is created, where the bits '0' and '1' have the same probability of occurring for all possible combinations of N_b bits [54]. Considering a linear conversion from the electrical domain to the optical domain, the OOK signal at the optical transmitter output in core c is defined by

$$s_c(t) = \sqrt{2P_c} \sum_{k=-\infty}^{+\infty} a_k p(t - kT_s), \quad c \in \{n, m\} \tag{3.1}$$

where T_s is the symbol time, equivalent to the bit period T_b, and P_c is the signal average power given by

$$P_c = \frac{1}{T_s} \int_{T_s} < |s_c(t)|^2 > dt \tag{3.2}$$

The amplitudes a_k represent the binary bits 0 and 1. The function, $p(t)$, represents the pulse shape, which is assumed as rectangular NRZ and is defined by

$$p(t) = \text{rect}\left(\frac{t}{T_s}\right) \tag{3.3}$$

where the rect function is defined by [53]:

$$rect\left(\frac{t}{\tau}\right) = \begin{cases} 1, & |t| < \frac{\tau}{2} \\ 0, & |t| > \frac{\tau}{2} \end{cases} \tag{3.4}$$

3.3 Multicore fiber

In this work, two models of the MCF impaired by ICXT are considered: 1) considering signals in one polarization, also known as single polarization model [18]; 2) considering signals in both polarization directions, also known as dual polarization model [25]. In both models, only a single interfering core is considered. Regardless of the model used, linear propagation through the MCF is assumed in the two cores, using the transfer function [34]

$$H_{SMF}(\omega) = \exp\left(-\alpha \cdot L\right) \exp\left(-j\beta_n(\omega)L\right) \tag{3.5}$$

where α is the fiber attenuation coefficient in Np/m, L is the MCF length, ω is the low-pass equivalent angular frequency and $\beta_n(\omega)$ is the intrinsic propagation constant of core n. A Taylor series expansion up to the second order in ω is considered for $\beta_n(\omega)$, i.e, propagation delay and chromatic fiber dispersion effects are considered in Eq. 3.5. Therefore, the propagation constant $\beta_n(\omega)$ is written

as [34]

$$\beta_n(\omega) = \beta_0 + \beta_1\omega + \frac{\beta_2}{2}\omega^2 \tag{3.6}$$

where β_0 is the phase constant, β_1 is the inverse of the group velocity and β_2 is the group velocity dispersion parameter, that rules the optical pulse broadening after propagation inside the fiber and is related to the dispersion parameter, D_λ, by $\beta_2 = -\frac{D_\lambda \lambda^2}{2\pi c}$ [34], where λ is the carrier wavelength and c is the speed of light in vacuum. PMD is not considered in this system model, and its inclusion is left for future work.

Regarding the ICXT, two models are under study, single and dual polarization DCMs, with the first proposed in [16] and later developed in [18], [21], [25] . To keep the simulation time acceptable and the model complexity low, the impact of ICXT is evaluated in time fractions separated by time intervals longer than the decorrelation time of the ICXT of the MCF [14]. With this, from time fraction to time fraction, the ICXT is not correlated, but in each time fraction it is, and from the ICXT viewpoint, one MCF realization is generated, which is not correlated with the other MCF realizations. One different MCF realization is calculated in each MC simulation iteration, and the bits of the CPRI signal to be transmitted in core m, in each iteration, are randomly generated. In subsections 3.3.1 and 3.3.2, the DCM models for single and dual polarization signals are presented and their differences are emphasized.

3.3.1 DCM with single polarization signals

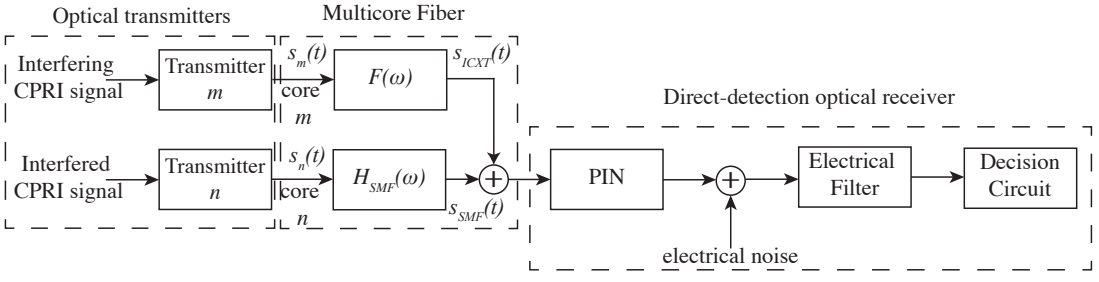

FIGURE 3.2: Single polarization equivalent system model used to study the impact of ICXT on a 5G fronthaul with direct detection.

Fig. 3.2 depicts the single polarization equivalent system model used to study the impact of the ICXT on a 5G fronthaul with direct detection. In core n, after passing through the linear propagation transfer function $H_{SMF}(\omega)$, the interfered CPRI signal at the output of core n is given by

$$s_{SMF}(t) = s_n(t) * \mathcal{F}^{-1}[H_{SMF}(\omega)] \tag{3.7}$$

being $s_n(t)$ the interfered CPRI signal and, where, $\mathcal{F}^{-1}[\ ]$ stands for the inverse Fourier transform and * stands for the convolution operator. The fiber attenuation is assumed the same in the two cores, and, therefore, the fiber attenuation level is not relevant in the analysis performed in this work. Hence, the receiver sensitivity will be considered as a metric for the signal power. For each MCF realization, the interfering signal in core n results from the ICXT caused by the signal in core m, and is obtained using the ICXT transfer function given by [18]

$$F(\omega) = -jK_{nm} \exp\left[-j\beta_n(\omega)L\right] \sum_{K=1}^{N_p} \exp\left[-j\Delta\beta_{mn}(\omega)z_k\right] \exp\left(-j\phi_k\right) \tag{3.8}$$

where K_{nm} represents the discrete coupling coefficient between cores n and m, z_k is the longitudinal coordinate of the k-th center point between consecutive phase-matching points (PMPs), defined by $z_k = (k-1)L/N_p + \zeta$, with N_p the number of PMPs and ζ is an uniformly distributed random variable between zero and L/N_p; The phase ϕ_k (with $1 \leqslant k \leqslant N_p$) is the k-th random phase shift (RPS) associated with the k-th PMP and is defined as a random variable uniformly distributed between [0,2π[, that models random fluctuations in bending radius, twist rate or other conditions of the MCF [18]. For equal powers at the output of the interfered and interfering cores, the ratio between the average crosstalk power and the average power of the signal, at the interfered core n output, X_c, is related to the parameters of Eq. 3.8 by $X_c = N_p|K_{nm}|^2$ [16], [18]. The skew between the interfering core, m and the interfered core, n, is given by $S_{mn} = d_{mn}L$, where d_{mn} is the walkoff between cores m and n and is related to Eq. 3.8 by $d_{mn} = \beta_{1,m} - \beta_{1,n}$, where $\beta_{1,m}$ is the inverse of the group velocity of core m, and $\beta_{1,n}$ is the inverse of the group velocity of core n. The difference of the intrinsic propagation constants between

cores m and n is given by [18]

$$\Delta\beta_{mn}(\omega) = \Delta\beta_{0,mn} + d_{mn}\omega - \frac{1}{2}\frac{\Delta D_{mn}\lambda^2}{2\pi c}\omega^2 \tag{3.9}$$

where $\Delta\beta_{0,mn}$ is the difference of propagation constants of cores m and n at zero frequency, ΔD_{mn} is the difference of the dispersion parameters of the interfering and interfered cores. $\Delta\beta_{0,mn}$ corresponds to $\Delta\beta_0$, $d_{mn}\omega$ refers to $\Delta\beta_1$, and $\frac{\Delta D_{mn}\lambda^2}{2\pi c}\omega^2$ corresponds to $\Delta\beta_2$. Thus, to obtain the interfering signal at the output of core n resulting from ICXT caused by the signal in core m, the signal at the input of core m is filtered by the transfer function given by Eq. 3.8

$$s_{ICXT,m}(t) = s_m(t) * \mathcal{F}^{-1}[F(\omega)] \tag{3.10}$$

3.3.2 DCM with dual polarization signals

Fig. 3.3 shows the dual polarization DCM system model used to study the impact of ICXT on a 5G fronthaul with direct detection.

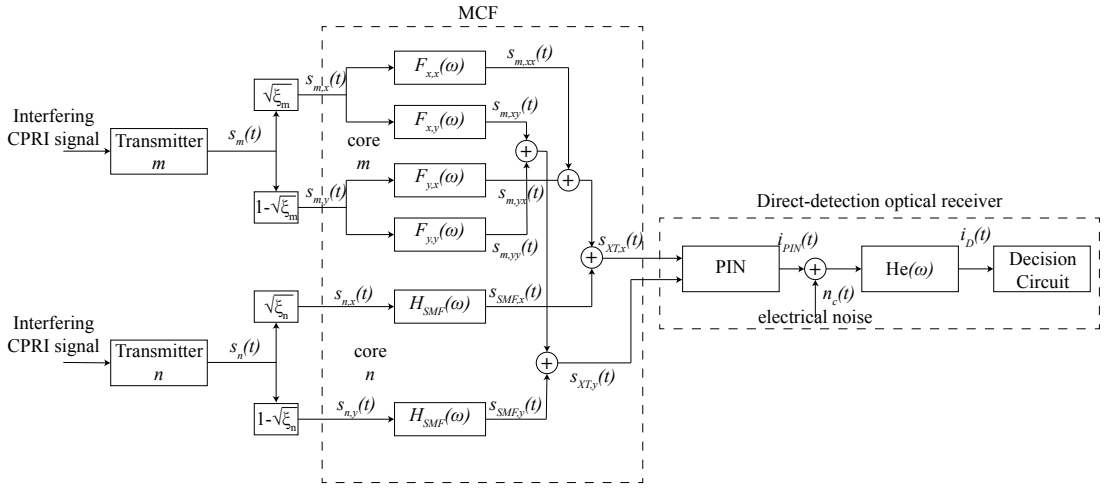

FIGURE 3.3: Dual polarization system model used to study the impact of ICXT on a 5G fronthaul with direct detection.

When compared to the single polarization model, the dual polarization model has the difference that, in both interfering and interfered cores, a power division of the transmitted CPRI signal between the polarizations x and y is performed,

as seen in Fig. 3.3, which is represented for core n as

$$\begin{aligned} s_{n,x}(t) &= s_n(t) \times\sqrt{\xi_n} \\ s_{n,y}(t) &= s_n(t) \times\sqrt{1-\xi_n} \end{aligned} \tag{3.11}$$

where $s_{n,x}(t)$ refers to the CPRI signal in polarization x and $s_{n,y}(t)$ corresponds to the CPRI signal in polarization y. The variable ξ_n controls the power distribution in both polarization directions and its value can vary between [0,1] [25]. The signal at the input of interfering core m is defined in both polarization directions by

$$\begin{aligned} s_{m,x}(t) &= s_m(t) \times\sqrt{\xi_m} \\ s_{m,y}(t) &= s_m(t) \times\sqrt{1-\xi_m} \end{aligned} \tag{3.12}$$

where $s_{m,x}(t)$ corresponds to the signal in polarization x, $s_{m,y}(t)$ corresponds to the signal in polarization y, and ξ_m defines how the signal power is distributed by the polarization directions in core m. Then, the signals $s_{m,x}$ and $s_{m,y}(t)$ are filtered by the ICXT transfer function for dual-polarization [25] defined by

$$F_{a,b}(\omega) = -\frac{j}{\sqrt{2}}\overline{K}_{nm} \exp\left[-j\overline{\beta}_n(\omega)L\right] \sum_{k=1}^{N_p} \exp\left[-j(\overline{\Delta\beta}_{mn}z_k)\right] \exp\left[-j\phi_k^{(a,b)}\right] \tag{3.13}$$

where $a, b \in \{x, y\}$, $\overline{K}_{nm}$ is the average discrete coupling coefficient of both polarizations, $\overline{K}_{nm}$=$(K_{nm}^{(x)} + K_{nm}^{(y)})/2$ [25], [42], $\overline{\beta}_m$ and $\overline{\beta}_n$ are the average of the propagation constants in the polarizations x and y of cores m and n and are given by $\overline{\beta}_m = (\beta_m^x + \beta_m^y)/2$ and $\overline{\beta}_n = (\beta_n^{(x)} + \beta_n^{(y)})/2$, respectively, and $\overline{\Delta\beta}_{mn} = \overline{\beta}_m - \overline{\beta}_n$ [25], is the difference of the average intrinsic propagation constants between cores m and n. Using Eq. 3.13, the signal due to ICXT at the output of core m is

obtained by

$$\begin{aligned} s_{m,xx}(t) &= s_{m,x}(t) * \mathcal{F}^{-1}[F_{xx}(\omega)] \\ s_{m,yx}(t) &= s_{m,y}(t) * \mathcal{F}^{-1}[F_{yx}(\omega)] \\ s_{m,xy}(t) &= s_{m,x}(t) * \mathcal{F}^{-1}[F_{xy}(\omega)] \\ s_{m,yy}(t) &= s_{m,y}(t) * \mathcal{F}^{-1}[F_{yy}(\omega)] \end{aligned} \tag{3.14}$$

where each of the transfer functions model the ICXT from the input of core m to the output of core n. The transfer functions $F_{xx}(\omega)$ and $F_{yx}(\omega)$ model the ICXT effect from the polarization x and polarization y of the interfering core to polarization x of the interfered core. The transfer functions $F_{xy}(\omega)$ and $F_{yy}(\omega)$ model the ICXT effect from both polarizations of core m to polarization y of core n. To ensure that these transfer functions are not correlated, it is necessary to generate the RPSs, $\phi_k^{(a,b)}$, independently. The signals at the output of the interfered core, corresponding to each one of the polarizations, are given, respectively, by

$$\begin{aligned} s_{XT,x}(t) &= s_{m,xx}(t) + s_{m,yx}(t) \\ s_{XT,y}(t) &= s_{m,xy}(t) + s_{m,yy}(t) \end{aligned} \tag{3.15}$$

where $s_{XT,x}$(t) corresponds to the ICXT signal in polarization x and $s_{XT,y}$(t) corresponds to the ICXT signal in polarization y at the output of core n.

3.4 Optical receiver

After passing through the MCF, the CPRI signal impaired by ICXT reaches the optical receiver, which is composed by a PIN photodetector, an electrical filter and a decision circuit.

3.4.1 PIN photodetector

The photodetector is characterized by being a PN photodiode with intrinsic material that is placed between the p-type and n-type materials, so that, incident

photons are absorbed in a depletion region with a very intense electric field [34], [35]. The presence of this electric field ensures that the electron-gap pairs, which arise due to photon absorption, are separated and collected at the terminals of the photodetector before they recombine. In a macro perspective, the optical signal is converted from the optical domain to the electrical domain using an ideal square-law model

$$i_{PIN}(t) = R_\lambda |s_o(t)|^2 = R_\lambda |s_{XT,x}(t)|^2 + R_\lambda |s_{XT,y}(t)|^2 \tag{3.16}$$

where $i_{PIN}(t)$ is the electrical-photo current and mixes both polarizations of the signal, and R_λ is the PIN responsivity, given by

$$R_\lambda = \frac{\eta q}{h\nu} \quad [\text{A/W}] \tag{3.17}$$

where q is the charge of the electron, h is equal to 6.6206×10^{-34} J/s and is the Planck constant [55] and η is the quantum efficiency of the photodetector. In this work, $R_\lambda = 1$ A/W and that the PIN bandwidth is assumed much larger than the CPRI signal bit rate in order to not introduce any bandwidth limitations.

3.4.2 Electrical filter

After passing through the photodector, the signal is passed through an electrical filter. The electrical filter is used to reduce the electrical noise power and minimize the intersymbol interference (ISI). For the electrical filter, a Butterworth filter, which is known for its bandpass gain flatness, is considered. The amplitude transfer function of the n-th order Butterworth filter is given by [53]

$$|H_e(f)| = \frac{1}{|P_n\left(j\frac{f}{f_{3dB}}\right)|} \tag{3.18}$$

with $|P_n(jf/f_{3dB})|$, the family of Butterworth polynomials, given by

$$|P_n(jf/f_{3dB})| = \sqrt{1 + \left(\frac{f}{f_{3dB}}\right)^{2n}} \tag{3.19}$$

At the cutoff frequency, f_{3dB}, the amplitude filter response decays -3 dB from its maximum and above this frequency, it decreases -20 dB/decade/order [56]. Increasing the Butterworth filter's order approaches the ideal rectangular filtering characteristic [53]. In this work, the cut-off frequency is set to $f_{3dB} = 0.65 \times R_b$, which is a typical value for direct-detection optical communications systems [34].

3.5 Noise from the receiver electrical circuit

At a finite temperature, the electrons move randomly in any type of conductor. The randomness of this movement manifests itself as a floating current, even if no tension is applied to the receiver. The resistor located at the front of the electrical circuit of the optical receiver adds these fluctuations to the photo current generated by the photodiode, $i_{PIN}(\mathrm{t})$, and, thus, thermal noise, $n_c(\mathrm{t})$, is added to the signal [34]. The noise power of the thermal noise after electrical filtering is given by [34]

$$\sigma_c^2 = R_\lambda^2 NEP^2 B_{e,n} \tag{3.20}$$

where NEP defines the Noise Equivalent Power (NEP) [34]. The NEP is defined as the minimum incident power that is required to generate a photocurrent equal to the noise current of the photodetector, at a specific frequency and within a specific bandwidth [34]. The NEP is defined by

$$NEP = \frac{\sqrt{S_c(f)}}{R_\lambda} \tag{3.21}$$

where $\sqrt{S_c(f)}$ is the square root of the power spectral density of the thermal noise. In this work, the NEP is set to 10^{-12} [W/$\sqrt{\mathrm{Hz}}$] [34]. $B_{e,n}$ is the electrical noise bandwidth of optical receiver, is given by [53]

$$B_{e,n} = \int_0^{+\infty} \left| \frac{H_e(f)}{H_e(0)} \right|^2 df \tag{3.22}$$

3.6 BER - Bit Error Rate

After correlation of the filtered current, $i_D(t)$, with the transmitted bits sequence in core n, to synchronize them, the eye pattern is obtained. The eye pattern, besides being a tool that allows analyzing the performance of the simulated system, is used to obtain the optimum sampling instant, t_{opt}, which is taken at the maximum eye-opening. Then, the received current is sampled at the sampling instants, $t_k = t_{opt} + kT_b$, and the BER is calculated.

The bit error probability is calculated, combining a semi-analytical method with MC simulation [14], [57]. The impact of the electrical noise on the system performance is taken into account analytically, and the effects of the fiber chromatic dispersion and ICXT are evaluated using waveform simulation in each MC simulation iteration.

The BER is, then, calculated by taking into account 2^N different levels of current at the sampling time instant, t_k. Let i denote the i-th iteration of the MC simulator, in which a different MCF realization is considered. The BER of the i-th iteration is given by [14]

$$BER_i = \frac{1}{2^N}\left\{\sum_{\substack{k=1\\a_k=0}}^{2^N} Q\left(\frac{F_i - m_{0,k,i}}{\sigma_{0,k,1}}\right) + \sum_{\substack{k=1\\a_k=1}}^{2^N} Q\left(\frac{m_{1,k,i} - F_i}{\sigma_{1,k,i}}\right)\right\} \tag{3.23}$$

where the function Q(x) [53] is defined by

$$Q(x) = \int_x^\infty \frac{1}{\sqrt{2\pi}} e^{-\frac{\xi^2}{2}} d\xi \tag{3.24}$$

$m_{j,k,i}$ and $\sigma_{j,k,i}$ are the mean and standard deviation of the current at the input of the decision circuit at time instants t_k and conditioned by bit j. As it is considered thermal noise, the noise power that affects the bits '0' and '1' is equal, σ_0^2=σ_1^2=σ_c^2.

To estimate the BER_{i}, the decision threshold, F_i, is optimized using the bi-section method [58], by solving

$$\sum_{k=1}^{2^N} \frac{1}{\sigma_{0,k,i}} \exp\left[-\frac{1}{2}\left(\frac{F_i - m_{0,k,i}}{\sigma_{0,k,i}}\right)^2\right] = \sum_{k=1}^{2^N} \frac{1}{\sigma_{1,k,i}} \exp\left[-\frac{1}{2}\left(\frac{m_{1,k,i} - F_i}{\sigma_{1,k}}\right)^2\right] \quad (3.25)$$

Then, the optimal threshold is used to minimize bit the BER_i. The average BER is defined by

$$\overline{BER} = \frac{1}{N_{MCF}} \sum_{i=1}^{N_{MCF}} BER_i \quad (3.26)$$

with the parameter N_{MCF} defining the number of iterations (MCF realizations) of the MC simulator. The number of MC simulation iterations needed to obtain a stabilized value of the average BER or a sufficient accurate outage probability is still to be determined and is analyzed in chapter 4.

3.7 BER assessment in presence of electrical noise

After describing and defining the discrete changes model for single and dual polarizations implemented in the simulation, it is necessary to validate the model and the BER assessment procedure described in section 3.6. The validation is performed using a simplified version of the model presented in Fig. 3.1, first in a back-to-back configuration and, then, including a single core dispersive fiber. Some validation results are compared with the results presented in [59].

First, it is necessary to find the optical power at the input of the optical receiver, in a back-to-back configuration, usually known as receiver sensitivity, at which a $BER = 10^{-12}$ is reached. In order to validate the model, it is necessary to check if the sensitivities obtained in the simulation are in accordance with the sensitivities obtained through the theoretical expression for the receiver sensitivity in a back-to-back configuration given by [34]

$$\overline{p_i} = QNEP\sqrt{B_{e,n}} \quad (3.27)$$

where Q represents the Q-factor (for BER$= 10^{-12}$, $Q = 7$) [34].

In Fig. 3.4, the theoretical and simulated BER are presented as a function of the optical power at the receiver input, for a bit rate $R_b = 40$ Gbps. By analyzing Fig. 3.4, it is possible to verify that, the theoretical and simulated BERs are in a very good agreement, and, that, for $R_b = 40$ Gbps, the target BER of 10^{-12} is reached when the sensitivity is approximately -16 dBm.

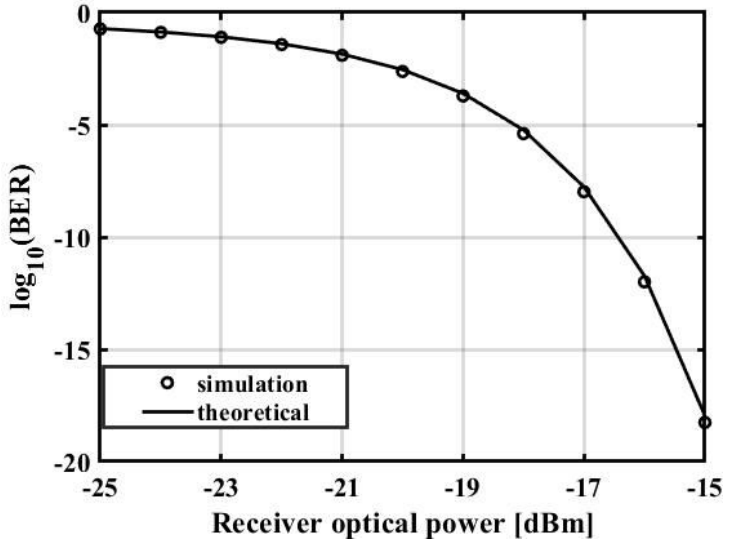

FIGURE 3.4: BER as a function of the optical power at the receiver input for $R_b = 40$ Gbps in a back-to-back configuration.

Besides of $R_b = 40$ Gbps, the comparison of the receiver sensitivity obtained from theory and simulation is performed for other bit rates than 40 Gbps. Table 3.1 shows the receiver sensitivity obtained using Eq. 3.27 and from numerical simulation as a function of R_b, for Q=7, NEP=1×10^{-12} W/$\sqrt{\text{Hz}}$ and $B_{e,n}$=$0.65\times R_b$ Gbps, and a back-to-back configuration.

TABLE 3.1: Receiver sensitivity comparison between theoretical and simulated values as a function of R_b, for Q=7, NEP=1×10^{-12} W/$\sqrt{\text{Hz}}$ and $B_{e,n}$=$0.65\times R_b$ Gbps, in a back-to-back configuration.

Rb [Gbps]	theoretical $\overline{p_i}$ [dBm]	simulated $\overline{p_i}$ [dBm]
1.2288	-37.04	-36.9
4.9152	-34.03	-33.89
10.1376	-32.045	-33.32
24.33024	-30.55	-30.42
40	-29.47	-29.34

From Table 3.1, it is possible to conclude that, in a back-to-back configuration, the higher the bit rate, the higher the receiver sensitivity required to reach the BER=10^{-12}. It is also possible to observe a very good agreement between the simulated and theoretical results, which validates the optical communication system in a back-to-back configuration.

Fig. 3.5 depicts the BER as a function of the fiber length for a lossless SCF with dispersion, for a transmitted optical power of -16 dBm, which corresponds to a BER=10^{-12} in a back-to-back configuration, with $D_\lambda = 17$ ps/(nm·km), $\lambda = 1550$ nm and $R_b = 40$ Gbps. By analyzing Fig. 3.5, it is possible to observe the BER degradation after 8 km due to fiber dispersion, which is in agreement with the results presented in [59]. Hence, Fig. 3.5 validates the implementation of the fiber chromatic dispersion in the simulator.

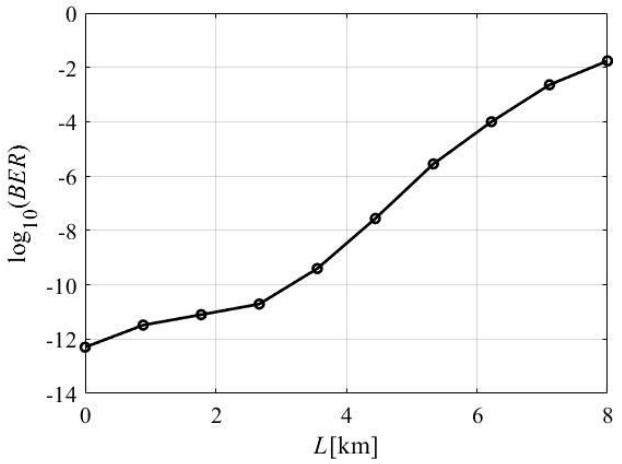

FIGURE 3.5: BER as a function of the fiber length for a transmitted optical power of -16 dBm, which corresponds to a BER=10^{-12} with $L = 0$ km, for $D_\lambda = 17$ ps/(nm·km), $\lambda_0 = 1550$ nm and $R_b = 40$ Gbps.

Extending this process to the CPRI bit rates, it is possible to observe that the higher the bit rate, shorter fiber lengths are reached. Fig. 3.6 shows the receiver sensitivity as a function of the fiber length, for a) $R_b = 10.1376$ Gbps, b) $R_b = 24.33024$ Gbps and c) $R_b = 40$ Gbps, and a target BER of 10^{-12}. From Fig. 3.6, by defining the maximum of power penalty due to dispersion as 2 dB [34], the maximum fiber length reached for each CPRI bit rate can be extracted.

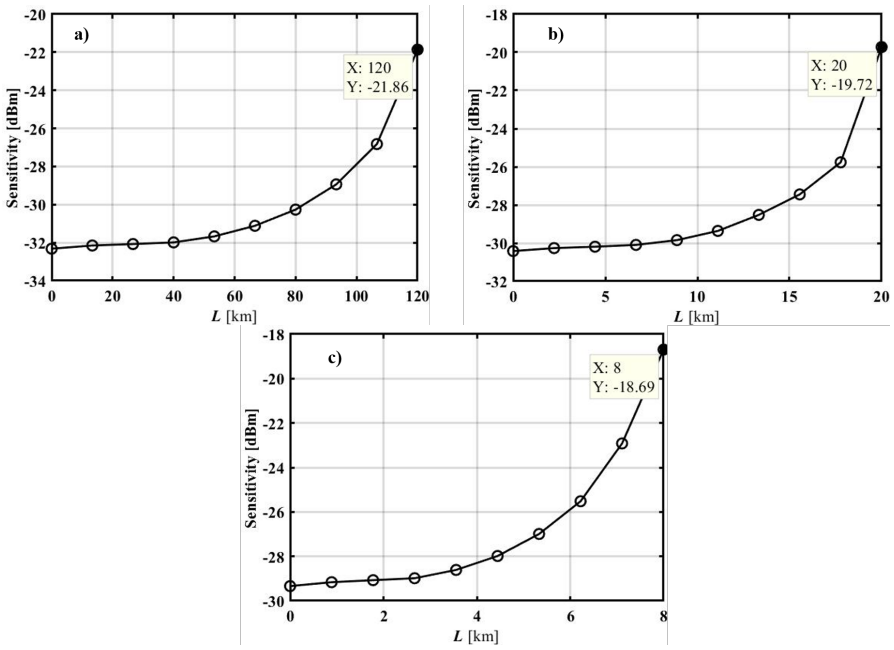

FIGURE 3.6: Receiver sensitivity as a function of the fiber length. a) R_b=10.1376 Gbps, b) R_b=24.33024 Gbps and c) R_b=40 Gbps

TABLE 3.2: Maximum fiber length achieved considering a 2 dB power penalty, due to fiber dispersion, and corresponding sensitivity.

CPRI bit rates	Sensitivity at L=0 km	L_{max} [km]	Sensitivity at L_{max}
1.2288 Gbps	−36.9 dBm	5333	−34.94 dBm
4.9152 Gbps	−33.89 dBm	335	−31.93 dBm
10.1376 Gbps	−32.32 dBm	80	−30.27 dBm
24.33024 Gbps	−30.42 dBm	14	−28.3 dBm
40 Gbps	−29.34 dBm	5	−27.42 dBm

Table 3.2, shows the maximum fiber length reached, considering a 2 dB power penalty due to fiber dispersion, by taking as a reference the back-to-back situation and the corresponding receiver sensitivity. The sensitivities obtained through simulation, in a back-to-back configuration, are also presented in Table 3.1, and are in accordance with the values obtained through Eq. 3.27. By analyzing Eq. 3.27, it is possible to conclude that when a bit rate is raised four times, the receiver sensitivity in a back-to-back configuration, decreases 3 dB. Table 3.2 shows this 3 dB difference in the sensitivity curves, in back-to-back configuration, when comparing R_b = 40 Gbps with R_b = 10.1376 Gbps or R_b = 4.9152 Gbps with R_b = 1.2288 Gbps. Furthermore, from Table 3.2, it is possible to verify that higher bit rates, lead to shorter maximum fiber lengths.

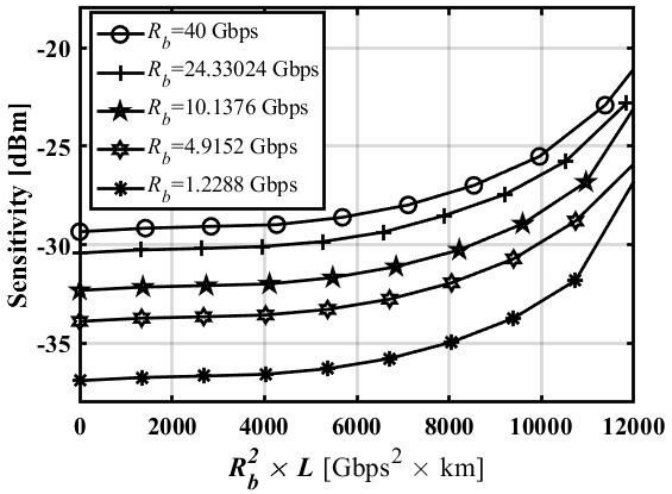

FIGURE 3.7: Receiver sensitivity as a function of ${R_b}^2 \times L$ for the bit rates of R_b=1.2268 Gbps, R_b=4.9152 Gbps, R_b=10.1376 Gbps, R_b=24.33024 Gbps and R_b=40 Gbps.

From Fig. 3.6, it is possible to represent the receiver sensitivity as a function of $R_b^2 \times L$, for all the bit rates considered in Table 3.2. Fig. 3.7 shows the receiver sensitivity as a function of $R_b^2 \times L$ for all the bit rates under study. From this figure, it is possible to conclude that the higher the bit rate, the higher the required sensitivity and, that, the 2 dB power penalty due to fiber dispersion is reached, for all bit rates, when $R_b^2 \times L \approx 8000$ Gbps^2×km.

Another method of validating the simulation model considering only fiber dispersion is through the observation of the eye-patterns. Fig. 3.8 shows the evolution of the noiseless eye-patterns according to the fiber length, up to a maximum limit of 8 km, for $R_b = 40$ Gbps, when only the effect of fiber dispersion is present. From Fig. 3.8, it is possible to conclude that the presence of fiber distortion degrades the system performance, since as the fiber length increases, the eye-closure increases. When comparing the eye-patterns and their corresponding amplitudes in Fig. 3.8 with the ones presented in [59], a very good agreement is observed.

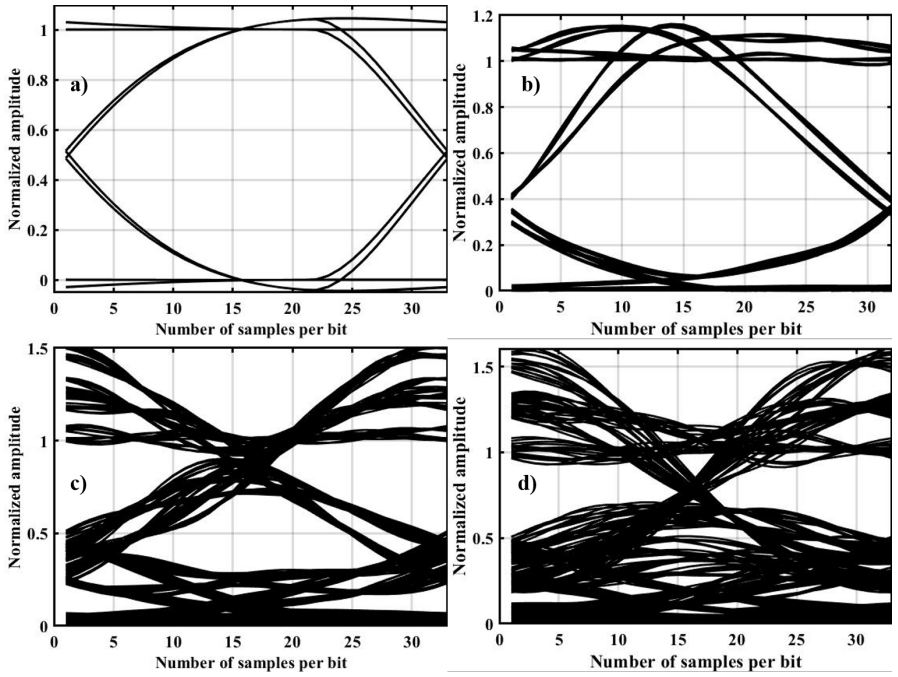

FIGURE 3.8: Eye-pattern evolution at the decision circuit input, for $R_b = 40$ Gbps and a) $L = 0$ km, b) $L = 2$ km, c) $L = 6$ km and d) $L = 8$ km.

Optical fiber attenuation has not been yet taken into account in the studies presented so far. When assuming fiber attenuation, the attenuation coefficient is considered to be 0.2 dB/km, for $\lambda = 1550$ nm [34]. Table 3.3 shows the optical power necessary at the optical fiber input, with and without considering losses, to achieve a BER=10^{-12}, for the maximum fiber length achieved with each bit rate. For $R_b = 4.9152$ Gbps (L =500 km) and $R_b = 1.2288$ Gbps (L=8000 km), the transmitted optical power obtained by simulation is not presented, since the attenuation is so strong, that leads to unfeasible transmitted optical powers.

TABLE 3.3: Theoretical optical power needed at the fiber input with and without attenuation for the maximum fiber length and all bit rates under study.

R_b [Gbps]	L [km]	Optical power without attenuation [dBm]	Attenuation [dB]	Optical power with attenuation [dBm]
40	8	−18.6	1.6	−17
24.3304	20	−22.8	4	−18.8
10.1376	120	−21.8	24	2.2
4.9152	500	−25.7	100	–
1.2288	8000	−26.4	1600	–

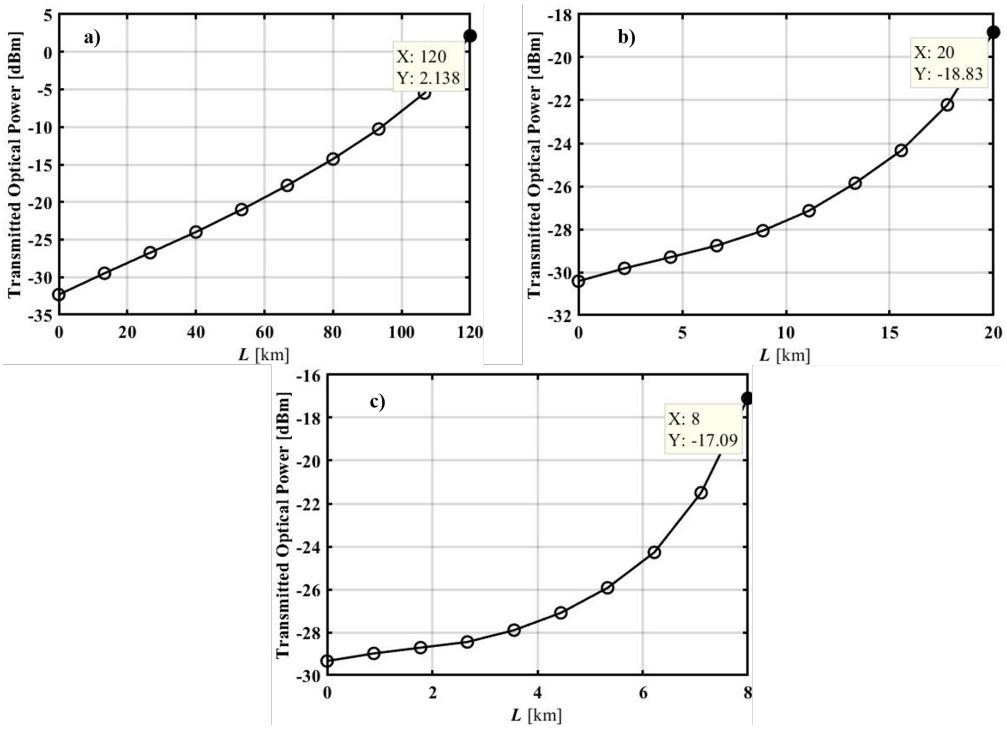

FIGURE 3.9: Transmitted optical power as a function of the fiber length with an attenuation coefficient of α=0.2 dB/km. a) R_b= 10.1376 Gbps; b) R_b= 24.33024 Gbps; and c) R_b= 40 Gbps.

In Fig. 3.9, it is possible to observe the transmitted optical power as a function of the fiber length for $R_b = 10.1376$ Gbps, $R_b = 24.33024$ Gbps and $R_b = 40$ Gbps, obtained through MC simulation. For $R_b = 10.1376$ Gbps, the obtained value for the transmitted optical power is 2.1 dBm, for $R_b = 24.3304$ Gbps is -18.8 dBm and for $R_b = 40$ Gbps is -17.1 dBm, at the maximum fiber length given by the 2 dB power penalty criterion. Hence, it is possible to conclude that the simulated results are in accordance with the theoretical results shown in Table 3.3.

3.8 Conclusion

In this chapter, the system model for the 5G fronthaul supported by MCFs and impaired by ICXT has been presented. Optical transmitter, MCF considering the single and dual polarization DCMs, and optical receiver composed by photodetector and the electrical filter have been described with some detail. The noise at the receiver electrical circuit is characterized, and the method of the BER estimation

using a combined technique of MC simulation and a semi-analytical calculation is described.

After presenting the 5G fronthaul model supported by MCFs and impaired by ICXT, the BER assessment in presence of electrical noise is performed in a back-to-back configuration and with fiber dispersion and losses. The good agreement between theoretical and simulated BERs validates the implemented system model without ICXT. The analysis and study of ICXT using the DCM models with one or two signal polarizations is left for chapter 4.

Chapter 4

Numerical results and discussion

In this chapter, by using the 5G fronthaul models presented in Chapter 3, the impact of the ICXT on the performance of CPRI signals transmitted in 5G fronthauls supported by weakly-coupled homogeneous MCFs is assessed and discussed. All numerical results are obtained using MC simulation combined with a semi-analytical method [14], where the impact of electrical noise is taken into account analytically and the effects of the MCF chromatic dispersion and ICXT on the performance are evaluated using waveform simulation, in each MC simulation iteration. In every MC simulation iteration, the average BER and the BER per MCF realization are estimated as defined in section 3.6.

4.1 CPRI bit rates and simulation parameters

The CPRI bit rates chosen to obtain the simulation results, the reasons for their choice and the simulation parameters utilized that remain the same along all this chapter are presented in this section. The CPRI bit rates chosen are the line option 7 with $R_b = 9.8304$ Gbps, 8B/10B line coding and without FEC and the CPRI bit rate line option 8 with $R_b = 10.1376$ Gbps, 64B/66B line coding and with FEC. These bit rates, around 10 Gbps, are the most common found in optical fiber telecommunication systems with OOK signal transmission and direct detection, since they lead to simpler and less expensive implementations [34], and are chosen

because they have been already studied in 5G networks fronthauls with single-core fibers [9], [60]. In systems that consider FEC, a target average BER of 10^{-3} is chosen [47], although it can change accordingly to the FEC implementation. For a system without FEC, a target average BER of 10^{-12} is considered [34].

Regarding the simulation parameters, the ones that remain the same along this chapter are presented in Table 4.1. The MCF length chosen is the one defined as the maximum reach of the 5G network fronthaul [52] and originates a slight ISI due to the chromatic dispersion at 10 Gbps. The same fiber dispersion is set for the two cores, ΔD_{mn}=0, the number of phase-matching points is set to define with precision the random-phase shift mechanism [18], [19]. The number of bits in each MC simulation iteration is set to get sufficient combinations of the bits sequences in both cores, in order to have the ICXT statistics properly characterized. Finally, two different skews are taken into account: a skew shorter than the bit period, $S_{mn}{\cdot}R_b \approx 0.2$, with $d_{mn} = 1$ ps/km, and $S_{mn}{\cdot}R_b \approx 10$, for $d_{mn} = 50$ ps/km, where the skew is much higher than the bit period.

Table 4.1: Simulation parameters

Simulation parameter	Value
Carrier wavelength	$\lambda = 1550$ nm
Fiber dispersion parameter	$D_\lambda = 17$ ps/(nm·km)
Fiber length	$L = 20$ km
Difference of propagation constants at zero frequency	$\Delta\beta_{0,mn} = 0$
Number of PMPs	$N_p = 1000$
Number of generated OOK bits per MCF realization	$N_b = 2^9$

4.2 Influence of the ICXT mechanism on the direct-detection system performance

The first goal of these studies is to assess the number of fiber realizations needed to achieve a stabilized average BER. The average BER in the absence of ICXT is set

two orders of magnitude below the target BER in order to allow a certain margin for the BER degradation due to ICXT. Consequently, the studies for CPRI line option 8 have a BER without ICXT of 10^{-5}. In this case, the receiver sensitivity is set to -34.40 dBm; in CPRI line option 7, the BER without ICXT is 10^{-14} and its respective sensitivity is -31.79 dBm. In subsections 4.2.1 and 4.2.2, the results for the number of MCF realizations needed to stabilize the average BER, the ICXT impact in each MCF realization and the corresponding eye-patterns for single polarization and dual polarization, respectively, are presented.

4.2.1 Single polarization results

In Figs. 4.1 and 4.2, the BER for each MCF realization (blue symbols) and the average BER as a function of the MCF realizations (red symbols), for a walkoff of $d_{mn} = 1$ ps/km are illustrated.

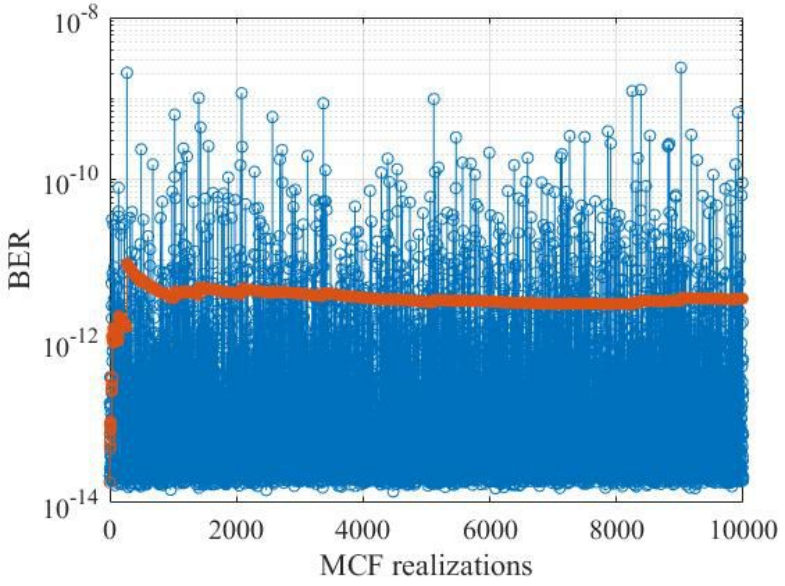

FIGURE 4.1: BER for each MCF realization (blue symbols) and average BER (red symbols) as a function of the MCF realizations, for R_b =9.8304 Gbps, $X_c = -30$ dB and $d_{mn} = 1$ ps/km. The BER in the absence of ICXT is 10^{-14}.

Fig. 4.1 corresponds to the CPRI signal with $R_b = 9.8304$ Gbps, that does not consider FEC, and to the crosstalk level $X_c = -30$ dB, that is chosen to lead to an average BER degradation relatively to the BER when no ICXT is considered, of two orders of magnitude. Observing Fig. 4.1, it is possible to see that a stabilized average BER of 3.33×10^{-12} is achieved after about 4000 MCF

realizations. For subsequent studies, for the CPRI line rate option 8, a conservative approach with 10^4 fiber realizations is adopted. In Fig. 4.1, it is possible to observe the degradation or the improvement of the BER per MCF realization (relative to the BER obtained in ICXT absence) caused by the randomness of the ICXT mechanism. In Fig. 4.1, the best BER per MCF realization obtained is 1.38×10^{-14} and the worst BER is 2.07×10^{-9}.

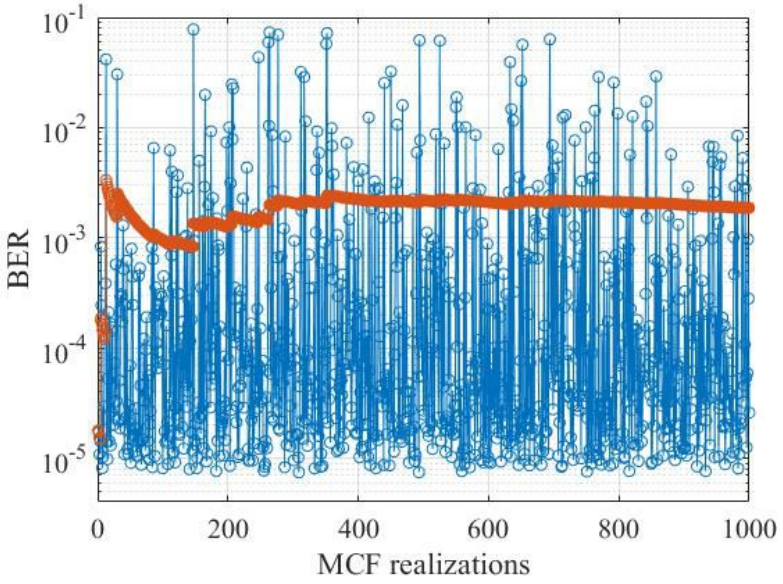

FIGURE 4.2: BER for each MCF realization (blue symbols) and average BER (red symbols) as a function of the MCF realizations, for R_b =10.1376 Gbps, $X_c = -15$ dB and $d_{mn} = 1$ ps/km. The BER in the absence of ICXT is 10^{-5}.

Fig. 4.2 shows the average BER as a function of the MCF realizations for the CPRI line rate option 8, $R_b = 10.1376$ Gbps, $X_c = -15$ dB and where FEC is considered. In this case, the stabilized value of the average BER is around 1.87×10^{-3} and is reached after about 400 MCF realizations. For the subsequent studies with CPRI line option 8, the total number of fiber realizations is set to 10^3. The difference between the number of MCF realizations needed to stabilize the average BER in Figs. 4.1 and 4.2 can be explained by the order of magnitude of the average BER in the absence of ICXT considered for each case. Regarding the randomness of the ICXT, Fig. 4.2 shows a best BER per MCF realization of 7.40×10^{-6} and a worst BER of 7.78×10^{-2}.

The impact of the ICXT can be analyzed in the eye-patterns corresponding to the BERs shown in Figs. 4.1 and 4.2. These eye-patterns do not show the effect of the electrical noise to make clear the ICXT effect and only consider the ISI

effect induced by the receiver electrical filtering and fiber chromatic dispersion. The amplitude of bit '1' in the absence of ISI is normalized to unity. Fig. 4.3 refers to the eye-pattern without ICXT at the decision circuit input after 20 km of fiber and, as the bit rate values are similar and the amplitude is normalized, the eye-patterns for both CPRI bit rates under analysis are similar.

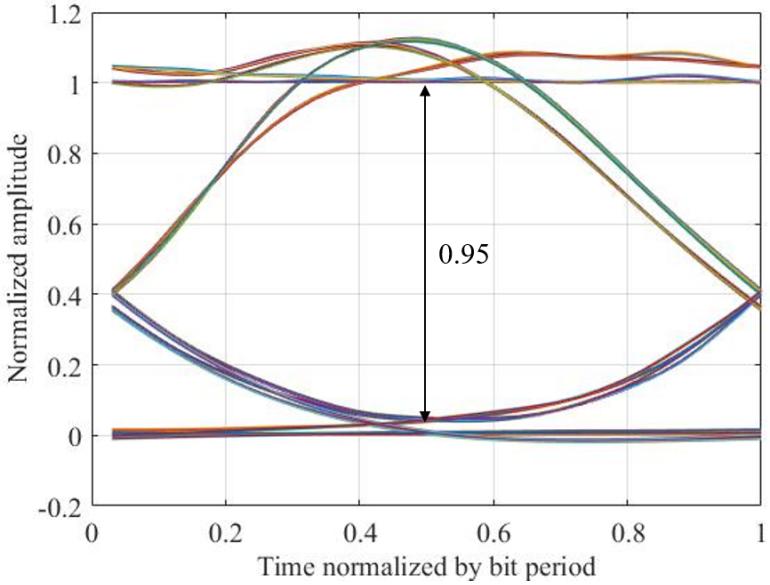

FIGURE 4.3: Eye-pattern at the decision circuit input corresponding to the absence of ICXT. The normalized eye opening is also depicted.

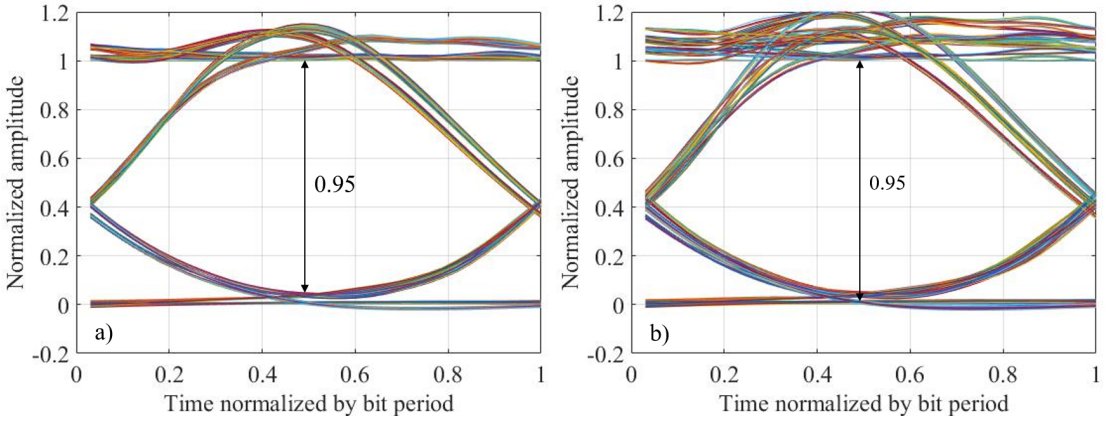

FIGURE 4.4: Eye-patterns at the decision circuit input corresponding to the best BER per MCF realization in Figs.4.1 and 4.2, for d_{mn} =1 ps/km. a) best BER per MCF realization, for R_b = 9.8304 Gbps; b) best BER per MCF realization, for R_b = 10.1376 Gbps. The normalized eye opening is also depicted.

Figs. 4.4 a) and b) exhibit the eye-patterns for the best BER per MCF realization, obtained in Figs. 4.1 and 4.2, for R_b = 9.8304 Gbps and for R_b = 10.1376 Gbps, respectively. In comparison with the case where no ICXT is considered, the normalized eye-patterns show a similar eye-opening. Fig. 4.4 b) represents an

example of an eye-pattern, where the BER per MCF realization has improved due to the ICXT presence relatively to absence of ICXT and this can be explained by the higher amplitudes of the bit '1' caused by the ICXT.

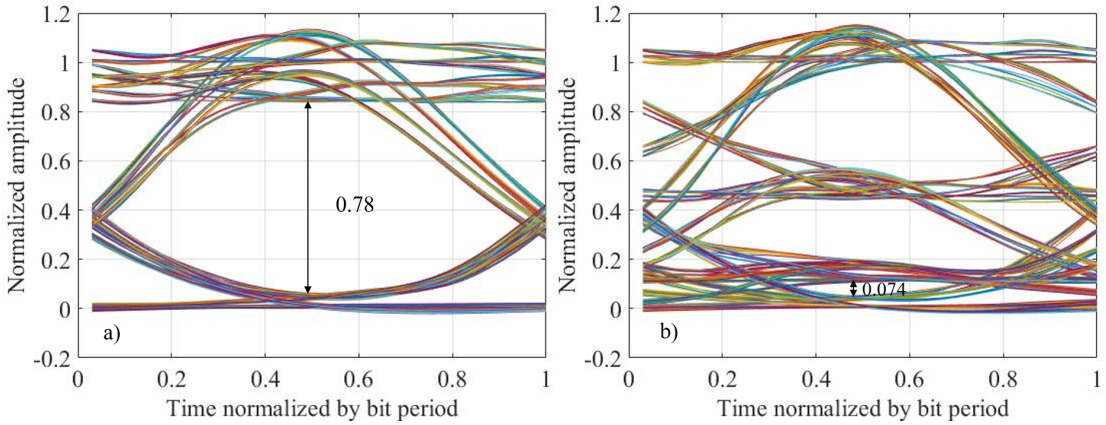

FIGURE 4.5: Eye-patterns at the decision circuit input corresponding to the worst BER per MCF realization, for d_{mn} =1 ps/km. a) worst BER per MCF realization, for R_b = 9.8304 Gbps; b) worst BER per MCF realization, for R_b = 10.1376 Gbps. The normalized eye opening is also depicted.

Fig. 4.5 a) and b) correspond to the MCF realizations in which the worst BER occurs, in Figs. 4.1 and 4.2, for R_b = 9.8304 Gbps and R_b = 10.1376 Gbps, respectively. In Fig. 4.5 a), it is possible to observe the eye-closure for the MCF realization with the worst BER is less severe than the one obtained in Fig. 4.5 b). This explains the higher number of MCF realizations needed to get a stabilized average BER for lower BERs (Fig. 4.1), since a slight signal distortion caused by ICXT can degrade the average BER by a few orders of magnitude. For higher BERs (Fig. 4.2), in order to get BERs per MCF realization with a few orders of magnitude above the reference BER of 10^{-5}, the crosstalk level is much higher, and leads to a very small normalized eye-opening of 0.074.

The analysis of Figs. 4.3, 4.4 and 4.5 reveals that the impact of the ICXT on the eye-pattern is mainly felt at the amplitudes of bit '1' creating new amplitude "rails" in these bits. At bit '0', the amplitude values remain essentially the same due to the null extinction ratio of the signal generated by the transmitter. For finite extinction ratios, it is expected that the amplitudes of the bit '0' suffer an ICXT effect similar to the one observed in the amplitudes of the bits '1'.

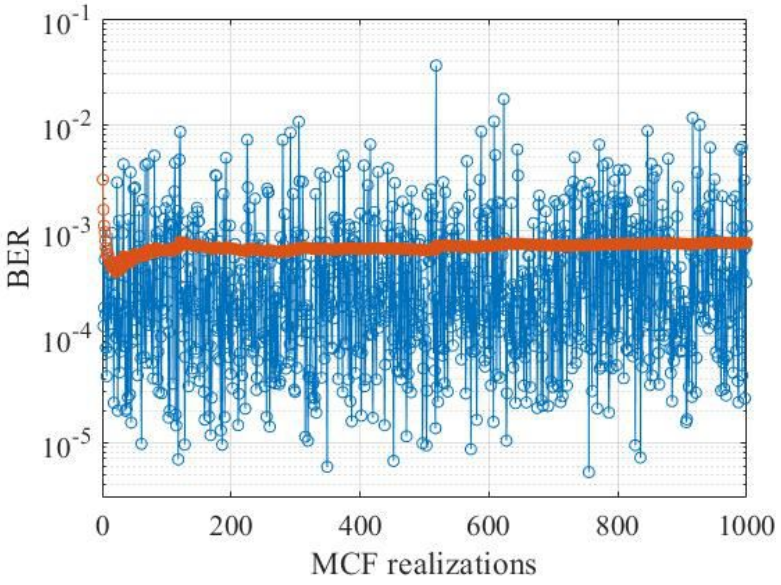

FIGURE 4.6: BER for each MCF realization (blue symbols) and average BER (red symbols) as a function of the MCF realizations for R_b =10.1376 Gbps, $X_c = -15$ dB and $d_{mn} = 50$ ps/km. In the absence of ICXT the BER is 10^{-5}.

An identical analysis to the one made in Figs. 4.1-4.5 has been performed for a skew much higher than the bit period, where $S_{mn} \cdot R_b \approx 10$ ($d_{mn} = 50$ ps/km). Fig. 4.6 presents the BER per MCF realization (blue symbols) and the average BER as a function of the MCF realizations for the CPRI signal with a bit rate $R_b = 10.1376$ Gbps and $X_c = -15$ dB. Fig. 4.6 shows, that in order to get a stabilized average BER of 7.67×10^{-4}, only 200 MCF realizations are required. For $d_{mn} = 50$ ps/km, the ICXT impact is lower than the one verified for a walkoff of $d_{mn} = 1$ ps/km [61]. Therefore, in comparison to Fig. 4.2, it is possible to conclude that for the same crosstalk level ($X_c = -15$ dB), a lower average BER is achieved with less MCF realizations. Besides that, Fig. 4.6 shows that in relation to Fig. 4.2, the best BER per MCF realization is lower (5.24×10^{-6} vs 7.40×10^{-6}) and the worst BER per MCF realization is also lower (3.62×10^{-2} vs 7.78×10^{-2}).

In Fig. 4.7 a) and b), the eye-patterns obtained for, respectively, the best and worst BERs per MCF realization in Fig. 4.6, are shown. The eye-pattern obtained without ICXT is the one depicted in Fig. 4.3. However, the best BER per MCF realization improves, since the amplitudes of the bit '1' are taken at sampling instants that have higher values than in the case of ICXT absence, similarly to what is observed with $d_{mn} = 1$ ps/km. The normalized eye-opening is equal to

the eye-opening obtained in Fig. 4.3. The worst BER happens due to a MCF realization that leads to a very small eye-opening.

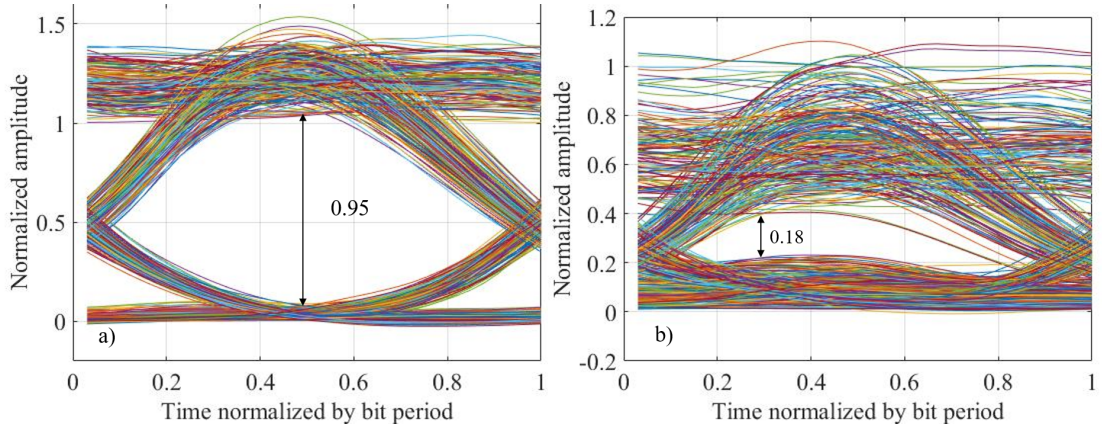

FIGURE 4.7: Eye-patterns at the decision circuit input corresponding a) best BER and b) worst BER obtained in Figure 4.6 for $d_{mn} = 50$ ps/km.

The analysis of the eye-patterns for $d_{mn} = 1$ ps/km and $d_{mn} = 50$ ps/km shows that they have a very distinctive behavior. For $d_{mn} = 1$ ps/km, the amplitude levels caused by the ICXT define discrete values on the eye-pattern. For a walkoff of $d_{mn} = 50$ ps/km, the amplitudes due to ICXT exhibit a "continuous" behavior at the sampling instant, which reminds a random behavior as the one provided by a noise source. The observed behavior is in agreement with the one observed in [43], where for an adequately broad signal, $S_{mn} \cdot R_b \approx 10$, the ICXT behaves similarly to white noise as shown in Fig. 4.7. In turn, for an adequately narrower signal, the ICXT leads to well-defined discrete amplitudes on the eye-pattern, as shown in Figs. 4.4 and 4.5, with a behavior named virtually static coupling [43].

4.2.2 Dual polarization results

The studies performed for the single polarization DCM are also made for the dual polarization model, following the scheme presented in Fig. 3.3. The parameters used are the same presented in Table 4.1, and an even power distribution between the polarization directions in the two cores is considered $\xi = \xi_m = \xi_n = 1/2$. Results are presented, for R_b =9.8304 Gbps and R_b =10.1376 Gbps and for two different skews, $S_{mn} \cdot R_b \approx 0.2$, ($d_{mn}$ =1 ps/km) and $S_{mn} \cdot R_b \approx 10$ (d_{mn} =50 ps/km).

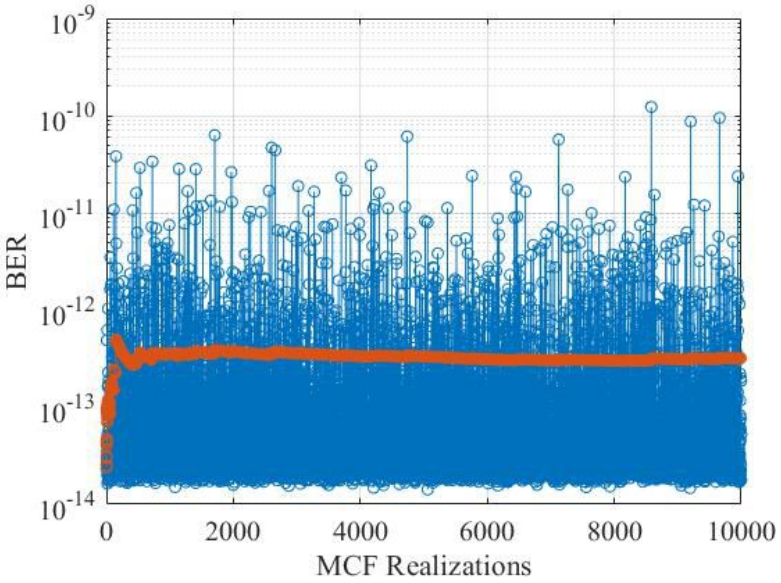

FIGURE 4.8: BER for each MCF realization (blue symbols) and average BER (red symbols) as a function of the MCF realizations, for R_b =9.8304 Gbps, $X_c = -30$ dB and $d_{mn} = 1$ ps/km. The BER in the absence of ICXT is 10^{-14}.

Fig. 4.8 shows the BER for each MCF realization and the average BER as a function of the MCF realizations obtained with the dual polarization DCM model for a CPRI signal with R_b =9.8304 Gbps, that does not consider FEC, and a crosstalk level, $X_c = -30$ dB. From Fig. 4.8, it is possible to see that a stabilized average BER of 3.18×10^{-13} is achieved after about 9500 MCF realizations. In comparison with single polarization scenario, more realizations are necessary to stabilize the BER because the ICXT impact is lower in the dual polarization DCM. For subsequent studies, for the CPRI line rate option 8, 10^4 fiber realizations are considered in the MC simulation. In Fig. 4.8, it is also possible to see the degradation or the improvement of the BER values per MCF realization (relative to the BER obtained in ICXT absence) caused by the randomness of the ICXT. Here, the best BER per MCF realization obtained is 1.42×10^{-14} and the worst BER is 1.23×10^{-10}, which is about one order of magnitude below the worst BER obtained in Fig. 4.1, for the single polarization model. By comparing Figs. 4.1 and 4.8, it is possible to observe that the ICXT impact on the dual polarization scenario is lower than for the single polarization case.

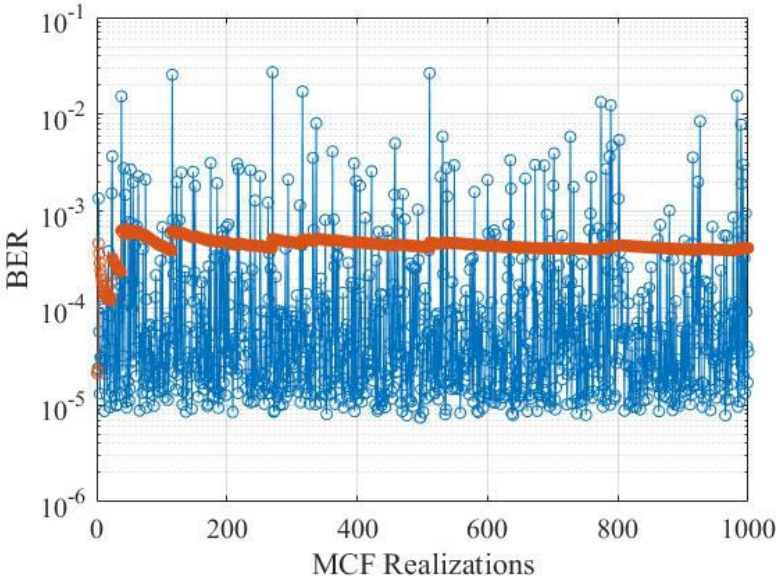

FIGURE 4.9: BER for each MCF realization (blue symbols) and average BER (red symbols) as a function of the MCF realizations, for R_b =10.1376 Gbps, $X_c = -15$ dB and $d_{mn} = 1$ ps/km. The BER in the absence of ICXT is 10^{-5}.

Fig. 4.9 shows the average BER as a function of the dual polarization MCF realizations for the CPRI line rate option 8, $R_b = 10.1376$ Gbps and ICXT level $X_c = -15$ dB. In this case, the average BER is 4.16×10^{-4}, and does not varies much after 800 MCF realizations. For the subsequent studies, the total number of fiber realizations is set to 10^3. The difference between the number of MCF realizations needed to stabilize the average BER in Figs. 4.8 and 4.9 can be explained again by the order of magnitude of the average BER considered for each CPRI bit rate. Fig. 4.9 shows a best BER per MCF realization of 7.42×10^{-6} and a worst BER of 2.7×10^{-2}. Analyzing Figs. 4.1, 4.2, 4.8 and 4.9, it is possible to conclude that under the same system conditions, the ICXT has less impact in the dual polarization weakly-coupled MCF, but more MCF realizations are needed to stabilize the average BER.

The study of the eye-patterns for the best BER per MCF realization, obtained in Figs. 4.8 and 4.9, for $R_b = 9.8304$ Gbps and $R_b = 10.1376$ Gbps, respectively, has been made and, in comparison with the case where only one polarization is taken into account, it was verified that for dual polarization, and without crosstalk the eye-pattern in ICXT absence, is the same as the one presented in Fig.4.3. Furthermore, since, for dual polarization, the best BER value per MCF realization

is similar to the the ones obtained for single polarization, for both bit rates, the eye-patterns have a similar aspect, are also an example where the higher amplitudes of bits '1' can explain why the BER has improved, and are not shown.

Fig. 4.10 a) and b) shows the eye-patterns corresponding to the MCF realizations in which the worst BER occurs for R_b = 9.8304 Gbps and R_b = 10.1376 Gbps, respectively in Figs. 4.8 and 4.9. Like in single polarization, the number of MCF realizations needed to stabilize the average BER can explain the less severe eye-closure in Fig. 4.10 a) when compared with Fig. 4.10 b). In comparison with Fig. 4.5, it is possible to see that for both Fig. 4.10 a) and b), due to the lower ICXT impact with the dual polarization MCF, the eye-opening is higher, for R_b =9.8304 Gbps (0.83 vs 0.78) and for R_b =10.1376 Gbps (0.32 vs 0.075).

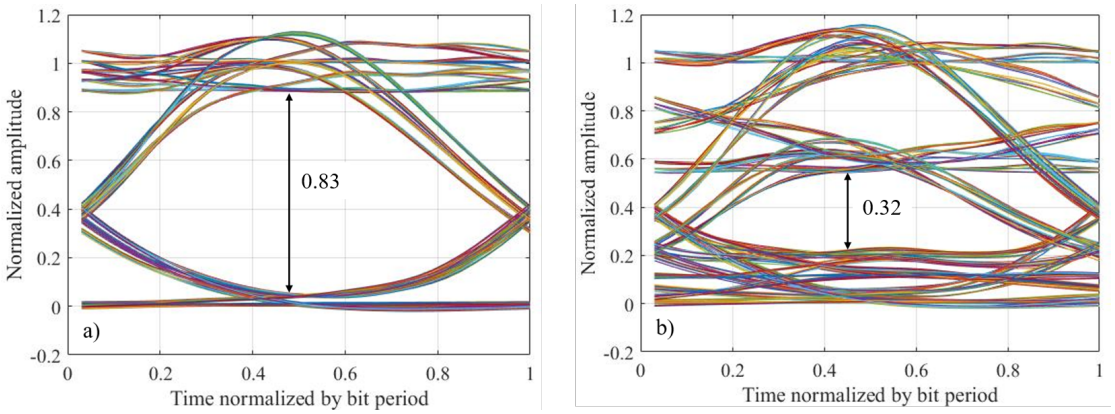

FIGURE 4.10: Eye-patterns at the decision circuit input corresponding to the worst BER per MCF realization, for d_{mn} =1 ps/km and the dual polarization DCM. a) is the worst BER per MCF realization for R_b = 9.8304 Gbps; b) is the worst BER per MCF realization for R_b = 10.1376 Gbps.

The analysis of Fig. 4.10 is similar to the one performed for single polarization. Hence, the impact of the ICXT on the eye-pattern is mainly felt at the amplitudes of bit '1' creating new amplitude "rails" in these bits and at bit '0', the amplitude values remain essentially the same due to the null extinction ratio of the signal generated by the transmitter.

As for the single polarization scenario, for the dual polarization case, an identical analysis to the one made in Figs. 4.8-4.10, has been made, for a skew much higher than the bit period, where $S_{mn} \cdot R_b \approx 10$ (d_{mn} = 50 ps/km). Fig. 4.11 presents the BER per MCF realization (blue symbols) and the average BER as a function of the MCF realizations for the CPRI signal with R_b = 10.1376 Gbps

and $X_c = -15$ dB. Fig. 4.11 shows, that in order to get a stabilized average BER of 1.98×10^{-4}, only 700 MCF realizations are required. For $d_{mn} = 50$ ps/km, the ICXT impact is lower than the one verified for $d_{mn} = 1$ ps/km [62]. Therefore, in comparison to Figure 4.9, is possible to conclude that for the same crosstalk level, $X_c = -15$ dB, a lower average BER is achieved with less MCF realizations. Besides that, Fig. 4.11 also shows that in relation to Fig. 4.9, the best BER per MCF realization is lower (3.52×10^{-6} vs 7.42×10^{-6}) and the worst BER per MCF realization is also lower (8.18×10^{-3} vs 2.7×10^{-2}). In comparison with the single polarization scenario (Fig.4.6), it is possible to conclude that, for the same skew and the same crosstalk level, more realizations are needed in order to stabilize the average BER, but the ICXT impact is lower for dual polarization scenario.

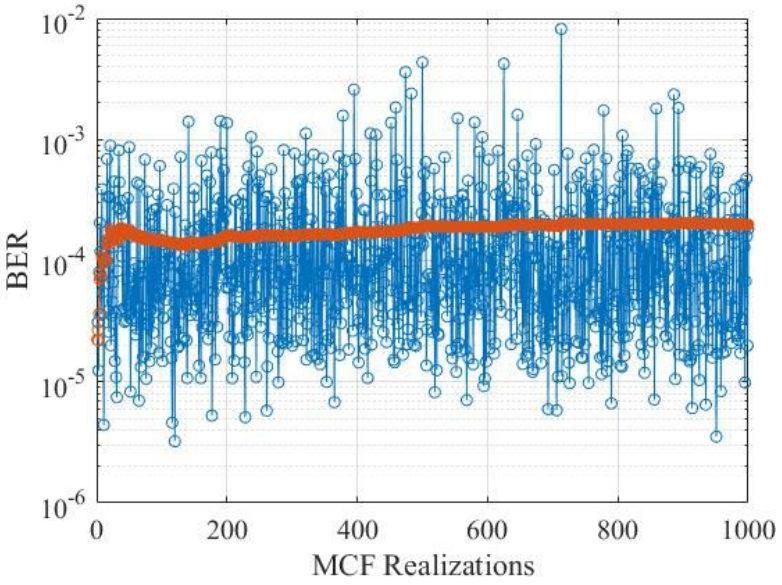

FIGURE 4.11: BER for each MCF realization (blue symbols) and average BER (red symbols) as a function of the MCF realizations for R_b =10.1376 Gbps, $X_c = -15$ dB and $d_{mn} = 50$ ps/km. In the absence of ICXT, the BER is 10^{-5}.

In Fig. 4.12 a) and b), the eye-patterns obtained for, respectively, the best and worst BERs per MCF realization in Fig. 4.11 are shown. The eye-pattern obtained without ICXT is the one depicted in Fig. 4.3. However, the best BER per MCF realization improves since the amplitudes of bit '1' are taken at sampling instants that have higher values than in the case of ICXT absence; the worst BER happens due to a MCF realization that leads to a very small eye-opening. In this case, the difference of the best and worst BER values, although not much different from the values obtained for the single polarization scenario, is caused by

the differences in the eye-closure as can be seen in Fig. 4.12. For the best BER and worst BER per MCF realization the eye-opening increases, 0.97 vs 0.95 and 0.35 vs 0.18, respectively. The analysis of the eye-patterns for, $d_{mn} = 1$ ps/km and $d_{mn} = 50$ ps/km, for the dual polarization case, shows that they have a very distinctive behavior, as commented previously for the single polarization scenario.

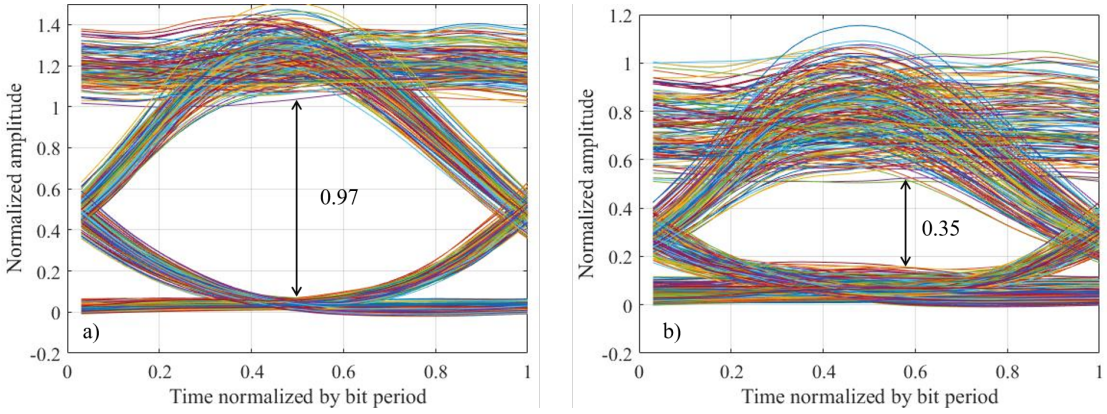

FIGURE 4.12: Eye-patterns at the decision circuit input corresponding to a) best BER and b) worst BER obtained in Fig. 4.11, for $d_{mn} = 50$ ps/km.

4.3 Power penalty due to ICXT

After the total number of MCF realizations required to have a stabilized average BER has been defined and the influence of the ICXT on the eye-pattern has been analyzed, the following studies focus on the influence of ICXT on the degradation of the average BER. Figs. 4.13 and 4.14 illustrate the average BER as a function of the ICXT level, a) for single polarization; b) for dual polarization, for $d_{mn} = 1$ ps/km and $d_{mn} = 50$ ps/km. Figure 4.13 corresponds to the CPRI signal with $R_b = 9.8304$ Gbps and Figure 4.14 refers to the CPRI signal with $R_b = 10.1376$ Gbps. As expected, with the increase of the crosstalk level, the average BER becomes higher.

In Fig. 4.13, as the BER in absence of ICXT is very low (10^{-14}), the values of the ICXT level that lead to a BER degradation over two orders of magnitude are also low. Having the average BER of 10^{-12} as a reference for the system performance, in Fig.4.13 a), this BER is reached, when $X_c = -31.7$ dB, for a walkoff of $d_{mn} = 1$ ps/km, and when $X_c = -29.6$ dB, for $d_{mn} = 50$ ps/km,

which represents an improvement of the ICXT tolerance of 2.1 dB for the higher walkoff in relation to $d_{mn} = 1$ ps/km. In Fig. 4.13 b), the BER is reached, when $X_c = -28.4$ dB, for $d_{mn} = 1$ ps/km, and, when $X_c = -26.1$ dB, for $d_{mn} = 50$ ps/km. In Fig. 4.13, it is shown that, an higher walkoff leads to an higher ICXT tolerance. Comparing the single polarization scenario with the dual polarization scenario allows to conclude that, for the target BER, for $d_{mn} = 1$ ps/km, the dual polarization system has a 3.3 dB higher ICXT tolerance than the single polarization system and, for $d_{mn} = 50$ ps/km, the system has a 3.5 dB higher ICXT tolerance.

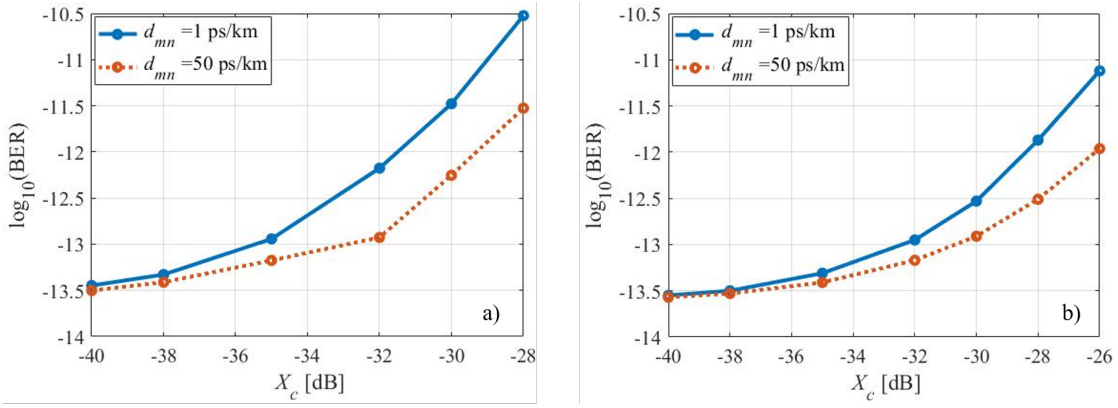

FIGURE 4.13: BER as a function of the crosstalk level, X_c, for $d_{mn} = 1$ ps/km (blue line) and $d_{mn} = 50$ ps/km (red line), for $R_b = 9.8304$ Gbps. a) single polarization DCM and b) dual polarization DCM.

In Fig. 4.14, as the BER without ICXT is 10^{-5}, higher crosstalk levels are required in order to have a significant BER deterioration. In this case, in Fig. 4.14 a), the average BER of 10^{-3} is reached when $X_c = -16.8$ dB, for $d_{mn} = 1$ ps/km, and when $X_c = -14.8$, for $d_{mn} = 50$ ps/km, which corresponds to an improvement of the ICXT tolerance of 2 dB for the higher walkoff. In Fig. 4.14 b), the average BER of 10^{-3} is reached when $X_c = -12.8$ dB, for $d_{mn} = 1$ ps/km, and $X_c = -11.8$ dB for $d_{mn} = 50$ ps/km, which corresponds to an improvement ICXT tolerance of 1 dB for the higher walkoff. The comparison of single and dual polarization shows a 4 dB ICXT tolerance improvement, for $d_{mn} = 1$ ps/km, and a 3 dB tolerance enhancement, for $d_{mn} = 50$ ps/km, which, like in Fig. 4.13, demonstrates the higher system tolerance to ICXT for the dual polarization scenario. The reduction of the impact of the ICXT with the increase of the walkoff between the cores is in qualitative accordance with the results obtained in [62],

where the ICXT impact is evaluated by obtaining the short term average crosstalk power at the MCF output.

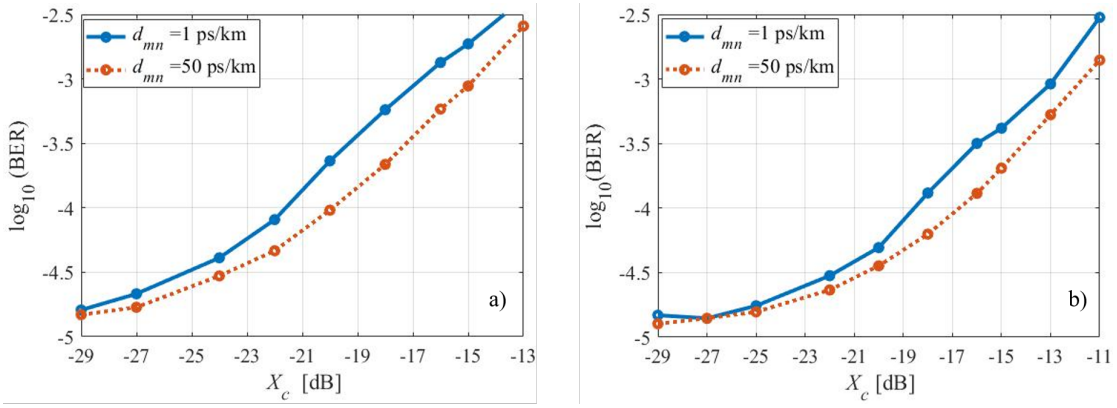

FIGURE 4.14: BER as a function of the crosstalk level, X_c, for $d_{mn} = 1$ ps/km (blue line) and $d_{mn} = 50$ ps/km (red line), for a CPRI signal with bit rate $R_b = 10.1376$ Gbps. a) single polarization DCM and b) dual polarization DCM.

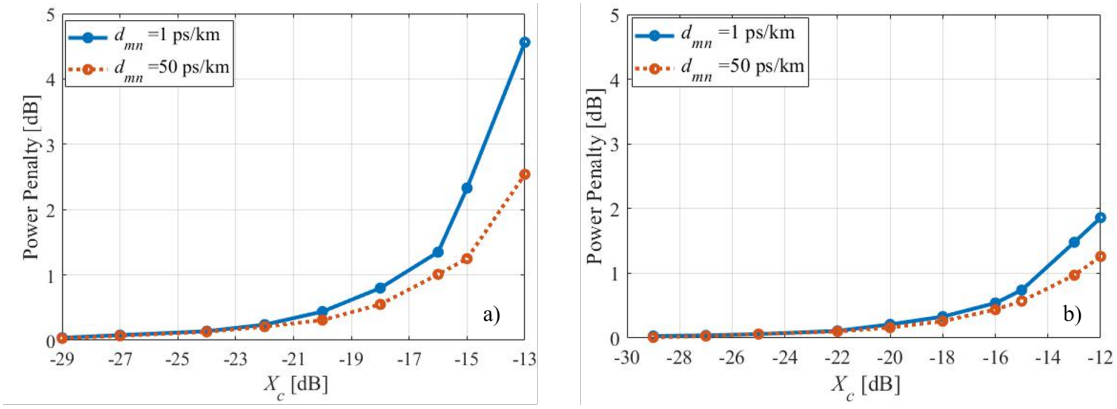

FIGURE 4.15: Power penalty as a function of the crosstalk level, X_c, for the CPRI signal with $R_b = 10.1376$ Gbps, for a target BER of 10^{-3}, $d_{mn} = 1$ ps/km (blue line) and $d_{mn} = 50$ ps/km (red line). a) single polarization DCM and b) dual polarization DCM.

Fig. 4.15 depicts the power penalty caused by the ICXT as a function of the crosstalk level for the CPRI bit rate of $R_b = 10.1376$ Gbps with an average target BER, for all X_c values, of 10^{-3}, for $d_{mn} = 1$ ps/km and $d_{mn} = 50$ ps/km, for both single and dual polarization DCMs. To reach the intended target BER, the receiver sensitivity is -35.86 dBm, in case of ICXT absence. For $d_{mn} = 1$ ps/km, a receiver power penalty of 1 dB is achieved when $X_c = -17.3$ dB, for the single polarization case, and $X_c = -14.3$ dB, for the dual polarization scenario. For a walkoff of $d_{mn} = 50$ ps/km, the 1 dB power penalty occurs for $X_c = -16$ dB, for the single polarization model, and for $X_c = -12.9$ dB, for the dual polarization scheme. Therefore, Fig. 4.15 shows, that the tolerance to the ICXT in CPRI

signal transmission through 5G fronthauls based on single polarization and dual polarization weakly-coupled MCFs with direct-detection can improve by about 1.3 dB, and 1.4 dB, respectively, for cores with higher skew, in relation to the walkoff of $d_{mn} = 1$ ps/km, because of the reduction of the ICXT impact on the system performance. By comparing the power penalties, for the same skew, but with two different polarization models, is possible to see that from single to dual polarization, the ICXT tolerance improves about 3 dB. This 3 dB improvement can be explained by the power of the signal-ICXT beating, which for the single polarization case, is twice above the power of the signal-ICXT beating for the dual polarization. Hence, the expected theoretical difference, 3 dB, is confirmed by the simulated results.

4.4 Outage probability

As concluded in Section 4.2, there are some specific MCF realizations that can degrade severely the BER, leading to system unavailability during the fraction of time in which that specific realization occurs. The time duration of the MCF realization depends on the correlation time of the ICXT, which strongly depends on the weakly-coupled MCF under study. Work [19] has studied a MCF with a measured decorrelation time up to two hours. On the other hand, work [22] reports decorrelation times of a few minutes. By taking as a reference, the MCF studied in [22], for a bit rate of 10 Gbps and, for example, by assuming a MCF realization that leads to system unavailability during 1 s, 10^{10} errored bits will occur in that particular MCF realization, which is unacceptable. Hence, the system unavailability must be studied when dealing with ICXT. A typical metric for measuring the unavailability of a communication system over a certain time interval is the outage probability [24], [62], [63]. The outage probability defines the probability of the system being unavailable for a target BER limit.

The outage probability in the simulation is estimated by counting the number of MCF realization occurrences that lead to a BER above the BER limit and

dividing this number by the total number of MCF realizations. In the simulations performed in this work, to define a reasonable number of occurrences above the defined BER limit, BER=10^{-3}, several outage probabilities have been estimated, with a different number of occurrences above the BER threshold in order to obtain an accurate outage probability. In Fig. 4.16, the outage probability is represented as a function of ICXT level for 50, 100, 150 and 200 error occurrences above the defined BER threshold of 10^{-3}, for the single polarization scenario, with $d_{mn} = 1$ ps/km and $R_b = 10.1376$ Gbps. In Fig. 4.16, it is verified that, with 200 occurrences, it is possible to obtain reasonably accurate estimates of the outage probability with very small fluctuations on the outage probability. Similar conclusions have been obtained, for $d_{mn} = 50$ ps/km with the single polarization DCM, and, for $d_{mn} = 1$ ps/km and $d_{mn} = 50$ ps/km with the dual polarization DCM.

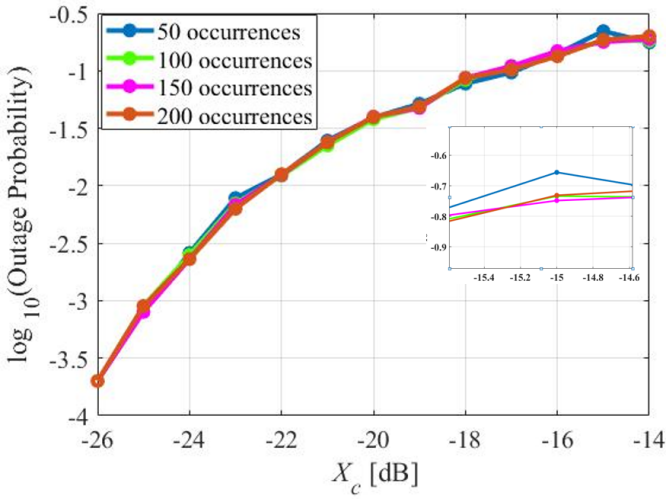

FIGURE 4.16: Outage probability as a function of the crosstalk level, X_c, for a BER in the absence of ICXT of 10^{-5}, $d_{mn} = 1$ ps/km, $R_b = 10.1376$ Gbps and single polarization DCM. Blue symbols: 50 BER occurences above the BER threshold, green symbols: 100 BER occurrences above the BER threshold, pink symbols: 150 occurrences above the BER threshold; and red symbols: 200 occurrences above the BER threshold.

Figure 4.17 depicts the outage probability as a function of the crosstalk level, for $d_{mn} = 1$ ps/km and $d_{mn} = 50$ ps/km. Fig. 4.17 a) and b) refer to results obtained with the single and dual polarization DCMs, respectively. When no ICXT is considered, the signal power at the optical receiver input is set to -34.40 dBm in order to reach a BER of 10^{-5}. The symbols represent the outage probability obtained by simulation. Usually, a typical acceptable outage probability is 10^{-5}

[64], but, with Monte-Carlo simulation, the computational time needed to reach this probability is too high and, consequently, unacceptable.

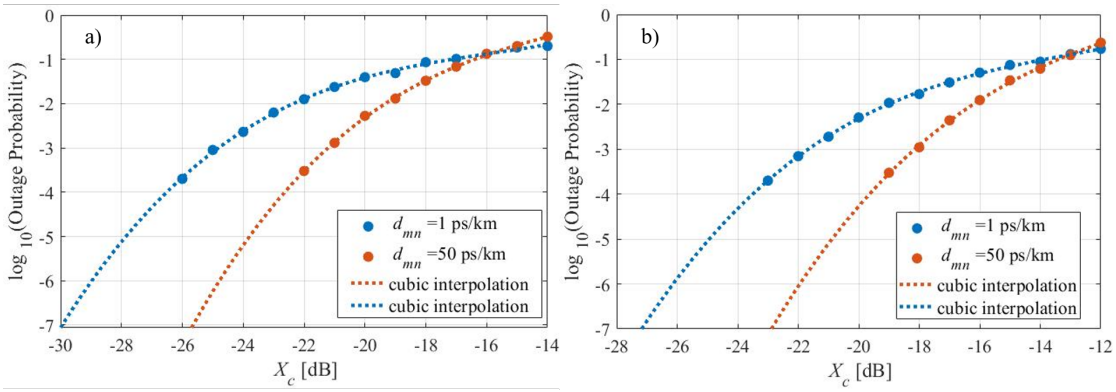

FIGURE 4.17: Outage probability as a function of the crosstak level, X_c, for a BER in the absence of ICXT of 10^{-5}, $d_{mn} = 1$ ps/km (blue symbols) and $d_{mn} = 50$ ps/km (red symbols), for a CPRI signal with $R_b = 10.1376$ Gbps. a) single polarization DCM and b) dual polarization DCM. In a) and b), the dashed lines correspond to cubic interpolations of the outage probability obtained by simulation.

To reach this value of outage probability, a cubic interpolation of the $\log_{10}(\quad)$ of the outage probabilities obtained by simulation has been used, and, an extrapolation has been done to obtain the outages below 10^{-4}. Fig. 4.17 a) shows that, for high crosstalk levels ($X_c \geq -16$ dB), the system is unavailable with a very high probability above 10^{-1}. For lower crosstalk levels, with $d_{mn} = 1$ ps/km, the system exhibits a higher outage probability than for $d_{mn} = 50$ ps/km. As an example, for the same outage probability of 10^{-5}, for $d_{mn} = 1$ ps/km, the maximum acceptable crosstalk level is around -27.8 dB, and for $d_{mn} = 50$ ps/km, around -23.8 dB. Therefore, a difference of 4 dB between the maximum tolerable crosstalk levels obtained for the two skews is observed. Fig. 4.17 b) shows that for high crosstalk levels ($X_c \geq -13$ dB) the system is unavailable with a high probability of 10^{-1}. For lower ICXT values, the system exhibits a higher outage probability, for $d_{mn} = 1$ ps/km, when compared with the results obtained for $d_{mn} = 50$ ps/km. For the outage probability of 10^{-5}, the maximum acceptable ICXT level is around -24.8 dB, for $d_{mn} = 1$ ps/km, and, -20.8 dB for $d_{mn} = 50$ ps/km. By comparing Fig. 4.17 a) and b), it is possible to conclude that for the same crosstalk level and target outage probability, the dual polarization scenario has a 3 dB higher ICXT

tolerance when compared with single polarization DCM, which is in agreement with the power penalty analysis made from Fig. 4.15.

In Table 4.2, a summary of the conclusions obtained from Figs. 4.15 and 4.17, for the single polarization scheme, regarding the maximum tolerable crosstalk level, corresponding to a receiver power penalty of 1 dB or to an outage probability of 10^{-5} is shown.

TABLE 4.2: Maximum tolerable crosstalk level to achieve 1 dB power penalty or an outage probability of 10^{-5} for single polarization DCM.

Performance metric	$d_{mn} = 1$ ps/km	$d_{mn} = 50$ ps/km
Power penalty of 1 dB	-17.3 dB	-16 dB
Outage probability of 10^{-5}	-27.8 dB	-23.8 dB

Table 4.2 shows that, the power penalty for 1 dB in a direct-detection OOK communication system impaired by ICXT is reached when the crosstalk level is around -17.3 dB. However, for this crosstalk level, Fig. 4.17 a), shows a very very high outage probability, above 8×10^{-2}. This means that the unavailability of the optical communication system is unacceptable since, in an one hour period, the system is unavailable during around 5 minutes. To ensure an outage probability of 10^{-5}, the crosstalk level must be below -27.8 dB, for both walkoffs, for one single interfering core, which is a much more restrictive condition than the one obtained considering a power penalty of 1 dB as a limit for the crosstalk level.

TABLE 4.3: Maximum tolerable crosstalk level to achieve 1 dB power penalty or an outage probability of 10^{-5} for dual polarization DCM.

Performance metric	$d_{mn} = 1$ ps/km	$d_{mn} = 50$ ps/km
Power penalty of 1 dB	-14.3 dB	-12.9 dB
Outage probability of 10^{-5}	-24.8 dB	20.8 dB

Table 4.3 shows that the power penalty for 1 dB in a direct-detection OOK communication system impaired by ICXT is reached when the crosstalk level is around -14.3 dB. However, for this crosstalk level, Fig. 4.17 b) shows a very high outage probability, above 8×10^{-2}. To ensure an outage probability of 10^{-5}, the crosstalk level must be below -24.8 dB, for $d_{mn} = 1$ ps/km, for one single

interfering core, which is a much more restrictive condition than the one obtained considering a power penalty of 1 dB as a limit for the crosstalk level. From Tables 4.2 and 4.3, it is possible to conclude that, when comparing the 1 dB power penalty with the outage probability, the best metric to evaluate the system performance, in presence of ICXT, for both single polarization and dual polarization models, is the outage probability. This last conclusion can be generalized to a MCF with N_i interfering cores. By assuming that the interfering signals have the same power and the different interfering cores induce equal crosstalk levels, an approach for the maximum tolerable crosstalk level per each core is obtained by $X_{c,max}$ [dB] $\leq X_{c,max,1} - 10 \cdot \log_{10}(N_i)$ [14], where $X_{c,max,1}$ denotes the maximum tolerable crosstalk level obtained for a single interfering core. For a minimum tolerable crosstalk level of $X_{c,max,1} = -27.8$ dB, for a MCF with 4 interfering cores in one interfered test core, the maximum tolerable crosstalk level per each interfering core is -33.8 dB. Furthermore, the outage probability obtained from simulation with one interfering core, has been confirmed with the theoretical developmetns presented in [65].

4.5 Conclusions

In this chapter, the ICXT impact on 10 Gbps CPRI signal transmission performance in a 5G network with a fronthaul supported by weakly-coupled MCFs, for single and dual polarization signals was studied through numerical simulation. The results obtained for both polarization models have shown that FEC-supported CPRI signals (with bit rate of 10.1376 Gbps) need less MCF realizations for the average BER to converge than CPRI signals without FEC (with bit rate of 9.8304 Gbps) due to the order of magnitude of the target BER. A smaller number of MCF realizations is required for the average BER to stabilize, when the MCF skew increases, as the ICXT impact is smaller. It is also demonstrated that the dual polarization scenario has a higher ICXT tolerance.

The effect of the ICXT on the received eye-pattern after direct-detection has also been studied, once again for single and dual polarization signals. For ideal

extinction ratio and low skew, the ICXT originates well-defined discrete amplitudes at the bit '1'. For high skew, the ICXT affects the amplitudes of bit '1' with a "white noise"-like behavior. These results are in qualitative agreement with the results presented in [43]. It was also seen that, when the crosstalk level is high, the degradation due to ICXT is mainly due to a severe eye-closure. These results were observed for both single and dual polarization models. Hence, although the results showed a similar behavior, for $R_b = 9.8304$ Gbps and $R_b = 10.1376$ Gbps, in both polarizations schemes, the eye-openings obtained with dual polarization system had a less severe eye-closure, when compared with the single polarization scenario, due to the higher ICXT tolerance.

The power penalty due to ICXT has also been studied for FEC-supported CPRI signals. By defining the power penalty of 1 dB as the maximum for performance degradation, we have shown that, for single polarization, for $d_{mn} = 1$ ps/km, the power penalty limit is reached for an ICXT level of -17.3 dB. For $d_{mn} = 50$ ps/km, the power penalty limit is reached for a -16 dB ICXT level. For the dual polarization model, the power penalty limit occurs for a crosstalk level of -14.3 dB with $d_{mn} = 1$ ps/km, and for -12.9 dB with $d_{mn} = 50$ ps/km. Making the comparison between single polarization and dual polarization, it is possible to see that for the dual polarization model, the system has a 3 dB higher ICXT tolerance for the power penalty of 1 dB.

Most importantly, this work has shown that is essential to study the outage probability for direct-detection optical communication systems impaired by ICXT. There are specific MCF realizations that can lead to system unavailability for long time periods, even if the average BER is set to be within prescribed limits. It has been shown that, for FEC-supported CPRI signals and crosstalk levels that lead to a power penalty above 1 dB, $X_c \geq -17.5$ dB, for the single polarization case, the system is unavailable with a very high probability (above 8×10^{-2}). To reach an acceptable outage probability, much lower crosstalk levels are required, $X_c < -27.8$ dB. As in single polarization, for the dual polarization scheme, the ICXT level that leads to a 1 dB power penalty, $X_c \geq -14.5$ dB, corresponds to a very high probability (above 8×10^{-2}) of the system being unavailable. To get an

acceptable outage probability, the ICXT level has to be at least $X_c < -24.8$ dB. When comparing both polarizations, once again, is possible to verify that using the same system parameters, the dual polarization system model has a 3 dB higher ICXT tolerance than the single polarization scheme, for an outage probability of 10^{-5}.

Chapter 5

Conclusions and future work

In this chapter, the dissertation final conclusions and some suggestions for future work are presented.

5.1 Final conclusions

The impact of ICXT of weakly-coupled MCFs on the transmission performance of CPRI signals in 5G network fronthauls with direct detection has been assessed by numerical simulation. In Chapter 2, a review of the fundamental concepts of the 5G fronthauls supported by MCFs has been presented: the 5G wireless networks evolution that led to the C-RAN implementation; the main characteristics of the optical fibers (with a particular focus on MCFs and ICXT); the proposal of C-RAN fronthauls supported by MCFs and the characteristics of the CPRI signals to be transmitted in such fronthauls. These concepts allow a better understanding of the theoretical framework used as the basis for this dissertation.

In Chapter 3, the system model used in this work for the 5G fronthaul supported by MCFs and impaired by ICXT is presented: optical transmitter, MCF (single and dual polarization models), and optical receiver composed by the photodetector and the electrical filter. Then, the BER assessment in presence of electrical noise without ICXT is performed, considering fiber dispersion and attenuation on the signal transmission in a single core fiber, for the purpose of

simulation and numerical results validation. This validation is performed in order to guarantee some reliability in the results obtained.

In Chapter 4, by using the 5G fronthaul models presented in Chapter 3, the impact of the ICXT on the performance of CPRI signals transmitted in 5G fronthauls supported by weakly-coupled homogeneous MCFs is assessed and discussed. The results, obtained for both DCM models, have shown that FEC-supported CPRI signals need less MCF realizations for the average BER to converge than CPRI signals without FEC due to the order of magnitude of the target BER. A smaller number of MCF realizations is required for the average BER to stabilize, when the MCF skew increases, as the ICXT impact is smaller, in this case. It is also demonstrated and explained the reason for the dual polarization scenario having a higher ICXT tolerance. The effect of the ICXT on the received eye-pattern after direct-detection is also analyzed. For ideal extinction ratio and low skew, the ICXT originates well-defined discrete amplitudes at the bit '1'. For high skew, the ICXT affects the amplitudes of bit '1' with a "white noise"-like behavior.

The power penalty due to ICXT has also been studied for FEC-supported CPRI signals. By defining the power penalty of 1 dB as the maximum for performance degradation, it was shown that, for single polarization, for $d_{mn} = 1$ ps/km, the power penalty limit is reached for an ICXT level of -17.3 dB. For $d_{mn} = 50$ ps/km, the power penalty limit is reached for a -16 dB ICXT level. For the dual polarization scenario, the power penalty limit occurs for a crosstalk level of -14.3 dB, for $d_{mn} = 1$ ps/km, and -12.9 dB for $d_{mn} = 50$ ps/km. Hence, by comparing the single and dual polarization models, it is possible to conclude that the dual polarization model has a 3 dB higher ICXT tolerance than the single polarization case, when considering the power penalty of 1 dB as a metric.

Most importantly, this work has shown that is essential to study the outage probability for direct-detection optical communication systems impaired by ICXT arising from weakly-coupled homogeneous MCFs. There are specific MCF realizations that can lead to system unavailability for long time periods, even if the average BER is set to be within prescribed limits. It has been shown that, for FEC-supported CPRI signals and crosstalk levels that lead to a power penalty

above 1 dB, above -17.5 dB, for the single polarization case, the system is unavailable with a very high probability. To reach an acceptable outage probability, much lower crosstalk levels are required, below -27.8 dB. For the dual polarization scheme, the ICXT level that leads to a 1 dB power penalty, -14.5 dB, corresponds to a very high probability of the system being unavailable. To get an outage probability of 10^{-5}, the ICXT level must be below -24.8 dB. When comparing both polarizations DCMs, it is possible to verify that, for the same outage probability, the dual polarization scenario has a 3 dB higher ICXT tolerance than the single polarization scheme.

5.2 Future work

Some topics for future investigation that were not addressed in this work are now proposed:

- Inclusion of the PMD effect on the DCM and study of its impact on the transmission;
- Insertion of an optical pre-amplifier at the receiver to reach longer distances in the fronthaul, which leads to amplified spontaneous emission noise dominance on the system performance instead of the electrical noise, and assess the ICXT impact in its presence [66];
- Generalize the study of the ICXT to multiple interfering cores;
- Adapt the system model to PAM-4 transmission, typical of intra and inter-datacenter connections [67] and analyze the ICXT impact on the performance of such systems;
- Introduction of laser phase noise on the simulation model and analysis of its impact on the system performance degradation in conjunction with ICXT [20].

Appendices

Appendix A

Publications

The publications originated from the work performed in this dissertation are presented in this appendix.

Transmission of CPRI signals along weakly-coupled multicore fibers for support of 5G networks

André S. Marques[2], João L. Rebola[1,2], Adolfo V. T. Cartaxo[1,2]
[1]*Optical Communications and Photonics Group, Instituto de Telecomunicações, Lisboa, Portugal*
[2]*Instituto Universitário de Lisboa (ISCTE-IUL), Lisboa, Portugal*
e-mail: afssm@iscte-iul.pt, joao.rebola@iscte-iul.pt, adolfo.cartaxo@iscte-iul.pt

ABSTRACT
The impact of intercore crosstalk (ICXT) of weakly-coupled multicore fibers on the transmission performance of a Common Public Radio Interface (CPRI) signal in 5G networks is studied by numerical simulation. The results show that forward error correction-supported CPRI signals (accepting higher bit error rates) have more tolerance to ICXT, which increases with the skew between cores. Improvement of the tolerance of CPRI signals to the ICXT, due to the increase of the skew, by 1.7 dB is shown.
Keywords: bit-error rate, intercore crosstalk, multicore fiber, 5G, CPRI

1. INTRODUCTION

The emergence of 5G and the steady growth of traffic in communication networks [1] led to new proposals on the radio access networks architecture in order to make data transmission more efficient and increase capacity. One of these proposals is the Cloud Radio Access Network [2]-[3] which proposes a physical separation between the base stations units (BBUs) and the transmitter/receiver remote radio-head (RRH) antennas [2]-[3], as shown in Fig. 1. With this new architecture, a new network segment known as fronthaul, which makes the connection between BBU and RRH, is deployed. One way to implement this link is through optical fiber using Radio over Fiber or Digital Radio over Fiber transmission using one of the protocols defined at the Common Public Radio Interface (CPRI) [4] with a bit rate around 10 Gbps [5]. Weakly-coupled multicore fibers (MCFs) are a good solution to support the fronthaul because they can accomplish the bit rate requirements, the fiber availability, the dynamic capacity allocation and the compatibility with the existing and future versions of passive optical networks [4]. However, the transmission in weakly-coupled MCFs, in which cores can be used as independent channels, is affected by intercore crosstalk (ICXT) [6].

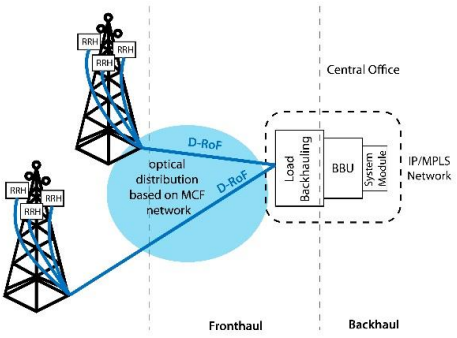

Figure 1. C-RAN architecture with MCFs.

In this work, we investigate, through numerical simulation, the transmission of CPRI signals along weakly-coupled MCFs and how the ICXT affects the transmitted signal performance. The paper is organized as follows. Section 2 presents the simulation model, the estimation of bit error rate (BER) and the type of CPRI signals investigated. Section 3 presents and discusses the numerical results. Section 4 provides the conclusions.

2. SIMULATION MODEL, BER CALCULATION AND CPRI BIT RATES

As a first assessment of the impact of ICXT on the CPRI signal transmission performance, we consider only a single interfering CPRI signal transmitted in core *m* that may degrade the performance of other similar CPRI signal transmitted in core *n*. Therefore, as illustrated in Fig. 2, two optical transmitters, each one generating an on-off keying (OOK) signal with the same CPRI bit rate and ideal extinction ratio, are considered.

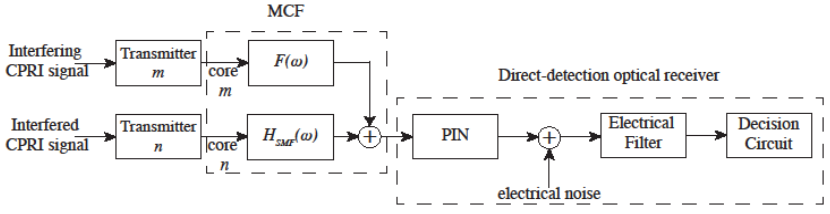

Figure 2. Equivalent system model used to study the impact of ICXT on a 5G fronthaul with direct detection.

Linear single-mode propagation is assumed in each core. The transmission in core *n* is modelled by the optical fiber transfer function $H_{SMF}(\omega)$ given by $H_{SMF}(\omega)= e^{-j\beta_n(\omega)L}$ where L is the fiber length, ω is the low-pass equivalent

angular frequency and $\beta_n(\omega)$ is the intrinsic propagation of core *n*. A Taylor series expansion up to the second order in ω is considered for $\beta_n(\omega)$, i.e. propagation delay and fiber dispersion effects are considered. The same fiber attenuation is assumed in the two cores. Hence, the fiber attenuation level is not relevant as our analysis considers the receiver sensitivity. The interfering signal in core *n* resulting from ICXT caused by the signal in core *m* is obtained using the transfer function [6]:

$$F(\omega)=-jK_{nm}e^{-j\beta_n(\omega)L}\sum_{k=1}^{N_p}e^{-j\Delta\beta_{mn}(\omega)z_k}e^{-j\phi_k} \quad (1)$$

where K_{nm} is the discrete coupling coefficient between cores *m* and *n*, $\Delta\beta_{mn}(\omega)$ is the difference of the intrinsic propagation constants of cores *m* and *n*, z_k is given by $z_k=(k-1)\,L/N_p+\xi$, with N_p the number of phase-matching points and ξ a random variable uniformly distributed between 0 and L/N_p. ϕ_k is a random variable uniformly distributed between $[0,2\pi]$ that models random fluctuations in bending radius, twist rate or other conditions of the MCF [6]. The ratio between the crosstalk power at the interfered core (*n*) output and the power of the signal at the interfering core (*m*), X_c, is related to the parameters of Eq. 1 by $X_c=N_p|K_{nm}|^2$. The skew between cores *m* and *n* is given by $S_{mn}=d_{mn}L$ where d_{mn}, is the walkoff between the cores *m* and *n* and is related to Eq. 1 by $\Delta\beta_{mn}(\omega)=\Delta\beta_{0,mn}+d_{mn}\omega-\frac{1}{2}\frac{\Delta D_{mn}\lambda^2}{2\pi c}\omega^2$ [6], where $\Delta\beta_{0,mn}$ is the difference of propagation constants of cores *m* and *n* at zero frequency, ΔD_{mn} is the difference of dispersion parameters of cores *m* and *n*, λ is the wavelength and *c* is the speed of light in vacuum. One fiber realization is calculated in each simulation iteration, where the bits of the CPRI signal to be transmitted in core *m* are randomly generated.

At the optical receiver, the signal at the MCF output is photodetected by a PIN with responsivity of 1 A/W. Then, it is filtered by an electrical filter modelled by a 2nd order Butterworth filter with a cut-off frequency of $0.65\times R_b$, being R_b the bit rate. The electrical noise, referred to the electrical filter input, is characterized by a noise equivalent power of 1×10^{-12} W/$\sqrt{\text{Hz}}$ [7]. After electrical filtering, the decision circuit samples the signal at the time instants $t_k=t_{opt}+kT_b$, where t_{opt} is the optimum sampling time, T_b is the bit period and k = 1, 2, …, N_b, with N_b being the number of bits generated in transmitter *n* in each simulation iteration, and decides on the transmitted bit.

We use semi-analytical simulation to evaluate the BER [8]. The impact of electrical noise on the performance is taken into account analytically, and the effects of fiber chromatic dispersion and intercore crosstalk on the BER are evaluated using waveform simulation of each simulation iteration. Hence, the BER is given by [8]:

$$\text{BER}=\frac{1}{N_b}\left\{\sum_{\substack{k=1\\ j=0}}^{N_b}Q\left(\frac{F-i_{0,k}}{\sigma_{0,k}}\right)+\sum_{\substack{k=1\\ j=1}}^{N_b}Q\left(\frac{i_{1,k}-F}{\sigma_{1,k}}\right)\right\} \quad (2)$$

where $Q(x)=\frac{1}{\sqrt{2\pi}}\int_x^{+\infty}e^{-\lambda^2/2}\,d\lambda$ [8] and $i_{j,k}$ and $\sigma_{j,k}$ are the mean and standard deviation of the current at the decision circuit input at time instants t_k, conditioned on the transmitted bit *j* (0 or 1). The decision threshold *F* is optimized using the bisection method to minimize the BER. Here, $\sigma_{0,k}=\sigma_{1,k}$ as we consider electrical noise only.

In this work, two CPRI bit rates are studied: (i) option 7, with R_b = 9.8304 Gbps, 8B/10B line coding and without Forward-Error Correction (FEC), and (ii) option 8, with R_b = 10.1376 Gbps, 64B/66B line coding and with FEC [4]. For systems without FEC, the target BER is 10^{-12} [4]. For systems with FEC, the target BER depends on the FEC implementation [9]. We assume the FEC implementation with the target BER set to 10^{-3} [9].

3. NUMERICAL RESULTS AND DISCUSSION

In this section, the impact of ICXT on the transmission performance of the CPRI signals is studied by simulation. The simulation parameters that are kept constant throughout this work are the nominal wavelength λ_0=1550 nm, the dispersion parameter D_λ=17 ps/(nm·km) (the same for both cores), the number of simulated OOK bits per fiber realization $N_b=2^9$, the N_p=1000, the fiber length L=20 km and $\Delta\beta_{0,mn}$=0.

First, we start by studying the number of fiber realizations that are necessary to achieve a stabilized value of the average BER. To provide a certain margin for BER degradation due to ICXT, we set the BER in the absence of ICXT to two orders of magnitude lower than the target BER. Hence, our studies for line option 8 consider the BER of 10^{-5} in the absence of ICXT. Following the same reasoning for systems without FEC, the BER in absence of ICXT is 10^{-14}. Fig. 3 a) and b) depict the BER for each MCF realization and the average BER as a function of the number of fiber realizations for d_{mn} = 1 ps/km. Fig. 3 a) refers to the CPRI signal with the bit rate of 9.8304 Gbps (which does not consider FEC and the BER without ICXT is 10^{-14}). The crosstalk level is X_c = –30 dB. Figure 3 b) refers to the CPRI signal with R_b = 10.1376 Gbps (which considers FEC and the BER without ICXT is 10^{-5}) and X_c = –15 dB. These crosstalk values are chosen to lead to an average BER degradation relative to the one in absence of ICXT by about two orders of magnitude. Fig. 3 a) shows that the average BER can be considered stabilized after about 4000 MCF realizations. In the subsequent studies for the CPRI signal with 9.8304 Gbps, we have set the number of fiber realizations to 10^4 as a conservative choice. Fig. 3 b) shows that the average BER is nearly stable after 400 MCF realizations. For the subsequent studies, we have set the number of MCF realizations to 10^3 as a conservative choice for the CPRI signal with 10.1376 Gbps. We have verified that the mentioned numbers of fiber realizations are more than sufficient to lead to a stabilized average BERs for different crosstalk levels, different fiber lengths (other than 20 km), different walk-offs between the fiber cores and CPRI signals

with different bit rates. The difference between the number of fiber realizations leading to a stabilized average BER is attributed to the order of magnitude of the average BERs considered in Fig. 3 a) and b).

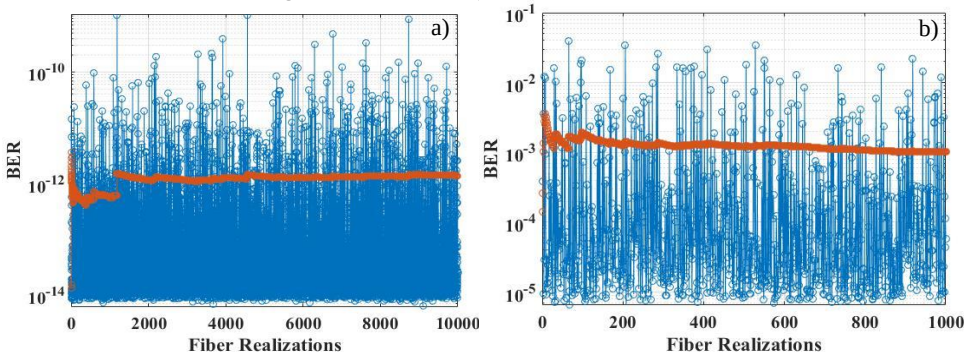

Figure 3. BER for each MCF realization (blue symbols) and average BER (red symbols) as a function of fiber realizations. In a), R_b=9.8304 Gbps, X_c= −30 dB and BER in the absence of ICXT is 10^{-14}. In b), R_b=10.1376 Gbps, X_c= −15 dB and BER in the absence of ICXT is 10^{-5}.

Fig. 3 a) and b) show that the randomness of the ICXT mechanism leads to a strong variation of the BER per fiber realization. The BER can be degraded severely or even improved. In Fig. 3 a), the best BER obtained per fiber realization is 6.3×10^{-15} and the worst BER is 1.1×10^{-9}. Fig. 3 b) exhibits a best BER of 6.3×10^{-6} and a worst BER of 3.9×10^{-2}. The eye-patterns corresponding to these BERs per fiber realization are presented in Fig. 4 where the ICXT impact on the eye-patterns can be seen. These eye-patterns do not show the effect of the electrical noise to make clear the ICXT effect. Fig. 4 a) and d) correspond to the cases where no ICXT is present. As the bit rates are similar in these plots, no significant difference is observed between the two eye-patterns. Fig. 4 b) and e) show the eye-patterns corresponding to the improvement of BER due to ICXT relative to the case of absence of ICXT. Fig. 4 c) and f) correspond to the MCF realizations in which the worst BER occurs. Fig. 4 c) shows that the eye-closure for the worst BER realization is not as severe as the one obtained in Fig. 4 f). This justifies the higher number of MCF realizations needed to get a stabilized average BER for lower BERs (see Fig. 3 a)), since any slight signal distortion caused by ICXT can degrade the average BER a few orders of magnitude. For higher BERs (see Fig. 3 b)), a higher crosstalk level is necessary to close the eye-pattern significantly in order to get BERs per fiber realization with a few orders of magnitude above the reference BER of 10^{-5}. Analysis of Fig. 4 a), b) and c) [and extending the same analysis to Fig. 4 d), e) and f)] reveals that the impact of the ICXT on the eye-pattern is felt only at the amplitudes of bit '1' while, at bit '0', the amplitude values remain essentially the same.

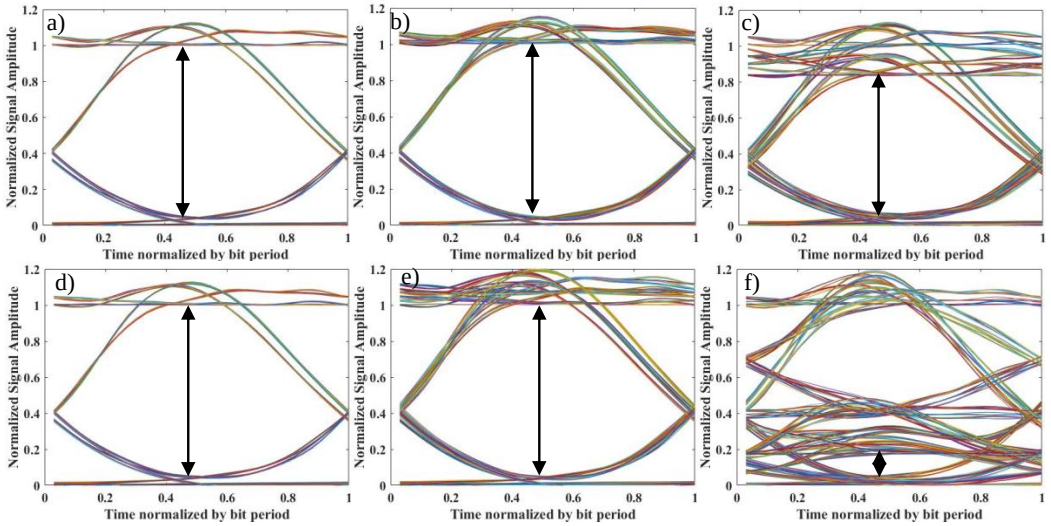

Figure 4. Eye-patterns at the receiver input corresponding to the BER without ICXT and the worst and best BER obtained in Fig. 3 a) and b). In a) and d) there is no ICXT. In b) and e): best BER cases for Fig 3 a) and b), respectively. In c) and f): worst BER cases for Fig. 3a) and b), respectively. The eye opening is indicated in each eye-pattern.

After having established the number of MCF realizations required to reach a stabilized value of the average BER, the performance degradation imposed by the increase of the crosstalk level is investigated. Figure 5 depicts the average BER as a function of the crosstalk level, for d_{mn} = 1 ps/km and d_{mn} = 50 ps/km. These values of walkoff correspond to two distinct levels of skew: one (d_{mn} = 50 ps/km), much higher than the bit period and other (1 ps/km) much lower than the bit period. Fig. 5 a) corresponds to the CPRI signal with 9.8304 Gbps and Fig. 5 b) relates to the CPRI signal with 10.1376 Gbps. As expected, the BER becomes higher with the increase of the crosstalk level. In Fig. 5 a), as the BER without ICXT is very low (10^{-14}), lower values of X_c lead to a significant BER degradation. An average BER of 10^{-12} is reached for X_c = –30 dB and X_c = –28.3 dB, for d_{mn} = 1 ps/km and for d_{mn} = 50 ps/km, respectively. In Fig. 5 b), as the BER without ICXT is higher (10^{-5}), higher ICXT levels are required to degrade the average BER. An average BER of 10^{-3} is reached for X_c = –15 dB and X_c = –13.7 dB, for d_{mn} = 1 ps/km and d_{mn} = 50 ps/km, respectively. The reduction of the impact of ICXT with the increase of the skew between the cores d_{mn} is in qualitative accordance with the results presented in [10].

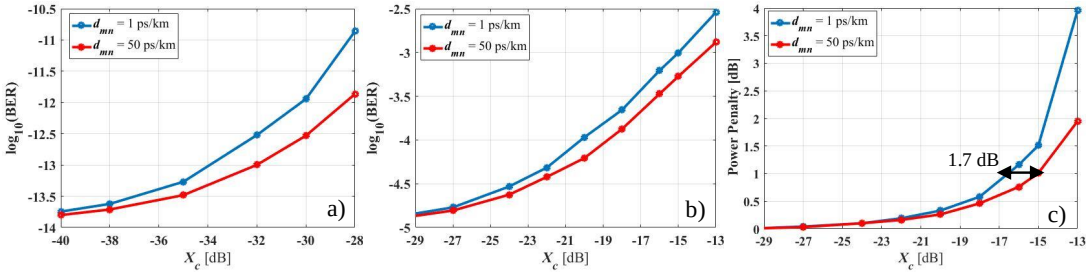

Figure 5. In a) and b), BER as a function of crosstalk level, X_c in dB, for d_{mn} = 1 ps/km (blue line) and *d_{mn} = 50 ps/km (red line). In a), CPRI signal with R_b=9.8304 Gbps; in b), CPRI signal with R_b=10.1376 Gbps. In c), power penalty as a function of crosstalk level X_c for a BER of 10^{-3} and R_b=10.1376 Gbps for d_{mn} = 1 ps/km (blue line)* and *d_{mn} = 50 ps/km (red line).*

We estimate also the system power penalty due to ICXT for the 10.1376 Gbps CPRI signal with BER=10^{-3} and the two levels of skew. Fig. 5 c) show the results obtained. For d_{mn} = 1 ps/km, a power penalty of 1 dB occurs for a ICXT level of −16.7 dB and, for d_{mn}= 50 ps/km, a power penalty of 1 dB occurs for a ICXT level of −15 dB. Therefore, we conclude that the skew effect can improve the tolerance of CPRI signals to the ICXT by 1.7 dB.

4. CONCLUSIONS

We have investigated the weakly-coupled MCF ICXT impact on the CPRI signal transmission performance in a 5G network. The results have shown that FEC-supported CPRI signals (accepting higher BER) have more tolerance to ICXT, which increases with the skew enhancement between cores. Improvement of the tolerance of CPRI signals to the ICXT, due to the increase of the skew, by 1.7 dB has been shown.

ACKNOWLEDGEMENTS

This work was supported in part by Fundação para a Ciência e a Tecnologia (FCT) from Portugal under the project of Instituto de Telecomunicações AMEN-UID/EEA/50008/2013.

REFERENCES

[1] C. Mobile, “C-RAN: the road towards green RAN,” White Paper, version 2.5, pp. 15–16, 2011.
[2] P. Chanclou *et al.*, “Optical fiber solution for mobile fronthaul to achieve cloud radio access network,” 2013 Future Network and Mobile Summit, pp. 1–11, 2013.
[3] J. M. Galve, I. Gasulla, S. Sales, and J. Capmany, “Reconfigurable radio access networks using multicore fibers,” IEEE J. of Quantum Elect., vol. 52, no. 1, pp. 1–7, January 2016.
[4] Common Public Radio Interface, “CPRI Specification V7.0,” Standard Document Specification, vol. 1, 2015.
[5] P. Parolari et al., “Operation of RSOA WDM PON self seeded transmitter over more 50 km of SSMF up to 10 Gb/s,” in Proc. Opt. Fiber Commun. Conf. Exhib., 2014, pp. 1–3.
[6] A. V. T. Cartaxo *et al.*, “Dispersion impact on the crosstalk amplitude response of homogeneous multi-core fibers,” IEEE Photon. Technol. Lett., vol. 28, no. 17, pp. 1858–1861, September 2016.
[7] G. P. Agrawal, Fiber-Optic Communication Systems, Third Edition, 2002.
[8] J. Rebola and A. Cartaxo, “Gaussian approximation for performance assessment of optically preamplified receivers with arbitrary optical and electrical filters,” IET Optoelectronics, vol. 148, no. 3, pp. 135–142, 2001.
[9] B. J. Puttnam *et al.*, “Impact of inter-core crosstalk on the transmission distance of QAM formats in multi-core fibers,” IEEE Photon. J., vol. 8, no. 5, April 2016, Art. ID. 0601109.
[10] G. Rademacher, R. S. Luis, B. J. Puttnam, Y. Awaji, and N. Wada, “Crosstalk dynamics in multi-core fibers,” Opt. Express, vol. 25, no. 10, pp. 12020–12028, May 2017.

10 Gbps CPRI signals transmission impaired by intercore crosstalk in 5G network fronthauls with multicore fibers

João L. Rebola[1,2] · Adolfo V. T. Cartaxo[1,2] · André S. Marques[2]

Received: / Accepted: / Published online: 2018

Abstract

The impact of intercore crosstalk (ICXT) of weakly-coupled multicore fibers (MCFs) on the transmission performance of a Common Public Radio Interface (CPRI) signal in 5G networks fronthaul is studied by numerical simulation. The results show that forward error correction-supported CPRI signals have more tolerance to ICXT due to the higher targeted bit error rate (of 10^{-3}). For a receiver power penalty of 1 dB, an improvement of the tolerance of CPRI signals to ICXT, due to the increase of the MCF skew by about 1 dB, is observed. However, for the crosstalk levels that lead to 1 dB power penalty, we have shown that, the system is unavailable with a high probability. The crosstalk level required for an acceptable outage probability is about 10 dB lower than the crosstalk level leading to 1 dB power penalty.

Keywords 5G wireless networks, Bit error rate, Common public radio interface, Intercore crosstalk, Multicore fiber, Outage probability.

1 Introduction

The emergence of 5G wireless networks and the continuous growth of traffic in communication networks [1]-[3] led to new proposals on the radio access networks architecture in order to increase data transmission efficiency and capacity. Cloud Radio Access Network (C-RAN) is expected to provide the 5G networks requirements in terms of network capacity, quality of service, latency and resources availability [4]-[7]. C-RAN proposes a physical separation between the base stations units (BBUs) and the transmitter/receiver remote radio-head (RRH) antennas [4], [5], as illustrated in Fig. 1. With this new architecture, a new network segment known as fronthaul, which includes the connection between BBUs (which are hosted at the same location in the central office and with centralized functionalities) and RRHs, is deployed. One way to cope with the high data transmission efficiency and capacity of the fronthaul is to consider optical fiber-based solutions such as radio over fiber or digital radio over fiber (D-RoF) transmission using, for example, the protocol defined at the Common Public Radio Interface (CPRI) [8]. In this work, we adopt the CPRI protocol because, it is currently by far the most common standard for connecting the BBUs to RRHs [2], [6], and allows to make RRHs very small and cheap, since no digital processing functions are required at the RRHs [6]. The CPRI is a serial data rate protocol that defines the transmission of digitized samples of the radio signals using digital binary baseband signals, whose payload is known as I/Q data [8]. The CPRI signals transmission involves the use of on-off keying (OOK) modulation in optical fibers with direct-detection at the receiver, which is attractive for its simpler and cheaper implementation. The 5G network fronthaul with CPRI protocol can demand very high capacities, depending on the radio-channel bandwidth, the number of sectors and number of antennas per sector [6], [9]. For a radio-channel bandwidth of 1 GHz and with 256 antenna ports, the 5G fronthaul capacity must reach an aggregate capacity of 12.8 Tbit/s using the CPRI protocol [3], [10]. This very high capacity is nowadays too hard to reach even considering the maximum CPRI signal bit rate of 24 Gbit/s per link defined in the specification

[8] and transmission in single core fiber with wavelength-division multiplexing (WDM) technology, since the number of WDM channels required is above 500. Hence, several works have proposed the use of multicore fibers (MCFs) in the fronthaul network segment to accomplish such high capacity [5], [11], [12].

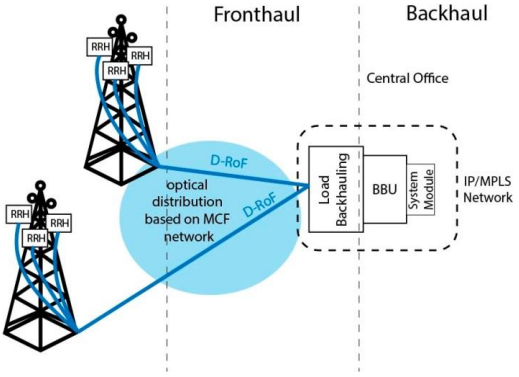

Fig. 1 C-RAN architecture with fronthaul supported by MCFs (based on [4]).

Homogeneous weakly-coupled MCFs have been reported as a promising technology to expand transmission capacity [12], [13]. The cores of homogeneous MCFs have similar physical properties, which lead to similar propagation times for signals transmitted in different cores. In 5G fronthauls, this similarity can be explored to use specialized transmission techniques and share receiver resources, as proposed for high capacity long distance transmission [14], [15]. In weakly-coupled MCFs, each single mode core guides one spatial mode, and the cores are sufficiently apart in the cladding, so that the power coupled from each core to other cores may be quite low [16]-[18]. Hence, the different cores can be used as independent channels. The intercore crosstalk (ICXT), i. e., power coupling between cores, is much stronger between adjacent cores than between non-adjacent cores, and its generation is distributed along the MCF [17], [19]. Furthermore, the ICXT has a random time varying frequency dependence, which may cause the random appearance of high levels of ICXT in short periods of time [20]-[23]. Hence, the ICXT may affect severely the signal quality, particularly for MCFs with a large number of adjacent cores and long path lengths.

With the aim of understanding and mitigating the impact of ICXT on MCF system performance, the characterization and suppression of ICXT in weakly-coupled MCFs has been investigated over the last years. The dependence of the mean ICXT power on MCF parameters (such as core refractive index and radius, bend and twisting, core pitch), dual polarization and wavelength have been reported [16], [17], [24]-[27]. The evolution of the random fluctuation of ICXT along the time has been investigated, and a model that provides the stochastic description of that evolution has been proposed and validated [22], [23]. ICXT decorrelation times of the order of a few minutes up to two hours have been measured [20], [23]. In order to achieve high capacity and long distance transmission, ICXT suppression has become one of the focus in weakly-coupled MCF research [17], [18], [28], [29]. In this direction, new structures of MCF [18], [30], and techniques for reduction of ICXT impact, for example, using signals transmitted in opposite directions on adjacent cores of the MCF [28], have been proposed.

As a consequence of the random evolution of ICXT along the time, two ICXT effects, that should be considered when evaluating the MCF transmission system performance, can be seen [31]. On one hand, for an analysis over short periods of time, the Q-factor varies randomly [32]; this effect is quantified by the degradation of the optical signal to noise ratio required for the same bit error rate (BER) in line-amplified transmission systems [31] or by the degradation of the receiver sensitivity in amplifier-less transmission systems. On the other hand, for an analysis over long periods of time, high levels of ICXT

occurring in short time intervals appear and cause outage periods of system operation [21], [31].

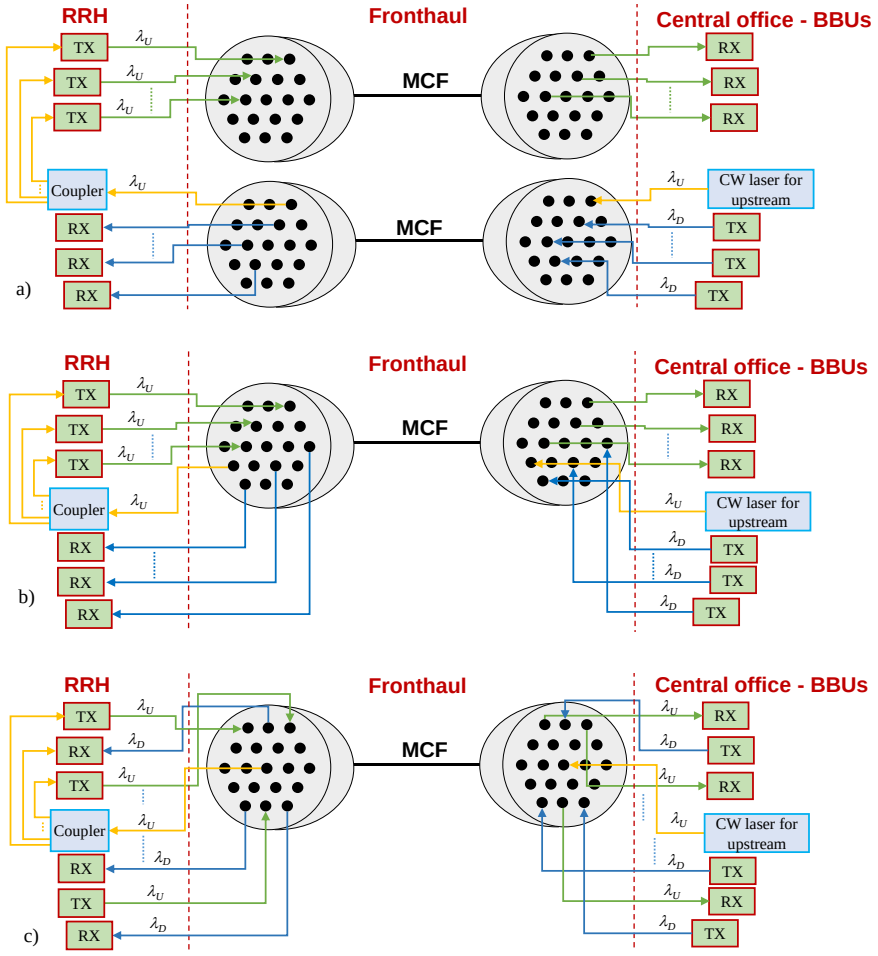

Fig. 2 Different configurations for the 5G fronthaul with MCFs. a) Two MCFs are used in the fronthaul for duplex transmission: one for upstream and other for downstream. b) One MCF is used in the fronthaul for duplex-transmission: the upper half cores are used for upstream and the lower half cores for the downstream. This is the solution proposed in [5], [12]. c) One MCF is used in the fronthaul for duplex-transmission: transmission directions are set in order that adjacent cores transmit in opposite directions in order to minimize ICXT [28]. In all three configurations, a single core is used to transmit a CW laser from the central office to the RRHs in order to provide the wavelength for the upstream direction. λ_U: upstream wavelength; λ_D: downstream wavelength; RX: receiver; TX: Transmitter.

Fig. 2 illustrates three possible configurations for the 5G fronthaul with MCFs. In all three configurations, it is assumed that a single channel (wavelength) is transmitted in a single core. WDM solutions can be also envisioned, however, with higher cost. The wavelengths used for the downstream transmission, λ_D, are the same, which means that the transmitters for the downstream direction are equal. The same idea is considered for the upstream transmission in the upstream wavelength λ_U. This wavelength is provided by the central office from a continuous-wave (CW) laser through transmission in a single dedicated MCF core and is distributed to the upstream transmitters. For connecting the MCFs to external equipment, MCF

connectors are assumed (which are not depicted in Fig. 2). These assumptions simplify the 5G network implementation and reduce its cost. Fig. 2 a) shows the configuration where, to guarantee duplex-transmission, one MCF is used for each transmission direction. Fig. 2 b) depicts the 5G fronthaul configuration that utilizes only one MCF to ensure duplex transmission: the upper cores are used for upstream transmission and the lower cores are used for downstream transmission. This configuration is the one proposed in [5], [12]. Fig. 2 c) illustrates a 5G fronthaul ICXT-"aware" configuration using one MCF, as it explores the fact that transmitting signals in opposite directions in adjacent cores reduces the ICXT effect [28]. Hence, in this configuration, the transmission directions in adjacent cores are set interchangeably in opposite directions. Even though, with this configuration, when many cores are used for transmission, the same transmission direction is employed in some adjacent cores.

In this work, we investigate numerically the transmission of 10 Gbps CPRI signals along 5G fronthauls supported by weakly-coupled MCFs systems with direct-detection and how the ICXT affects the transmitted signal performance. Numerical results are obtained through the combination of Monte Carlo (MC) simulation to assess the ICXT impact on the performance, with a semi-analytical method for noise evaluation. The performance metrics used for this assessment are the analysis of the eye-pattern, BER, power penalty and outage probability.

The paper is organized as follows. Section 2 presents the fronthaul equivalent simulation model, how the BER is estimated and the type of CPRI signals chosen. Section 3 presents and discusses the numerical results. Section 4 provides the conclusions.

2 System model, BER calculation and CPRI bit rates

In this section, the system model developed to assess, through numerical simulation, the impact of ICXT on the performance of a 5G fronthaul with weakly-coupled MCF and direct-detection is described. The BER estimation using MC simulation of the transmitted signal and ICXT combined with a semi-analytical method to account for the noise influence is also explained. A discussion about the CPRI signals bit rates used in this work is presented as well.

2.1 System model

As a first assessment of the impact of ICXT on the CPRI signal transmission performance, we consider only a single interfering CPRI signal transmitted in core *m* that may degrade the performance of other similar CPRI signal transmitted in core *n*. An extension of the main achievements to multiple interfering cores is presented in subsection 3.3.

Fig. 3 depicts the equivalent system model used to study the impact of ICXT on the OOK signal transmission performance in 5G fronthauls with MCFs and direct-detection. As each CPRI link is assigned to a single core of the MCF to perform a connection between the pool of BBUs and one RRH, our model considers a point-to-point link between a transmitter and a receiver, which uses core *n* to transmit the CPRI signal. This model holds for both downstream or upstream directions.

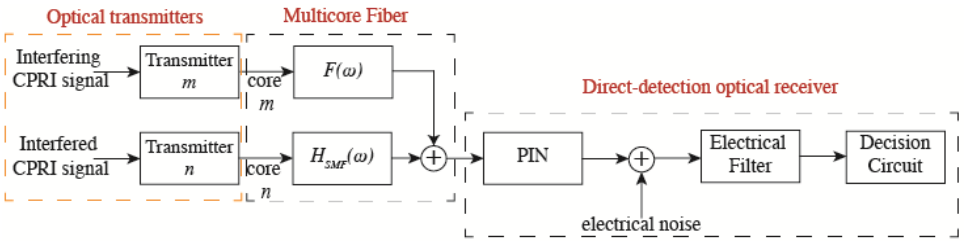

Fig. 3 Equivalent system model with two interfering cores used to study the impact of ICXT on a 5G fronthaul with weakly-coupled MCF and direct detection.

As illustrated in Fig. 3, two chirpless optical transmitters, each one generating an OOK signal with rectangular pulse shape and infinite extinction ratio, are considered. The OOK signals at the input of the interfered core *n* and the interfering core *m* are generated with the same CPRI bit rate and their bit transitions are aligned in time.

Linear single-mode propagation is assumed in each core. In core *n*, the transmission is modelled by the single mode fiber (SMF) transfer function $H_{SMF}(\omega)$ given by $H_{SMF}(\omega) = \exp[-j\beta_n(\omega)\cdot L]$, where L is the fiber length, ω is the low-pass equivalent angular frequency and $\beta_n(\omega)$ is the intrinsic propagation constant of core *n*. A Taylor series expansion up to the second order in ω is considered for $\beta_n(\omega)$, i.e., propagation delay and fiber dispersion effects are considered. The same fiber attenuation is assumed for the two cores. Hence, the fiber attenuation level is not relevant in our analysis, as the average signal power at the optical receiver input, i.e., the receiver sensitivity is considered to obtain the system performance.

We model the ICXT by the discrete changes model, introduced in [17] and later further developed in [19], [22], [23], [25], [26]. To keep the complexity and time of simulation at acceptable levels, we analyse the evolution of the impact of ICXT on system performance in time fractions (corresponding to the duration of several thousand of bits, i.e., much shorter than the ICXT decorrelation time), separated by time intervals longer than the decorrelation time of ICXT of the MCF. This means that, from time fraction to time fraction, the ICXT is uncorrelated and, within each time fraction, is totally correlated. This simplifies the simulation of the ICXT as, in each time fraction, from the ICXT viewpoint, one MCF realization is generated that is uncorrelated to all other MCF realizations associated with other fractions of time. In this case, in each time fraction, a MCF realization, corresponding to the interfering signal in core *n* resulting from ICXT caused by the signal in core *m*, is obtained from the ICXT field transfer function [19]:

$$F(\omega) = -jK_{nm}e^{-j\beta_n(\omega)L}\sum_{k=1}^{N_p} e^{-j\Delta\beta_{mn}(\omega)\cdot z_k}\cdot e^{-j\phi_k} \tag{1}$$

where K_{nm} is the discrete coupling coefficient between cores *m* and *n*, z_k is the longitudinal coordinate of the *k*-th point between consecutive phase-matching points (PMPs), given by $z_k=(k-1)\,L/N_p+\xi$, with N_p the number of PMPs and ξ a random variable uniformly distributed between 0 and L/N_p. ϕ_k (with $1\le k\le N_p$) is the *k*-th random phase shift (RPS), associated with the *k*-th point, that models random fluctuations in bending radius, twist rate or other conditions of the MCF. Each ϕ_k is modelled by a random variable uniformly distributed between [0,2π[and different ϕ_k are uncorrelated [19]. The skew between

cores m and n is given by $S_{mn} = d_{mn} \cdot L$, with d_{mn} the walkoff parameter between cores m and n. In Eq. (1), $\Delta\beta_{mn}(\omega)$ is the difference of the intrinsic propagation constants between cores m and n and is given by [19]

$$\Delta\beta_{mn}(\omega) = \Delta\beta_{0,mn} + d_{mn}\omega - \frac{1}{2} \cdot \frac{\Delta D_{mn}\lambda^2}{2\pi c}\omega^2 \tag{2}$$

where $\Delta\beta_{0,mn}$ is the difference of propagation constants of cores m and n at zero frequency, ΔD_{mn} is the difference of dispersion parameters of cores m and n, λ is the carrier wavelength and c is the speed of light in a vacuum. For equal powers at the interfered and interfering cores and same core losses, the ratio between the crosstalk power at the output of the interfered core n and the power of the signal at the output of the interfering core m, X_c, is related to the parameters of Eq. (1) by $X_c = N_p|K_{nm}|^2$ [17], [19]. To obtain the interfering signal at the output of core n resulting from ICXT caused by the signal in core m, we filter the signal at the input of core m by the filter with transfer function given by Eq. (1). The different MCF realizations are obtained by generating randomly different sets of N_p RPSs. In each iteration of the MC simulator, one MCF realization is generated, and the bits of the interfering CPRI signal transmitted in core m are randomly generated.

At the optical receiver, the signal at the MCF output is photodetected by a PIN with unit responsivity and bandwidth much larger than the CPRI signal bit rate. The signal at the PIN output is filtered by an electrical filter modelled by a 2nd order Butterworth filter with a −3 dB cut-off frequency of $0.65 \times R_b$, being R_b the OOK signal bit rate. The electrical noise, referred to the electrical filter input, is characterized by a noise equivalent power of 1×10^{-12} W/$\sqrt{\text{Hz}}$ [33]. After electrical filtering, the decision circuit samples the signal at the time instants $t_l = t_{opt} + lT_b$, where t_{opt} is the optimum sampling time extracted from the eye-pattern (different from MCF realization to MCF realization), T_b is the bit period and l = 1, 2, …, N_b, with N_b, the number of bits considered for BER assessment in each MCF realization.

2.2 Semi-analytical BER estimation

To evaluate the BER, we use MC simulation combined with a semi-analytical technique [34]. The impact of electrical noise on the performance is taken into account analytically, and the effects of fiber chromatic dispersion and ICXT on the BER are evaluated using waveform simulation in each MC simulation iteration. Let i denote the i-th iteration of the MC simulator, in which a different MCF realization is used. Hence, the BER of the i-th iteration is given by [34]

$$BER_i = \frac{1}{N_b}\left\{\sum_{\substack{l=1\\ j=0}}^{N_b} Q\left(\frac{F_i - m_{0,l,i}}{\sigma_{0,l,i}}\right) + \sum_{\substack{l=1\\ j=1}}^{N_b} Q\left(\frac{m_{1,l,i} - F_i}{\sigma_{1,l,i}}\right)\right\} \tag{3}$$

where $Q(x)$ is the Q-function defined by [35]

$$Q(x) = \frac{1}{\sqrt{2\pi}}\int_x^{+\infty} e^{-\lambda^2/2}\, d\lambda \tag{4}$$

and $m_{j,l,i}$ and $\sigma_{j,l,i}$ are the mean and standard deviation of the current at the decision circuit input at the time instants t_l, conditioned on the transmitted bit j (0 or 1). Here, $\sigma_{0,l,i}=\sigma_{1,l,i}$, as we consider electrical noise

only. The ICXT and intersymbol interference (ISI) from fiber dispersion affect the mean $m_{j,l,i}$ components by the waveform distortion taken from the eye-pattern at the time instants t_l. The decision threshold F_i is optimized in each iteration of the MC simulator using the bisection method to minimize the BER per MCF realization. The average BER is defined by

$$\overline{BER} = \frac{1}{N_{MCF}} \cdot \sum_{i=1}^{N_{MCF}} BER_i \tag{5}$$

with the parameter N_{MCF} defining the number of iterations (MCF realizations) of the MC simulator. The number of MC simulation iterations needed to obtain a stabilized value of the average BER or a sufficient accurate outage probability is still to be determined and is discussed in section 3.

2.3 CPRI bit rates

In this work, two CPRI bit rates are studied: (i) option 7, with R_b = 9.8304 Gbps, 8B/10B line coding and without Forward-Error Correction (FEC), and (ii) option 8, with R_b = 10.1376 Gbps, 64B/66B line coding and with FEC [8]. For systems without FEC, the target BER is 10^{-12} [8]. For systems with FEC, the target average BER depends on the FEC implementation [31]. We assume the CPRI signal option 8 with a target average BER before performing FEC set to 10^{-3} [31]. We have chosen CPRI bit rates near 10 Gbps per MCF core, since, this bit rate has been already studied for the fronthaul of 5G networks with single core fibers in [4], [36]. Furthermore, this bit rate is the most common found in optical fiber telecommunication systems with OOK signal transmission and direct-detection, hence, leading to a simpler and cheaper implementation [33].

3 Numerical results and discussion

In this section, the impact of ICXT on the performance of CPRI signals transmitted in 5G fronthauls supported by weakly-coupled MCFs is investigated by numerical simulation. The simulation parameters that are kept constant throughout this work are shown in Table 1. The same fiber dispersion parameter is considered for the two cores, i. e., $\Delta D_{mn} = 0$. The length of the MCF is set for the maximum reach defined for the 5G fronthaul [10] and originates a slight ISI due to chromatic dispersion at the CPRI bit rates investigated. As mentioned, fiber attenuation is the same in both cores. The number of PMPs is set to characterize accurately the mechanism of the RPSs [19], [20], [37]. The number of generated OOK bits per MCF realization is set to take into account the ISI of the communication system in a rigorous way. Two different skews are considered: a skew shorter than the bit period, $S_{mn} \cdot R_b \approx 0.2$, which corresponds to d_{mn} = 1 ps/km; and a skew much higher than the bit period, $S_{mn} \cdot R_b \approx 10$ obtained with d_{mn} = 50 ps/km.

Table 1. Simulation parameters.

Parameter	Value
Carrier wavelength, λ	1550 nm
Fiber dispersion parameter, D_λ	17 ps/nm/km
Fiber length	20 km
Difference of propagation constants at zero frequency, $\Delta\beta_{0,mn}$	0
Number of PMPs, N_p	1000
Number of generated OOK bits per MCF realization	2^9

8

3.1 Influence of the ICXT mechanism on the direct-detection system performance

First, we start by assessing the number of fiber realizations that are necessary to achieve a stabilized value of the average BER. To provide a certain margin for BER degradation due to ICXT, we set the BER in the absence of ICXT to two orders of magnitude below the target BER. Hence, our studies for the CPRI line option 8 consider the BER of 10^{-5} in absence of ICXT. The receiver sensitivity corresponding to this BER is −34.40 dBm. Following the same reasoning for systems without FEC, the BER in the absence of ICXT is defined as 10^{-14}, which corresponds to the receiver sensitivity of −31.79 dBm. Figs. 4 and 5 depict the BER for each MCF realization (green symbols) and the average BER (black symbols) as a function of the number of MCF realizations, for d_{mn} = 1 ps/km. Fig. 4 refers to the CPRI signal with the bit rate of 9.8304 Gbps (which does not consider FEC) and for the crosstalk level, X_c = −30 dB. Figure 5 refers to the CPRI signal with R_b = 10.1376 Gbps (which considers FEC) and X_c = −15 dB. These crosstalk values are chosen to lead to an average BER degradation relative to the one obtained in ICXT absence by about two orders of magnitude. Fig. 4 shows that the average BER can be considered stabilized after about 4000 MCF realizations. The achieved average BER in this case is 3.33×10^{-12}. In the subsequent studies for the CPRI signal with 9.8304 Gbps, we have set the number of fiber realizations to 10^4 as a conservative choice. Fig. 5 shows that the average BER is nearly stable at about 1.87×10^{-3} after 400 MCF realizations. For the subsequent studies, we have set the number of MCF realizations to 10^3 as a conservative choice for the CPRI signal with 10.1376 Gbps. The large difference between the number of MCF realizations required to get a stabilized average BER shown in Figs. 4 and 5 is attributed to the order of magnitude of the average BERs considered in each case.

Figs. 4 and 5 show that the randomness of the ICXT mechanism can lead to severe BER degradation or even to BER improvement per MCF realization. In Fig. 4, the best BER obtained per MCF realization is 1.38×10^{-14} and the worst BER is 2.07×10^{-9}. Fig. 5 exhibits a best BER of 7.40×10^{-6} and a worst BER of 7.78×10^{-2}. The eye-patterns corresponding to the MCF realization that led to these BERs are presented in Fig. 6. In this figure, the ICXT impact on the eye-patterns can be analyzed. These eye-patterns do not show the effect of the electrical noise to make clear the ICXT effect. The amplitude of bit '1' in the absence of ISI is normalized to unit. The normalized eye-opening is also shown. Fig. 6 a) shows the eye-pattern corresponding to the case where no ICXT is present. As the bit rates are similar and the amplitude is normalized, the eye-pattern is similar for both cases in Figs. 4 and 5, and exhibits only the ISI effect induced by dispersion and electrical filtering. Fig. 6 b) shows an example of an eye-pattern that leads to a BER improvement due to ICXT relative to the case of ICXT absence. Notice that the eye-opening is similar in comparison with the eye-opening obtained in the absence of ICXT. The BER improvement is obtained because amplitudes of bit '1', that have higher values than in the case of ICXT absence, occur due to the ICXT. Figs. 6 c) and d) correspond to the MCF realizations in which the worst BER occurs in Figs. 4 and 5, respectively. Fig. 6 c) shows that the eye-closure for the MCF realization with the worst BER is not so severe as the one obtained in Fig. 6 d). This explains the higher number of MCF realizations needed to get a stabilized average BER for lower BERs (see Fig. 4)), since a slight signal distortion caused by ICXT can degrade the average BER by a few orders of magnitude. For higher BERs (see Fig. 5), in order to get BERs per MCF realization with a few orders of magnitude above the reference BER of 10^{-5}, the crosstalk level must be much higher, and leads to a very small eye-opening. Analysis of Fig. 6 reveals that the impact of the ICXT on the eye-pattern is felt mainly at the amplitudes of bit '1' creating new amplitude "rails" in these bits. At bit '0', the amplitude values remain essentially the same due to the infinite extinction ratio of the signal generated by the transmitter. For finite extinction ratios, it is expected that the amplitudes of the bit '0' suffer also from an ICXT effect similar to the one observed in the amplitudes of bit '1'.

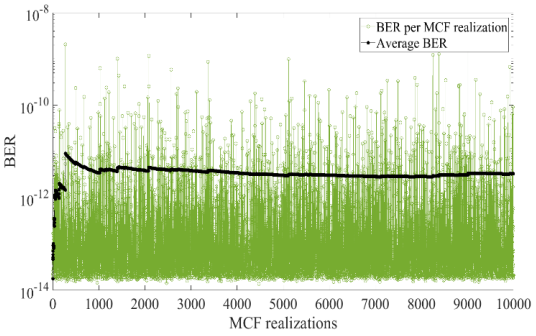

Fig. 4 BER for each MCF realization (green symbols) and average BER (black symbols) as a function of the MCF realizations, for R_b =9.8304 Gbps, X_c= −30 dB and d_{mn} = 1 ps/km. The BER in the absence of ICXT is 10^{-14}.

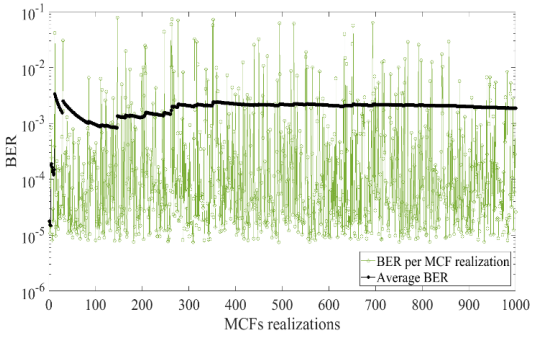

Fig. 5 BER for each MCF realization (green symbols) and average BER (black symbols) as a function of the MCF realizations, for R_b =10.1376 Gbps, X_c = −15 dB, and d_{mn} = 1 ps/km. The BER in the absence of ICXT is 10^{-5}.

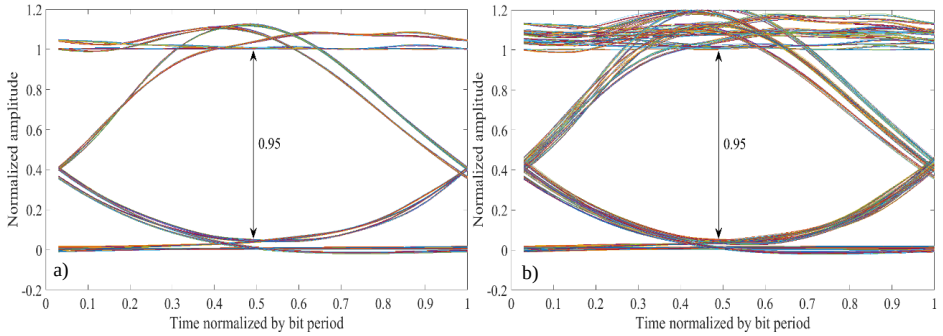

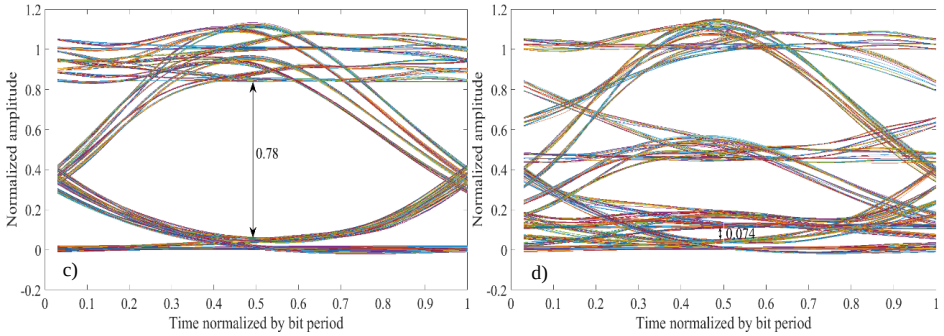

Fig. 6 Eye-patterns at the decision circuit input corresponding to the BER without ICXT and the worst and best BER obtained in Figs. 4 and 5, for d_{mn} = 1 ps/km. In a), the ICXT is absent. In b): best BER case for Fig. 5. In c) and d): worst BER cases for Figs. 4 and 5, respectively. The eye opening is indicated in each eye-pattern.

A study similar to the one performed in Figs. 4-6 has been performed for $S_{mn} \cdot R_b \approx 10$ (with d_{mn} = 50 ps/km). Fig. 7 shows the BER for each MCF realization (green symbols) and the average BER (black symbols) as a function of the number of MCF realizations for the CPRI signal with R_b = 10.1376 Gbps, X_c = –15 dB and d_{mn} = 50 ps/km. Fig. 7 shows that 200 MCF realizations are enough to reach the stabilized average BER of 7.67×10^{-4}. For d_{mn} = 50 ps/km, the impact of ICXT on the performance is reduced in comparison with d_{mn} = 1 ps/km [37], [38]. Therefore, Fig. 7 exhibits, for the same crosstalk level, X_c = –15 dB, a lower average BER than the one shown in Fig. 5, which needs less MCF realizations to stabilize. Fig. 7 shows also that the worst BER of all MCF realizations is lower, 3.62×10^{-2}, than the one presented in Fig. 5 given by 7.78×10^{-2}. The best BER of all MCF realizations in Fig. 7 is 5.24×10^{-6}, which is also lower than the best BER per realization presented in Fig. 5.

Figs. 8 a) and b) show the corresponding eye-patterns obtained for the best and worst BERs presented in Fig. 7, respectively. The eye-pattern in the case of absence of ICXT is the same as in Fig. 6 a). The best and worst BERs per MCF realization shown in Fig. 7 can be explained by similar reasons to the ones presented for Fig. 5. For the best BER, the eye-opening is the same as in the case of ICXT absence, but the BER per MCF realization improves, because there are amplitudes of bit '1' taken at the sampling instants that have higher values than in the case of ICXT absence. The worst BER occurs due to a MCF realization that leads to a very small eye-opening. However, there is a very distinctive behavior between the eye-patterns shown for the two fiber walkoffs. For d_{mn} = 1 ps/km, the amplitudes due to ICXT define discrete values on the eye-pattern. For d_{mn} = 50 ps/km, the amplitudes due to ICXT exhibit a "continuous" behavior at the sampling instant, which reminds a random behavior as the one provided by a noise source. The observed behavior is in agreement with the one observed in [32], where, for an adequately broad signal, $S_{mn} \cdot R_b \approx 10$, the ICXT behaves similarly to white noise as shown in Fig. 8. For an adequately narrower signal, the ICXT leads to well-defined discrete amplitudes on the eye-pattern, as shown in Fig. 6, with a behavior named virtually static coupling [32].

We have verified that the aforementioned numbers of MCF realizations are more than sufficient to lead to stabilized average BERs for different crosstalk levels, different fiber lengths (other than 20 km), different walkoffs between fiber cores and CPRI signals with different bit rates.

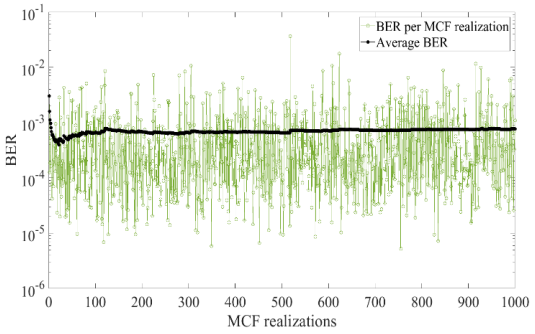

Fig. 7 BER for each MCF realization (green symbols) and average BER (black symbols) as a function of the MCF realizations, for R_b =10.1376 Gbps, X_c = −15 dB, and d_{mn} = 50 ps/km. The BER in the absence of ICXT is 10^{-5}.

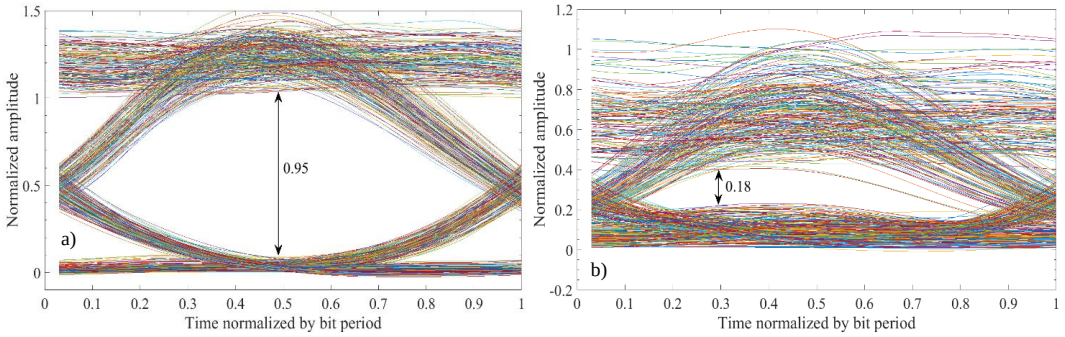

Fig. 8 Eye-patterns at the decision circuit input corresponding to the a) best BER and b) worst BER obtained in Fig. 7, for d_{mn} = 50 ps/km. The eye opening is indicated in each eye-pattern.

3.2 Power penalty due to ICXT

After having identified the number of MCF realizations required to reach a stabilized average BER, the influence of the ICXT on the average BER degradation is studied. Figs. 9 and 10 depict the average BER as a function of the crosstalk level, for d_{mn} = 1 ps/km and d_{mn} = 50 ps/km. Fig. 9 corresponds to the 9.8304 Gbps CPRI signal and Fig. 10 refers to the 10.1376 Gbps CPRI signal. As expected, the average BER becomes higher with the increase of the crosstalk level. In Fig. 9, as the BER without ICXT is very low (10^{-14}), lower values of the crosstalk level lead to a BER degradation above two orders of magnitude. By taking the average BER of 10^{-12} as a reference for the system performance, this BER is reached for X_c = –31.7 dB with d_{mn} = 1 ps/km, and for X_c = –29.6 dB with d_{mn} = 50 ps/km, which gives an improved tolerance to ICXT of 2.1 dB for the higher MCF walkoff. In Fig. 10, as the BER in absence of ICXT is higher (10^{-5}), higher ICXT levels are required to degrade the average BER significantly. An average BER of 10^{-3} is reached for about X_c = –17.4 dB and X_c = –15.4 dB, for d_{mn} = 1 ps/km and d_{mn} = 50 ps/km, respectively, which leads to an ICXT tolerance improvement of 2 dB for higher walkoff. The reduction of the impact of the ICXT with the increase of the walkoff between the cores is in qualitative accordance with the results presented in [38], where the ICXT impact is evaluated by obtaining the short term average crosstalk power at the MCF output.

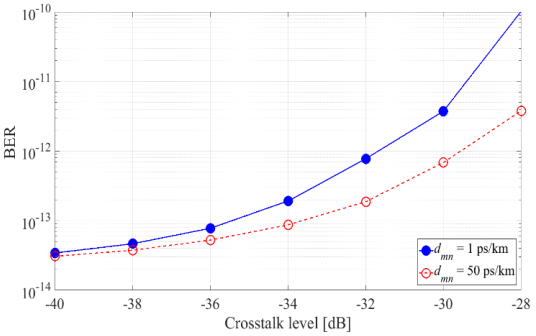

Fig. 9 BER as a function of crosstalk level, X_c, in dB, for d_{mn} = 1 ps/km (blue line) and d_{mn} = 50 ps/km (red line), for a CPRI signal with R_b=9.8304 Gbps.

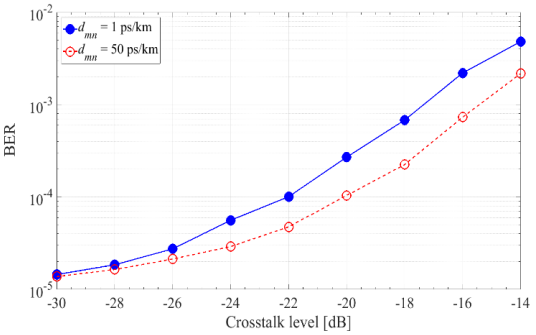

Fig. 10 BER as a function of crosstalk level, X_c, in dB, for d_{mn} = 1 ps/km (blue line) and d_{mn} = 50 ps/km (red line), for a CPRI signal with R_b=10.1376 Gbps.

Fig. 11 depicts the power penalty due to ICXT as a function of the crosstalk level for the 10.1376 Gbps CPRI signal with a target average BER of 10^{-3}, for d_{mn} = 1 ps/km and d_{mn} = 50 ps/km. The receiver sensitivity to reach the target BER is –35.86 dBm. For d_{mn} = 1 ps/km, a power penalty of 1 dB is reached for a crosstalk level of −17.7 dB, while, for d_{mn}= 50 ps/km, the power penalty of 1 dB occurs for a crosstalk level of −16.7 dB. Therefore, our results show that the tolerance to the ICXT in CPRI signals transmission through 5G fronthauls based on MCFs with direct-detection can improve by about 1 dB for pairs of cores with higher skew, due to the reduction of the ICXT impact on the system performance.

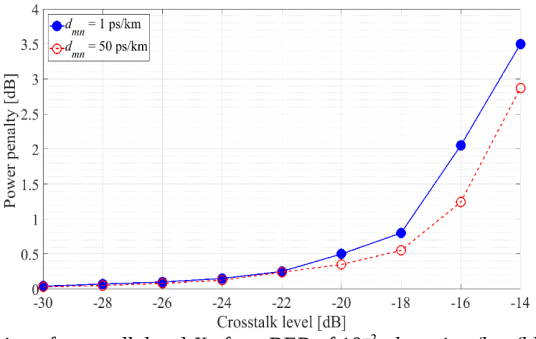

Fig. 11 Power penalty as a function of crosstalk level X_c, for a BER of 10^{-3}, d_{mn} = 1 ps/km (blue line) and d_{mn} = 50 ps/km (red line), for a CPRI signal with R_b=10.1376 Gbps.

3.3 Outage probability due to ICXT

Section 3.1 has shown that specific MCF realizations can degrade severely the BER, leading to system unavailability during the fraction of time in which each one of those specific MCF realizations occurs. The time duration of the MCF realization depends on the correlation time of the ICXT, which depends strongly on the weakly-coupled MCF under study. Work [20] studies a MCF and measures a decorrelation time up to two hours. On the other hand, work [23] reports decorrelation times of a few minutes. By taking as a reference, the MCF studied in [23], a bit rate of 10 Gbps and, for example, by assuming a MCF realization that leads to system unavailability during 1 s, 10^{10} errored bits will occur in that particular MCF realization, what is unacceptable. Hence, the system unavailability must be studied when dealing with ICXT. A typical metric for measuring the unavailability of a communication system over a certain time interval is the outage probability [31], [39], [40]. The outage probability defines the probability of the system being unavailable for a target BER limit. In the simulation, the outage probability is estimated by counting the number of MCF realization occurrences that lead to a BER above the BER limit and dividing this number by the total number of MCF realizations. In our simulations, we have seen that 200 occurrences are enough to obtain reasonably accurate estimates of the outage probability. The following results consider the CPRI option 8 with R_b = 10.1376 Gbps, the BER in the absence of ICXT is set to 10^{-5}, and the system is considered to be unavailable when a MCF realization leads to a BER that overcomes the BER limit of 10^{-3}.

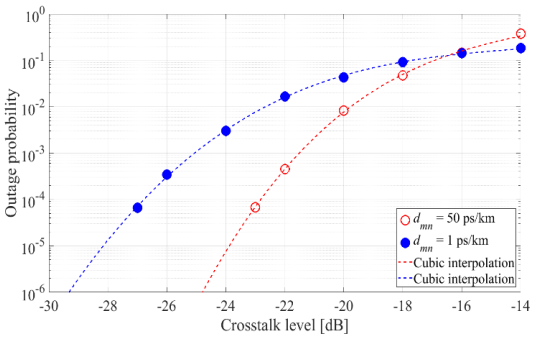

Fig. 12 Outage probability as a function of the crosstalk level, X_c, for a BER in the absence of ICXT of 10^{-5} and a BER limit of 10^{-3}, d_{mn} = 1 ps/km (blue symbols) and d_{mn} = 50 ps/km (red symbols), for a CPRI signal with R_b=10.1376 Gbps. The lines represent a cubic interpolation of the $\log_{10}(\ )$ of the outage probability.

Fig. 12 shows the outage probability as a function of the crosstalk level, for d_{mn} = 1 ps/km and d_{mn} = 50 ps/km. In the absence of ICXT, the signal power at the optical receiver input is set to –34.40 dBm to reach a BER of 10^{-5}. The symbols represent the outage probability obtained from the simulation model. Typically, the maximum acceptable outage probability is 10^{-5} [31], [39], however, with MC simulation, the computational time needed to reach this probability is very high and almost unacceptable. To reach this value of outage probability, a cubic interpolation for the points obtained by MC simulation has been used and, then, extrapolation has been used to obtain BERs below 1×10^{-4}. Fig. 12 shows that, for high crosstalk levels (X_c > –16 dB), the system is unavailable with a very high probability, above 10^{-1}. For lower crosstalk levels, with d_{mn} = 1 ps/km, the system exhibits a higher outage probability than with d_{mn} = 50 ps/km. For example, for the outage probability of 10^{-5}, the maximum tolerable crosstalk level is about –28.2 dB for d_{mn} = 1 ps/km, and –23.9 dB for d_{mn} = 50 ps/km. A difference between the maximum tolerable crosstalk levels obtained for the two skews of 4.3 dB is observed.

Table 2 summarizes the conclusions taken from Figs. 11 and 12, regarding the maximum tolerable

crosstalk level acceptable for a receiver power penalty of 1 dB and an outage probability of 10^{-5}. Table 2 shows that the power penalty of 1 dB in a direct-detection communication system impaired by ICXT is reached when the crosstalk level is higher than –18 dB. However, for this crosstalk level, Fig. 12 shows a very high outage probability, above 5×10^{-2}. This means that the unavailability of the optical communication system is unacceptable since, in one hour period, the system will be unavailable during 3 minutes. To ensure an outage probability of 10^{-5}, the crosstalk level must be below –28.2 dB, for both walkoffs, for one single interfering core, which is a much more stringent condition than the one obtained considering a power penalty of 1 dB as a limit for the crosstalk level.

This last conclusion can be generalized to a MCF with N_i interfering cores. By assuming that the interfering signals have the same power and the different interfering cores induce equal crosstalk levels, an approach for the maximum tolerable crosstalk level per each core is given by $X_{c,max}$ [dB] $\leq X_{c,max,1}$ [dB] $- 10\cdot\log_{10}(N_i)$, where $X_{c,max,1}$ denotes the maximum tolerable crosstalk level obtained for a single interfering core. For $X_{c,max,1} = -28.2$ dB as given in Table 2, for a MCF with 4 interfering cores in one interfered test core, the maximum tolerable crosstalk level per each interfering core is –34.2 dB.

Table 2. Maximum tolerable crosstalk level to achieve a 1 dB power penalty or an outage probability of 10^{-5}.

Maximum tolerable crosstalk level		
Performance metric limit	d_{mn} = 1 ps/km	d_{mn} = 50 ps/km
Power penalty of 1 dB	–17.7 dB	–16.7 dB
Outage probability of 10^{-5}	–28.2 dB	–23.9 dB

Therefore, our results indicate that in direct-detection optical communication systems impaired by ICXT, the study of the outage probability can be far more important than the assessment of the power penalty degradation related to the average BER. The random nature of ICXT can lead, with very high probability, to large periods of system unavailability, even if the average BER is set to be within its pre-defined limits.

4 Conclusion

In this work, we have studied, through numerical simulation, the ICXT impact on 10 Gbps CPRI signal transmission performance in a 5G network with a fronthaul supported by weakly-coupled MCFs. The results have shown that FEC-supported CPRI signals (with bit rate of 10.1376 Gbps) need less MCF realizations for the average BER to converge than CPRI signals without FEC (with bit rate of 9.8304 Gbps) due to the order of magnitude of the target BER. A smaller number of MCF realizations is required for the average BER to stabilize, when the MCF skew increases, as the ICXT impact is smaller.

The effect of the ICXT on the received eye-pattern after direct-detection has also been studied. For infinite extinction ratio and low skew, the ICXT originates well-defined discrete amplitudes at the bit '1'. For high skew, the ICXT affects the amplitudes of bit '1' with a "white noise"-like behavior. These results are in qualitative agreement with the results presented in [32]. We have also seen that, when the crosstalk level is high, the degradation due to ICXT is mainly due to a severe eye-closure.

The power penalty due to ICXT has also been studied for FEC-supported CPRI signals. By defining the power penalty of 1 dB as the maximum for performance degradation, we have shown that, for d_{mn} = 1 ps/km, the power penalty limit is reached for an ICXT level of −17.7 dB, while, for d_{mn}= 50 ps/km, the power penalty of 1 dB occurs for an ICXT level of −16.7 dB.

Most importantly, our studies have shown that is essential to study the outage probability for direct-

detection optical communication systems impaired by ICXT. There are specific MCF realizations that can lead to system unavailability for long time periods, even if the average BER is set to be within prescribed limits. We have shown that, for FEC-supported CPRI signals and crosstalk levels that lead to a power penalty of 1 dB, $X_c > -18$ dB, the system is unavailable with a very high probability (above 5×10^{-2}), which is unacceptable. Much lower tolerable crosstalk values, $X_c < -28.2$ dB, are required to get an acceptable outage probability. MCFs with higher walkoffs between the cores are more resilient to ICXT, since they require higher crosstalk levels to reach a pre-defined outage probability than MCFs with lower walkoff. A difference of about 4.3 dB has been observed for a BER limit of 10^{-5}.

Acknowledgments

This work was supported in part by Fundação para a Ciência e a Tecnologia (FCT) from Portugal under the project of Instituto de Telecomunicações AMEN-ID/EEA/50008/2013.

References

[1] China Mobile: C-RAN: the road towards green RAN. White Paper, version 2.5, 15–16, https://pdfs.semanticscholar.org/eaa3 (2011)
[2] Pizzinat, A., Chanclou, P., Saliou, F., Diallo, T.: Things you should know about fronthaul. IEEE/OSA J. Lightw. Technol., **33**(5), 1077–1083 (2015)
[3] Shafi, M., Molisch, A., Smith, P., Haustein, T., Zhu, P., Silva, P., Tufvesson, F., Benjebbour, A., Wunder, G.: 5G: A tutorial overview of standards, trials, challenges, deployment, and practice. IEEE J. Sel. Areas Commun., **35**(6), 1201–1221 (2017)
[4] Chanclou, P., Pizzinat, A., Clech, F., Reedeker, T., Lagadec, Y., Salliou F., Guyader, B., Guillo, L., Deniel, Q., Gosselin, S., Le, S., Diallo, T., Brenot, R., Lelarge, F., Marazzi, L., Parolari, O., Martinelli, M., Dull, S., Gebrewold, S., Hillerkuss, D., Leuthold, J., Gavioli, G., Galli, P.: Optical fiber solution for mobile fronthaul to achieve cloud radio access network. In: Future Network and Mobile Summit 2013, Lisbon, Portugal (2013)
[5] Galve, J.M., Gasulla, I., Sales, S., Capmany, J.: Reconfigurable radio access networks using multicore fibers. IEEE J. Quantum Electron., **52**(1), 1–7 (2016)
[6] Alimi, I., Teixeira, A., Monteiro, P.: Towards an efficient C-RAN optical fronthaul for the future networks: a tutorial on technologies, requirements, challenges and solutions. IEEE Commun. Surveys Tuts., **20**(1), 708–769 (2018)
[7] Dat, P., Kanno, A., Kawanishi, T.: Radio-on-radio-over-fiber: efficient fronthauling for small cells and moving cells. IEEE Wireless Commun., **22**(5), 67–75 (2015)
[8] Common Public Radio Interface: CPRI Specification V7.0. Standard Document Specification, vol. 1, (2015)
[9] Pfeiffer, T.: Next generation mobile fronthaul and midhaul architectures. IEEE/OSA J. Opt. Commun. Netw., **7**(11), B38–45 (2015)
[10] Telecommunications Standardization Sector of ITU-T: Transport network support of IMT-2020/5G. ITU-T Technical Report, (2018), https://www.itu.int/md/T17-SG15-170619-TD-GEN-0078/en
[11] Macho, A., Morant, M., Llorente, R.: Next-generation optical fronthaul systems using multicore fiber media. IEEE/OSA J. Lightw. Technol., **34**(20), 4819–4827 (2016)
[12] Galve, J., Gasulla, I., Sales., S., Capmany, J.: Fronthaul design for radio access networks using multicore fibers. Waves Magaz., **7**(1), 69–80 (2015)
[13] Sakaguchi, J., Puttnam, B., Klaus, W., Awaji, Y., Wada, N., Kanno, A., Kawanishi, T., Imamura, K., Inaba, H., Mukasa, K., Sugizaki, R., Kobayashi, T., Watanabe, M.: 305 Tb/s space division multiplexed transmission using homogeneous 19-core fiber. IEEE/OSA J. Lightw. Technol., **31**(4), 554-562 (2013)
[14] Puttnam, B., Luís, R., Mendinueta, J., Sakaguchi, J., Klaus, W., Awaji, Y., Wada, N., Kanno, A., Kawanishi, T.: High-capacity self-homodyne PDM-WDM-SDM transmission in a 19-core fiber. Opt. Expr., **22**(18), 21185–21191 (2014)
[15] Feuer, M., Nelson, L., Zhou, X., Woodward, S., Isaac, R., Zhu, B., Taunay, T., Fishteyn, M., Fini, J., Yan, M.: Joint digital signal processing receivers for spatial superchannels. IEEE Photon. Techn. Lett., **24**(21), 1957–1960 (2012)
[16] Igarashi, K., Tsuritani, T., Morita, I., Tsuchida, Y., Maeda, K., Tadakuma, M., Saito, T., Watanabe, K., Imamura, K., Sugizaki, R., Suzuki, M.: Super-Nyquist-WDM transmission over 7,326-km seven-core fiber with capacity-distance product of 1.03 Exabit/s·km. Opt. Expr., **22**(2), 1220-1228 (2014)
[17] Hayashi, T., Taru, T., Shimakawa, O., Sasaki, T., Sasaoka, E.: Design and fabrication of ultra-low crosstalk and low-loss multicore fiber. Opt. Expr., **19(**17), 16576-16592 (2011)

[18] Tu, J., Saitoh, K., Koshiba, M., Takenaga, K., Matsuo, S.: Design and analysis of large-effective-area heterogeneous trench-assisted multi-core fiber. Opt. Expr., **20(**14), 15157-15170 (2012)
[19] Cartaxo, A., Luís, R., Puttnam, B., Hayashi, T., Awaji, Y., Wada, N.: Dispersion impact on the crosstalk amplitude response of homogeneous multi-core fibers. IEEE Photon. Technol. Lett., 28(17), 1858–1861 (2016)
[20] Luís, R., Puttnam, B., Cartaxo, A., Klaus, W., Mendinueta, J., Awaji, Y., Wada, N., Nakanishi, T., Hayashi, T., Sasaki, T.: Time and modulation frequency dependence of crosstalk in homogeneous multi-core fibers. IEEE/OSA J. Lightw. Technol., **15**(2), 441–447 (2016)
[21] Alves, T., Cartaxo, A., Luís, R., Puttnam, B., Awaji, Y., Wada, N.: Intercore crosstalk in direct-detection homogeneous multicore fiber systems impaired by laser phase noise. Opt. Expr., **25**(23), 29417-29431 (2017)
[22] Alves, T., Cartaxo, A.: Intercore crosstalk in homogeneous multicore fibers: theoretical characterization of stochastic time evolution. IEEE/OSA J. Lightw. Technol., **35(**21), 4613-4623 (2017)
[23] Alves, T., Cartaxo, A.: Characterization of the stochastic time evolution of short-term average intercore crosstalk in multicore fibers with multiple interfering cores. Opt. Expr. **26**(4), 4605-4620 (2018)
[24] Koshiba, M., Saitoh, K., Takenaga, K., Matsuo, S.: Analytical expression of average power-coupling coefficients for estimating intercore crosstalk in multicore fibers. IEEE Photon. J., **4**(5), 1987–1995 (2012)
[25] Cartaxo, A., Alves, T.: Discrete changes model of inter-core crosstalk of real homogeneous multi-core fibers. IEEE/OSA J. Lightw. Technol, **35**(12), 2398-2408 (2017)
[26] Soeiro, R., Alves, T., Cartaxo, A.: Dual polarization discrete changes model of inter-core crosstalk in multi-core fibers. IEEE Photon. Technol. Lett., **29(**16), 1395-1398 (2017)
[27] Ye, F., Tu, J., Saitoh, K., Takenaga, K., Matsuo, S., Takara, H., Morioka, T.: Wavelength dependence of inter-core crosstalk in homogeneous multi-core fibers. IEEE Photon. Technol. Lett., **28(**1), 27-30 (2016)
[28] Sano, A., Takara, H., Kobayashi, T., Miyamoto, Y.: Crosstalk-managed high capacity long haul multicore fibre transmission with propagation-direction interleaving. IEEE/OSA J. Lightw. Technol., **32**(16), 2771–2779 (2014)
[29] Takenaga, K., Arakawa, Y., Tanigawa, S., Guan, N., Matsuo, S., Saitoh, K., Koshiba, M.: Reduction of crosstalk by trench-assisted multi-core fiber. In: Proc. Optical Fiber Communication Conference and Exhibition, OFC 2011, Los Angeles, USA, (2011)
[30] Hayashi, T., Taru, T., Shimakawa, O., Sasaki, T., Sasaoka, E.: Characterization of crosstalk in ultra-low-crosstalk multi-core fiber. IEEE/OSA J. Lightw. Technol., **30**(4), 583-589 (2012)
[31] Puttnam, B., Luís, R., Eriksson, T., Klaus, W., Mendinueta, J., Awaji, Y., Wada, N.: Impact of inter-core crosstalk on the transmission distance of QAM formats in multi-core fibers. IEEE Photon. J., **8**(5), Art. ID. 0601109 (2016)
[32] Hayashi, T., Sasaki, T., Sasaoka, E.: Behavior of inter-core crosstalk as a noise and its effect on Q-factor in multi-core fiber. IEICE Trans. Commun., **E97-B**(5), 936–944 (2014)
[33] Agrawal, G.P.: Fiber-optic communication systems, 4th edn. John Wiley & Sons, New Jersey, USA (2010)
[34] Rebola, J., Cartaxo, A.: Gaussian approximation for performance assessment of optically preamplified receivers with arbitrary optical and electrical filters. IET Optoelectron., **148**(3), 135–142 (2001)
[35] Carlson, A. Crilly, P.: Communication systems: an introduction to signals and noise in electrical communication, 5th edn. McGraw-Hill, New York, USA (2010)
[36] Parolari, P., Marazzi, L., Brunero, M., Martinelli, M., Maho, A., Barbet, S., Lelarge, F., Brenot, R., Gavioli, G., Simon, G., Saliou, F., Deniel, Q., Chanclou, P.: Operation of RSOA WDM PON self-seeded transmitter over more 50 km of SSMF up to 10 Gb/s. In: Proc. Optical Fiber Communication Conference and Exhibition, OFC 2014, San Francisco, USA, (2014)
[37] Pinheiro, B., Rebola, J., Cartaxo, A.: Impact of inter-core crosstalk on the performance of multi-core fibers-based SDM systems with coherent fetection. In: Proc. International Conference on Photonics, Optics and Laser Technology, Photooptics 2018, Funchal, Portugal, (2018)
[38] Rademacher, G., Luís, R., Puttnam, B., Awaji, Y., Wada, N.: Crosstalk dynamics in multi-core fibers. Opt. Expr., **25**(10), 12020–12028 (2017)
[39] Cvijetic, N., Wilson, S., Qian, D.: System outage probability due to PMD in high-speed optical OFDM transmission. IEEE/OSA J. Lightw. Technol., **26**(14), 2118–2127 (2008)
[40] Winzer, P., Foschini, G.: MIMO capacities and outage probabilities in spatially multiplexed optical transport systems. Opt. Expr., **19**(17), 16680–16696 (2011)

Outage Probability due to Intercore Crosstalk in Multicore Fiber Links with Direct-Detection

João L. Rebola, Adolfo V. T. Cartaxo, Tiago M. F. Alves, and André S. Marques

***Abstract*— The outage probability in short-haul direct-detection optical links supported by multicore fibers (MCFs) impaired by intercore crosstalk (ICXT) is studied analytically and a closed-form expression for the outage probability in such systems is proposed. This expression shows that direct-detection links with nonzero extinction ratio are more robust to outage, with a 1.5 dB improvement in the required ICXT level, when comparing an extinction ratio of 0.1 with null extinction ratio, for an outage of 10^{-5}. The expression is in very good agreement with results obtained from simulation and is valid for small intersymbol interference, a single interfering core and low MCF skew. For higher skews, it provides a worst-case prediction.**

***Index Terms*— Bit error rate, Direct-detection, Intercore crosstalk, Multicore fiber, Outage probability**

I. Introduction

Multicore fibers (MCFs) provide a good solution for the expected growth of data traffic in future optical networks, since they allow space division multiplexing and joint signal processing [1]. MCF have been recently proposed for short-haul links (radio-over-fiber, access networks, or datacenters interconnects), where optical amplification is not required [2]-[4]. Direct-detection at the receiver is also needed for low cost and complexity in short reach MCF optical links [2], [4]. Weakly-coupled homogeneous MCFs can provide the solution for the required capacity, since individual cores can be used as independent channels with similar propagation delays. However, in such MCFs, power coupling between signals in different cores, an effect known as intercore crosstalk (ICXT), limits the MCF reach and performance [5], [6]. The ICXT effect is reasonably well studied in the literature [5], [6], and several models have been proposed to assess the impact of ICXT on the system performance [7]-[9]. Due to the random evolution of ICXT along time [7], two ICXT effects affect the performance: random variations of the bit error rate (BER) over short time periods [5], and over long time periods when high levels of ICXT cause outage periods of system operation [1], [10]. The outage in weakly-coupled MCF-based systems with direct detection has been obtained from measuring the error vector magnitude [6] and by simulation [11]. However, a theoretical analysis of the outage probability, which provides a more comprehensive insight of the ICXT impact, is still to be developed.

In this letter, a theoretical closed-form expression for the outage probability in direct-detection unamplified short-haul links using weakly-coupled homogeneous MCFs impaired by ICXT is proposed. The theoretical expression is valid for systems with skew lower than the bit period and that takes into account the ICXT level and signal extinction ratio Its predictions are corroborated with numerical results obtained from Monte Carlo (MC) simulation.

This work was supported in part by Fundação para a Ciência e a Tecnologia (FCT) from Portugal under the project of Instituto de Telecomunicações AMEN-ID/EEA/50008/2013.

J. Rebola and A. Cartaxo are with Instituto de Telecomunicações, 1049-001, Lisboa, Portugal, and with ISCTE-Instituto Universitário de Lisboa, 1649-026, Lisboa, Portugal (e-mail: joao.rebola@iscte-iul.pt; adolfo.cartaxo@lx.it.pt).

T. Alves is with Instituto de Telecomunicações, 1049-001, Lisboa, Portugal (e-mail: tiago.alves@lx.it.pt).

A. Marques is with ISCTE-Instituto Universitário de Lisboa, 1649-026, Lisboa, Portugal (e-mail: Andre_Silva_Marques@iscte-iul.pt).

II. System Model and Outage Probability Derivation

In this section, the system model used to assess the ICXT impact on the MCF link performance and the analytical derivation of the outage probability are presented.

A. System Model

The impact of ICXT on the on-off keying (OOK) signal transmission performance in short-haul MCF links with direct-detection is studied using the equivalent system model proposed in [11], adapted for dual-polarization ICXT [8]. In this model, the OOK signal transmitted in the interfering core *m* may degrade the performance of another similar OOK signal transmitted in the tested core *n*. Two chirpless optical transmitters, each one generating an OOK signal with nonzero extinction ratio are considered. The OOK signals at the input of cores *n* and *m* are generated with the same bit rate and extinction ratio and their bit transitions are aligned in time.

Single-mode propagation is considered in each core. Fiber attenuation is assumed similar in the two cores. We model the ICXT by the dual-polarization discrete changes model proposed in [8]. This model has been developed to keep the complexity and time of simulation at acceptable levels in relation to other models used in the literature [8]. We analyze the ICXT impact evolution on system performance in time fractions separated by time intervals longer than the ICXT decorrelation time, but with a duration that can include several thousands of bits [7]. This means that, from time fraction to time fraction, the ICXT is uncorrelated and, within each time fraction, is totally correlated. In this case, in each time fraction, a MCF realization, corresponding to the interfering signal in core *n* resulting from ICXT caused by the signal in core *m*, is obtained from the ICXT field transfer function referring to the polarization directions **x** and **y** [8]

$$F_{b,d}(\omega) = -j\frac{\overline{K}_{nm}}{\sqrt{2}} e^{-j\beta_n(\omega)L} \sum_{k=1}^{N_p} e^{-j\bar{d}_{mn}\omega z_k} e^{-j\phi_k^{(b,d)}} \quad (1)$$

where $b, d \in \{x,y\}$, $\beta_n(\omega)$ is the intrinsic propagation constant of core n, $\overline{K}_{nm}$ is the discrete coupling coefficient, z_k is the longitudinal coordinate of the k-th point between consecutive phase-matching points (PMPs), N_p is the number of PMPs, L is the MCF length and $\phi_k^{(b,d)}$ is the k-th random phase shift (RPS), associated with the k-th PMP [8]. Each RPS is modelled by a random variable (r.v.) uniformly distributed between [0,2π[and different RPS are uncorrelated [8]. The skew between cores m and n is defined by $S_{mn} = d_{mn} \cdot L$, with d_{mn} the walkoff parameter between cores m and n. For equal powers at the output of the tested and interfering cores, the ICXT level, i.e., the ratio between the ICXT and signal powers at the output of core n, is related to the parameters of (1) by $X_c = N_p \left|\overline{K}_{nm}\right|^2$ [8]. The different MCF realizations are obtained by generating randomly different sets of N_p RPSs.

At the optical receiver, the signal is photodetected by a PIN with unit responsivity and bandwidth much larger than the OOK signal bit rate and is electrically filtered [12]. Only electrical noise is considered in our analysis.

To evaluate the BER using simulation, we use MC simulation combined with a semi-analytical technique [11]: the impact of electrical noise on the performance is taken into account analytically, and the effects of fiber chromatic dispersion and ICXT on the BER are evaluated using waveform simulation in each MC simulation iteration.

B. Derivation of the outage probability

At the transmitter output, the electrical field of the signals, within one bit period, are modeled by $s_c(t) = \sqrt{\zeta_c} a_c \mathbf{x} + \sqrt{1-\zeta_c} a_c \mathbf{y}$, where ζ_c controls the signal power distribution between the polarization directions (with c referring to core n or m); and a_c is the level corresponding to the bit transmitted in core c, with $a_{c,1} = \sqrt{2\overline{p_c}/(1+r)}$, for a bit '1' and $a_{c,0} = \sqrt{r} \cdot a_{c,1}$, for a bit '0', where $\overline{p_c}$ is the average power of the signal at the input of core c and r is the extinction ratio defined by the ratio between the average powers corresponding to bits '0' and '1'.

The current due to ICXT after photodetection in the tested core n is approximated by

$$i_{ICXT}(t) \approx 2\,\mathrm{Re}\left\{E_{n,x}(t) \cdot s_{out,x}^*(t) + E_{n,y}(t) \cdot s_{out,y}^*(t)\right\} \quad (2)$$

where Re{z} stands for the real part of z, $s^*(t)$ stands for the complex conjugate of $s(t)$, the ICXT-ICXT beating has been neglected, $s_{out,b}(t)$ is the electrical field of the signal at the MCF output in core n in the b direction (assuming an identical power splitting as in $s_c(t)$), and $E_{n,b}(t)$ is the electrical field of the interfering signal at the MCF output in the b direction, which, by assuming low skew between cores, negligible fiber dispersion and using (1), is given by

$$E_{n,b}(t) = -j\frac{\overline{K}_{nm}}{\sqrt{2}} a_m \sum_{k=1}^{N_p} \left[\sqrt{\zeta_m} e^{-j\phi_k^{(b,x)}} + \sqrt{1-\zeta_m} e^{-j\phi_k^{(b,y)}}\right] \quad (3)$$

where intersymbol interference (ISI) from electrical filtering and fiber dispersion has been neglected. The current in (2) can be written as $i_{ICXT}(t) = \sqrt{2}\left|\overline{K}_{nm}\right| a_n a_m \mu_m = a_n a_m x_m$, where

$$\mu_m = \sqrt{\zeta_n} \sum_{k=1}^{N_p} \left[\sqrt{\zeta_m} \sin\left(\phi_k^{(x,x)}\right) + \sqrt{1-\zeta_m} \sin\left(\phi_k^{(x,y)}\right)\right] + \sqrt{1-\zeta_n} \sum_{k=1}^{N_p} \left[\sqrt{\zeta_m} \sin\left(\phi_k^{(y,x)}\right) + \sqrt{1-\zeta_m} \sin\left(\phi_k^{(y,y)}\right)\right] \quad (4)$$

which, for large N_p and according to the central limit theorem, is a Gaussian r.v. with null mean and variance given by $N_p/2$. Hence, x_m is a zero mean Gaussian r.v. with variance X_c.

The BER conditioned to ICXT is given by

$$P_b = \frac{1}{2} Q\left(\frac{a_{n,1} - i_L + i_{ICXT}^{(1)}}{\sigma}\right) + \frac{1}{2} Q\left(\frac{i_L - a_{n,0} - i_{ICXT}^{(0)}}{\sigma}\right) \quad (5)$$

where $Q(x)$ is the Q-function [12], i_L is the decision threshold, σ is the standard deviation of the electrical noise, and $i_{ICXT}^{(1)}$ and $i_{ICXT}^{(0)}$ correspond to (2), when the bit transmitted in core n is, respectively, '1' or '0'. In absence of ICXT and with the decision threshold optimized, the BER simplifies to a very well-known result for OOK binary systems, $P_{b,NICXT} = Q\left[\left(a_{n,1} - a_{n,0}\right)/\left(2\sigma\right)\right]$. We have observed from analysis of the eye-patterns obtained from simulation that, in the presence of ICXT, the optimized threshold is obtained at half distance between the average of the amplitudes of bits '1' and the average of amplitudes of bits '0' occurring due to ICXT. Hence, in presence of ICXT and low skew, the optimized threshold can be written as

$$i_{L,opt} = \left(a_{n,1} + a_{n,0}\right)/2 + A x_m \quad (6)$$

with $A = \left(a_{n,1} + a_{n,0}\right)\left(a_{m,1} + a_{m,0}\right)/4$.

By assuming that bits '1' in core n have a major contribution to the BER degradation, the second term in (5) is neglected. Then, by considering that $i_{ICXT}^{(1)}$ is higher when bits '1' occur in core m and is smaller for bits '0', (5) can be simplified to

$$P_b \approx \frac{1}{4} Q\left(\frac{a_{n,1} - a_{n,0}}{2\sigma} - \frac{F}{\sigma}\right) \quad (7)$$

where $F = \left(A - a_{n,1} a_{m,1}\right) x_m$ is a zero mean Gaussian r.v. with standard deviation given by $\sigma_F = W\left(a_{n,1} - a_{n,0}\right)/2$, with $W = \sqrt{X_c}/2\left[4 - \left(1+\sqrt{r}\right)^2\right]/\left(1-r\right)$.

The outage probability, P_{out}, is the probability of the communication system becoming unavailable, i. e., the probability of the BER becoming above a BER limit, P_{lim}, [1], [10], and is given by

$$P_{out} = \Pr\{P_b \geq P_{lim}\} = \Pr\left\{F \geq \left(a_{n,1} - a_{n,0}\right)/2 - \sigma Q^{-1}\left(4P_{lim}\right)\right\} \quad (8)$$

Taking into account that F has a Gaussian distribution, the outage probability in direct-detection systems with nonzero extinction ratio impaired by ICXT is given by

$$P_{out} = Q\left(\frac{1}{W}\cdot\left[1 - \frac{Q^{-1}\left(4P_{lim}\right)}{Q^{-1}\left(P_{b,NICXT}\right)}\right]\right) \quad (9)$$

Analysis of (9) and the dependence of W on the extinction ratio shows that nonzero extinction ratio leads to lower outage probabilities, increasing the system robustness to ICXT. By solving (9) as a function of the ICXT level, for $P_{out} = 10^{-5}$, $P_{lim} = 10^{-3}$ and $P_{b,NICXT} = 10^{-5}$, the ICXT level obtained for $r = 0.1$ is 1.52 dB above the ICXT level obtained with $r = 0$.

Eq. (9) is valid for a single interfering core, zero ISI, very small skew and is independent of the signal power distribution between the polarization directions in both cores.

III. Numerical Results and Discussion

In this section, the ICXT effect on the eye-pattern and BER of a direct-detection MCF short-haul link is analyzed, in order to show how ICXT can lead to system unavailability. Then, the outage probability in such systems is studied.

A short-haul link with OOK signaling at $R_b = 10.1376$ Gbps, emulating a 5G fronthaul is considered as a showcase [11]. The system parameters are shown in Table 1. The MCF length is set for the maximum defined for the 5G fronthaul [11], originating low ISI due to fiber dispersion. The number of PMPs is set to describe accurately the ICXT mechanism [8]. The number of bits in each MC simulation iteration is set to get sufficient combinations of the bits sequences in both cores, in order to have the ICXT statistics properly characterized.

Table 1. System parameters.

Parameter	Value
Carrier wavelength, λ	1550 nm
Fiber dispersion parameter, D_λ	17 ps/nm/km
Fiber length, L	20 km
Number of PMPs, N_p	1000
−3 dB bandwidth of the 4th order Bessel electrical receiving filter	10.14 GHz
Noise equivalent power	1 pW×Hz$^{1/2}$
Number of OOK bits in each MC simulation iteration	2^9
BER (in absence of ICXT), $P_{b,NICXT}$	10^{-5}
BER limit, P_{lim}	10^{-3}

Fig. 1 shows the BER per normalized time interval (estimated in each time fraction corresponding to a MCF realization) and the average BER, for $X_c = -12$ dB and $r = 0.1$, for the average signal power at the receiver input of −32.9 dBm. A skew shorter than the bit period, $S_{mn}\cdot R_b \approx 0.2$, which corresponds to $d_{mn} = 1$ ps/km, is considered.Fig. 1 shows that the average BER is nearly stable at about 4.57×10^{-4} after averaging 800 BERs per normalized time interval. Fig. 1 shows also that the randomness of the ICXT mechanism can lead to severe BER degradation or to slight BER improvement. Fig. 1 exhibits a best BER of 6.76×10^{-6} and a worst BER of 5.14×10^{-2}. The eye-patterns corresponding to these BERs are presented in Fig. 2. These eye-patterns do not include the effect of electrical noise to make clear the ICXT effect. The amplitude of bit '1' in the absence of ISI and ICXT is normalized to unity. Fig. 2 a) shows the eye-pattern that leads to the best BER in Fig. 1. The eye-opening is the same as the one obtained in the absence of ICXT (shown in the inset). The BER improves because some bit '1' levels, which occur due to ICXT, have higher values than in case of ICXT absence [11]. Fig. 2 b) shows the received eye-pattern corresponding to the worst BER with a very reduced eye-opening. Analysis of Fig. 2 reveals that the ICXT impact on the eye-pattern creates new amplitude levels in both bits in core n due to the two possible amplitude levels corresponding to the bits in core m. This effect is more visible in the bit '1' amplitudes. From observation of the eye-patterns and by comparison with the decision threshold optimized to minimize the BER in each normalized time interval [11], we have confirmed the optimum threshold given by (6).

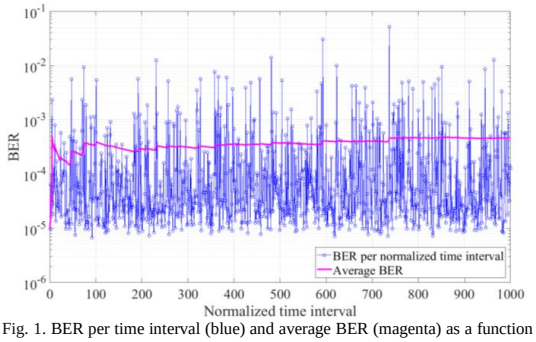

Fig. 1. BER per time interval (blue) and average BER (magenta) as a function of the normalized time interval, for $X_c = -12$ dB, $d_{mn} = 1$ ps/km and $r = 0.1$.

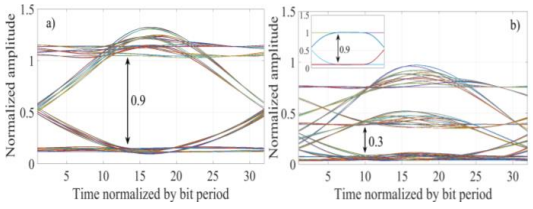

Fig. 2. Eye-patterns (without the electrical noise effect) at the decision circuit input corresponding to a) the best BER and b) worst BER obtained in Fig. 1. An inset with the eye-diagram obtained in the absence of ICXT is also depicted. The normalized eye opening is indicated in each eye-pattern.

Figs. 1 and 2 show that, in specific time intervals, the BER is severely degraded, leading to system unavailability during these intervals. This unavailability caused by ICXT can be suitably characterized by the outage probability [1], [10]. In the simulation, the outage probability is estimated by counting the number of BERs per normalized time interval above the BER limit and dividing it by the total number of time intervals

[11]. To obtain reasonably accurate outage probabilities, 200 BER occurrences are enough.

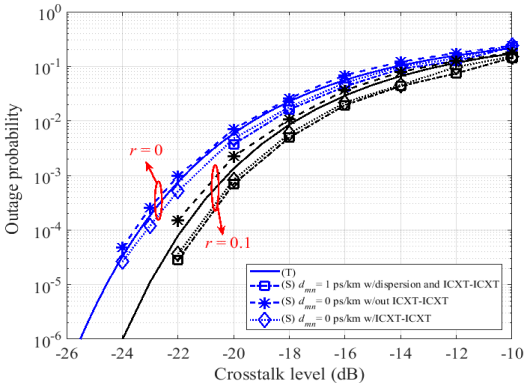

Fig. 3. Outage probability as a function of the ICXT level for $r = 0$ (blue) and $r = 0.1$ (black): theoretical (T); simulation (S) for three situations: $d_{mn} = 0$ without ICXT-ICXT beating; $d_{mn} = 0$ with ICXT-ICXT beating; and $d_{mn} = 1$ ps/km with fiber dispersion and ICXT-ICXT beating.

Fig. 3 shows the outage probability as a function of the ICXT level, for $r = 0$ and $r = 0.1$. The outage probability is estimated theoretically through (9), and using MC simulation in three situations: (1) without ISI and ICXT-ICXT beating and with null skew ($d_{mn} = 0$), which corresponds to the conditions within which (9) has been derived; (2) without ISI and with ICXT-ICXT beating and null skew; and (3) with ISI (considering a dispersive fiber with $L = 20$ km), ICXT-ICXT beating and $d_{mn} = 1$ ps/km. Fig. 3 shows a very good agreement between the outage probabilities obtained with (9) and from simulation without the ICXT-ICXT beating. For $P_{out} = 10^{-4}$, the difference between the ICXT levels predicted by both methods, for $r = 0$ and $r = 0.1$, is, respectively, 0.18 dB and 0.4 dB. Eq. (9) underestimates the outage probability in relation to the results obtained from simulation without the ICXT-ICXT beating, since the BER in (7) neglects the influence of the bits '0' from both cores. Fig. 3 shows also that the ICXT-ICXT beating has a reduced impact on the outage probability, as assumed in the derivation of (9). In fact, simulation results including this beating show a ICXT level difference from theoretical estimates, for $P_{out} = 10^{-4}$, of only 0.26 dB and 0.5 dB, respectively, for $r = 0$ and $r = 0.1$. The eye-patterns show that the improvement of the outage probability with the ICXT-ICXT beating inclusion, increases the noise margin of the bits '1', since the amplitude levels corresponding to these bits become higher. The inclusion of MCF dispersion and skew ($d_{mn} = 1$ ps/km) in the simulation gives outage probabilities very similar to the ones obtained with null skew and ICXT-ICXT beating. Hence, (9) still provides a good prediction of the outage probability considering fiber dispersion, low skew and ICXT-ICXT beating. This good agreement is found for both extinction ratios. Fig. 3 confirms that signals with nonzero extinction ratio reduce the outage probability relative to $r = 0$, as predicted by (9). When comparing the ICXT levels obtained with $r = 0.1$ and $r = 0$, for $P_{out} = 10^{-5}$, the improvement of 1.5 dB is clearly seen. From the eye-patterns analysis, the higher noise margin of the bits '1' attained for higher extinction ratio leads to this improvement.

For larger skew, the ICXT impact is lower, and the outage probability is reduced [11]. In this case, (9) provides a worst-case prediction, as it has been derived for small skews.

By assuming $P_{out} = 10^{-5}$, 10^{-4} and 10^{-3} in (9), the required ICXT levels increase, respectively, 1 dB, 2.2 dB and 3.8 dB in relation to the ICXT level that leads to $P_{out} = 10^{-6}$. This conclusion is independent of the extinction ratio.

IV. Conclusion

A theoretical analysis of the outage probability in short-haul direct-detection optical links supported by weakly-coupled MCFs impaired by ICXT has been presented. A closed-form expression for the outage probability has been derived, which takes into account nonzero extinction ratio and the ICXT level, and allows concluding that direct-detection links with nonzero extinction ratio are more robust to outage due to ICXT. Comparison with MC simulation results has shown that the proposed expression provides very good outage estimates, with maximum discrepancies below 0.6 dB. The proposed expression is valid for small ISI, a single interfering core and low skew, and provides a wider physical insight on the ICXT impact on the performance.

References

[1] P. Winzer, and G. Foschini, "MIMO capacities and outage probabilities in spatially multiplexed optical transport systems," *Opt. Expr.*, vol. 19, no. 17, pp. 16680–16696, Aug. 2011.

[2] J. Galve, I. Gasulla, S. Sales, and J. Capmany, "Reconfigurable radio access networks using multicore fibers," *IEEE J. Quantum Electron.*, vol. 52, no. 1, pp. 1–7, Jan. 2016.

[3] Z. Feng *et al.*, "Multicore-fiber-enabled WSDM optical access network with centralized carrier delivery and RSOA-based adaptive modulation," *IEEE Photon. J.*, vol. 7, no. 4, Art. ID 7201309, Nov. 2015.

[4] D. Butler *et al.*, "Space division multiplexing in short reach optical interconnects," *IEEE/OSA J. Lightw. Technol.*, vol. 35, no. 4, pp. 677–682, Feb. 15 2017.

[5] T. Hayashi, T. Sasaki, and E. Sasaoka, "Behavior of inter-core crosstalk as a noise and its effect on Q-factor in multi-core fiber," *IEICE Trans. Commun.*, vol. E97-B, no. 5, pp. 936–944, May 2014.

[6] T. Alves *et al.*, "Intercore crosstalk in direct-detection homogeneous multicore fiber systems impaired by laser phase noise," *Opt. Expr.*, vol. 25, no. 23, pp. 29417-29431, Nov. 2017.

[7] T. Alves, and A. Cartaxo, "Characterization of the stochastic time evolution of short-term average intercore crosstalk in multicore fibers with multiple interfering cores," *Opt. Expr.*, vol. 26, no. 4, pp. 4605-4620, Feb. 2018.

[8] R. Soeiro, T. Alves, and A. Cartaxo, "Dual polarization discrete changes model of inter-core crosstalk in multi-core fibers," *IEEE Photon. Technol. Lett.*, vol. 29, no. 16, pp. 1395-1398, Aug. 15 2017.

[9] A. Macho *et al.*, "Birefringence effects in multicore fiber: Coupled local-mode theory," *Opt. Expr.*, vol. 24, no. 19, pp. 21415-21434, Sep. 2016.

[10] B. Puttnam *et al.*, "Impact of inter-core crosstalk on the transmission distance of QAM formats in multi-core fibers," *IEEE Photon. J.*, vol. 8, no. 5, Art. ID. 0601109, Feb. 2016.

[11] J. Rebola, A. Cartaxo, and A. Marques, "10 Gbps CPRI signals transmission impaired by intercore crosstalk in 5G networks fronthauls with multicore fibers," submitted for Springer Photonics Network Communications Journal.

[12] G. Agrawal, "Fiber-optic communication systems", 4th edn. John Wiley & Sons, New Jersey, USA, 2010.

5G fronthauls with multicore fibers: CPRI signals performance degradation induced by intercore crosstalk

Authors: João L. Rebola, Tiago M. F. Alves, Adolfo V. T. Cartaxo, and André S. Marques

Weakly-coupled multicore fibers (MCFs) have been proposed to support the huge data capacity demanded by future 5G fronthauls. However, in MCFs, intercore crosstalk (ICXT), i.e. crosstalk between different MCF cores, can degrade significantly the performance of the 5G fronthaul, particularly, when using Common Public Radio Interface (CPRI) signals and direct-detection at the optical receiver. In this work, the performance degradation induced by ICXT in 5G fronthauls with MCFs and direct-detection is assessed by numerical simulation and experimentally. We show that the study of the outage probability is essential to ensure the reliability and the good quality of service in 5G fronthauls supported by MCFs with CPRI signals, where ICXT is significant. The crosstalk level that leads to an outage probability of 10^{-5} is more than 7 dB lower than the crosstalk level necessary to reach the power penalty of 1 dB.

Bibliography

[1] S. Vij and A. Jain, "5G : Evolution of a Secure Mobile Technology," *3rd International Conference on Computing for Sustainable Global Development (INDIAcom)*, pp. 2192–2196, New Dehli, India, Mar. 2016.

[2] M. Peng, Y. Li, Z. Zhao, and C. Wang, "System Architecture and Key Technologies for 5G Heterogeneous Cloud Radio Access Networks," *IEEE Network*, vol. 29, no. 2, pp. 6–14, Mar.-Apr. 2015.

[3] A. Sharma, "Generations of Wireless Communication. From 0G to 5G," Sai Institute of Engineering and Technology, Amritsar, India, Mar. 2013.

[4] J. Andrews, S. Buzzi, W. Choi, S. Hanly, A. Lozano, A. Soong, and J. Zhang, "What Will 5G Be?," *IEEE Journal on Selected Areas in Communications*, vol. 32, no. 6, pp. 1–17, Jun. 2014.

[5] S. Onoe, "Evolution of 5G Mobile Technology Toward 2020 and Beyond," *IEEE International Solid-State Circuits Conference (ISSCC)*, pp. 23–28, San Francisco, CA, USA, Feb. 2016.

[6] Qorvo, *Comparing 4G and 5G*, Sept. 2017. https://www.qorvo.com/design-hub/blog/getting-to-5g-comparing-4g-and-5g-system-requirements, (accessed Oct. 20, 2018).

[7] I. Alimi, A. Teixeira, and P. Monteiro, "Toward an Efficient C-RAN Optical Fronthaul for the Future Networks: A Tutorial on Technologies, Requirements, Challenges, and Solutions," *IEEE Communications Surveys and Tutorials*, vol. 20, no. 1, pp. 708–769, Nov. 2018.

[8] S. Park, K. Lee, C. Song, and I. Lee, "Joint Design of Fronthaul and Access Links for C-RAN With Wireless Fronthauling," *IEEE Signal Processing Letters*, vol. 23, no. 11, pp. 1657–1661, Nov. 2016.

[9] P. Chanclou, A. Pizzinat, F. Clech, T.-l. Reedeker, Y. Lagadec, F. Saliou, B. Guyader, L. Guillo, Q. Deniel, S. Gosselin, S. Le, T. Diallo, S. Dúill, S. A. Gebrewold, D. Hillerkuss, J. Leuthold, G. Gavioli, and P. Galli, "Optical Fiber Solution for Mobile Fronthaul to Achieve Cloud Radio Access Network," *2013 Future Network and Mobile Summit*, Lisbon, Portugal, Jul. 2013.

[10] J. M. Galve, I. Gasulla, S. Sales, and J. Capmany, "Reconfigurable Radio Access Networks Using Multicore Fibers," *IEEE Journal of Quantum Electronics*, vol. 52, no. 1, Article Sequence Number 0600507, Jan. 2016.

[11] Z. Feng, B. Li, M. Tang, L. Gan, R. Wang, R. Lin, Z. Xu, S. Fu, L. Deng, W. Tong, S. Long, L. Zhang, H. Zhou, R. Zhang, S. Liu, and P. P. Shum, "Multicore-fiber-enabled WSDM optical access network with centralized carrier delivery and rsoa-based adaptive modulation," *IEEE Photonics Journal*, vol. 7, no. 4, Article Sequence Number 7201309, Aug. 2015.

[12] D. L. Butler, M. J. Li, S. Li, Y. Geng, R. R. Khrapko, R. A. Modavis, V. N. Nazarov, and A. V. Koklyushkin, "Space Division Multiplexing in Short Reach Optical Interconnects," *Journal of Lightwave Technology*, vol. 35, pp. 677–682, Feb. 15 2017.

[13] J. M. Galve, I. Gasulla, S. Sales, and J. Capmany, "Fronthaul design for Radio Access Networks using Multicore Fibers," *Waves Magazine*, vol. 7, no. 1, pp. 69–80, Mar. 2015.

[14] J. Rebola, A. Cartaxo, and A. Marques, "10 Gbps CPRI signals transmission impaired by intercore crosstalk in 5G network fronthauls with multicore fibers," *submitted to Springer Photonic Network Communications*, pp. 1–16, Oct. 2018.

[15] K. Saitoh and S. Matsuo, "Multicore Fiber Technology," *Journal of Lightwave Technology*, vol. 34, no. 1, pp. 55–66, Jan. 1 2016.

[16] T. Hayashi, T. Taru, O. Shimakawa, T. Sasaki, and E. Sasaoka, "Design and fabrication of ultra-low crosstalk and low-loss multi-core fiber," *Optics Express*, vol. 19, no. 17, pp. 16576–16592, Jun. 2011.

[17] A. Sano, H. Takara, T. Kobayashi, and Y. Miyamoto, "Crosstalk-managed high capacity long haul multicore fiber transmission with propagation-direction interleaving," *Journal of Lightwave Technology*, vol. 32, no. 16, pp. 2771–2779, Aug. 2014.

[18] A. Cartaxo, R. Luís, B. Puttnam, T. Hayashi, Y. Awaji, and N. Wada, "Dispersion Impact on the Crosstalk Amplitude Response of Homogeneous Multi-Core Fibers," *IEEE Photonics Technology Letters*, vol. 28, no. 17, pp. 1858–1861, Sep. 1 2016.

[19] R. Luis, B. Puttnam, A. Cartaxo, W. Klaus, J. Mendinueta, Y. Awaji, N. Wada, T. Nakanishi, T. Hayashi, and T. Sasaki, "Time and Modulation Frequency Dependence of Crosstalk in Homogeneous Multi-Core Fibers," *Journal of Lightwave Technology*, vol. 34, no. 2, pp. 441–447, Jan. 15 2016.

[20] T. Alves, A. Cartaxo, R. Luis, B. Puttnam, Y. Awaji, and N. Wada, "Intercore crosstalk in direct-detection homogeneous multicore fiber systems impaired by laser phase noise," *Optics Express*, vol. 25, no. 23, pp. 29417–29431, Nov. 2017.

[21] T. Alves and A. Cartaxo, "Intercore Crosstalk in Homogeneous Multicore Fibers: Theoretical Characterization of Stochastic Time Evolution," *Journal of Lightwave Technology*, vol. 35, no. 21, pp. 4613–4623, Nov. 1 2017.

[22] T. Alves and A. Cartaxo, "Characterization of ICXT in DD-OFDM MCF-based Systems," *European Conference on Optical Communication (ECOC)*, P2.SC6.29, Gothenburg, Sweden, Sep. 2017.

[23] D. Kumar and R. Ranjan, "Estimation of crosstalk in homogeneous multicore fiber for high core count under limited cladding diameter," *2017 Conference on Information and Communication Technology (CICT)*, Gwalior, India, Nov. 2017.

[24] B. Puttnam, R. Luís, W. Klaus, J. Mendinueta, Y. Awaji, N. Wada, and T. Eriksson, "Impact of inter-core crosstalk on the transmission distance of QAM formats in multi-core fibers," *IEEE Photonics Journal*, vol. 8, no. 2, Article Sequence Number 0601109, Apr. 2016.

[25] R. O. Soeiro, T. M. Alves, and A. V. Cartaxo, "Dual Polarization Discrete Changes Model of Inter-Core Crosstalk in Multi-Core Fibers," *IEEE Photonics Technology Letters*, vol. 29, no.16, pp. 1395–1398, Aug. 2017.

[26] A. Al-Fuqaha, M. Guizani, M. Mohammadi, M. Aledhari, and M. Ayyash, "Internet of Things: A Survey on Enabling Technologies, Protocols, and Applications," *IEEE Communications Surveys & Tutorials*, vol. 17, no. 4, no. 4, pp. 2347–2376, Jun. 2015.

[27] Ineconomics, *Mobile communication evolution: from 1G to 5G*, 2018. http://www.ineconomics.com/1g-2g-3g-4g-5g/, (accessed Oct. 18, 2018).

[28] A. Osseiran, F. Boccardi, V. Braun, K. Kusume, P. Marsch, M. Maternia, O. Queseth, M. Schellmann, H. Schotten, H. Taoka, H. Tullberg, M. A. Uusitalo, B. Timus, and M. Fallgren, "Scenarios for 5G mobile and wireless communications: The vision of the METIS project," *IEEE Communications Magazine*, vol. 52, no. 5, pp. 26–35, May 2014.

[29] Q. Li, H. Niu, A. Papathanassiou, and G. Wu, "5G network capacity: Key elements and technologies," *IEEE Vehicular Technology Magazine*, vol. 9, no. 1, pp. 71–78, Mar. 2014.

[30] A. Alexiou, P. Demestichas, and A. Georgakopoulos, "5G Vision, Enablers and Challenges for the Wireless Future," *Wireless World Research Forum, White Paper*, Piraeus, Greece, Apr. 2015.

[31] V. Ziegler, T. Theimer, C. Sartori, J. Prade, N. Sprecher, K. Albal, and A. Bedekar, "Architecture Vision for the 5G Era: Cognitive and Cloud Network Evolution," *2015 IEEE 81st Vehicular Technology Conference (VTC Spring)*, Glasgow, UK, May 2015.

[32] China-Mobile, "C-RAN: the road towards green RAN," *White Paper,* ver. 2.5, 2011.

[33] C. Chang, R. Schiavi, N. Nikaein, T. Spyropoulos, and C. Bonnet, "Impact of packetization and functional split on C-RAN fronthaul performance," *2016 IEEE International Conference on Communications (ICC)*, Kuala Lumpur, Malaysia, May 2016.

[34] G. Agrawal, *Fiber-Optic Communications Systems.* John Wiley & Sons, 4^{th} ed., New Jersey, USA, 2010.

[35] H. Venghaus and N. Grote, *Fibre Optic Communication: Key Devices.* Springer-Verlag, 2^{nd} ed., Berlin, Germany, 2012.

[36] J. Senior and M. Jamro, *Optical Fiber Communications: Principles and Practice.* Pearson Education Limited, 3^{rd} ed., Essex, England, 2009.

[37] E. Virgillito, "Limitations of PM-QAM based multicore fiber transmission systems due to intercore crosstalk," Master's thesis, Telecommunications engineering, Instituto Superior Técnico, 2016.

[38] J. M. Galve, I. Gasulla, and J. Capmany, "Space-division multiplexing for the next generation of fiber-wireless access networks," *International Conference on Transparent Optical Networks (ICTON)*, paper Mo.B5.4, Jul. 2015.

[39] T. Hayashi and T. Nakanishi, "Multi-core optical fibers for the next-generation communications," *SEI Technical Review,* no. 86, pp. 23–28, Apr. 2018.

[40] T. Hayashi, T. Taru, T. Nagashima, O. Shimakawa, and T. Sasaki, "Multi-core Fiber for High-Capacity Long-Haul Spatially- Multiplexed Transmission," *SEI Technical Review*, vol. 77, no. 3, pp. 14–22, Oct. 2013.

[41] T. Hayashi, T. Nakanishi, O. Shimakawa, F. Sato, T. Taru, and T. Sasaki, "125-Mm-Cladding 8-Core Fiber for Short-Reach Optical Interconnects," *SEI Technical Review,* no. 83, pp. 21–25, Oct. 2016.

[42] A. Cartaxo and T. Alves, "Discrete Changes Model of Inter-core Crosstalk of Real Homogeneous Multi-core Fibers," *Journal of Lightwave Technology*, vol. 35, no. 12, pp. 2398–2408, Jun. 15 2017.

[43] T. Hayashi, T. Sasaki, and E. Sasaoka, "Behavior of inter-core crosstalk as a noise and its effect on Q-factor in multi-core fiber," *IEICE Transactions on Communications*, vol. E97-B, no. 5, pp. 936–944, May 2014.

[44] A. Macho, M. Morant, and R. Llorente, "Next-Generation Optical Fronthaul Systems Using Multicore Fiber Media," *Journal of Lightwave Technology*, vol. 34, no. 20, pp. 4819–4827, Oct. 15 2016.

[45] B. Ballal and S. Nema, "Performance Comparison of Analog and Digital Radio Over Fiber Link," *International Journal of Computer Science & Engineering Technology*, vol. 3, no. 6, pp. 193–198, Jun. 2012.

[46] A. Ng'oma, "Radio-over-fibre technology for broadband wireless communication systems". PhD thesis, Electrical Engineering, Technische Universiteit Eindhoven, Jun. 2005.

[47] Common Public Radio Interface, "CPRI Specification V7.0," *Standard Document Specification*, vol. 1, 2015.

[48] JDSU, "Cloud-RAN Deployment with CPRI Fronthaul Technology," *White Paper*, 2013.

[49] D. Chitimalla, K. Kondepu, L. Valcarenghi, M. Tornatore, and B. Mukherjee, "5G Fronthaul–Latency and Jitter Studies of CPRI Over Ethernet," *Journal of Optical Communications and Networking*, vol. 9, no. 2, pp. 172–182, Feb. 2017.

[50] Y. Chun-Hui and C. Xin, "Research of CPRI protocol based on high-speed fiber link," *2nd International Conference on Information Technology and Computer Science*, pp. 336–339, Kiev, Ukraine, Jul. 2010.

[51] J. Wang, Z. Yu, K. Ying, J. Zhang, F. Lu, M. Xu, L. Cheng, X. Ma, and G. Chang, "Digital Mobile Fronthaul Based on Delta–Sigma Modulation for

32 LTE Carrier Aggregation and FBMC Signals," *Journal of Optical Communications and Networking*, vol. 9, no. 2, pp. A233–A244, Feb. 2017.

[52] ITU-T, "Transport network support of IMT-2020/5G," Technical Report, Feb. 2018.

[53] A. Carlson and P. Crilly, *Communication Systems*. McGraw-Hill International Editions, 5^{th} ed., New York, USA, 2010.

[54] M. Jeruchim, P. Balaban, and S. Shanmugan, *Simulation of Communication Systems*. Kluwer Academic Publishers, 2 nd ed., New York, USA, 2002.

[55] M. J. Milton, R. Davis, and N. Fletcher, "Towards a new SI: A review of progress made since 2011," *Metrologia*, vol. 51, no. 3, pp. R21–R30, May 2014.

[56] J. Karki, "Active Low-Pass Filter Design," *Texas Instruments,* Aplication Report, Sep. 2002.

[57] J. Rebola and A. Cartaxo, "Gaussian approximation for performance assessment of optically preamplified receivers with arbitrary optical and electrical filters," *IEE Proceedings- Optoelectron*, vol. 148, no. 3, pp. 135–142, Jun. 2001.

[58] M. Carpentier, *Análise Numérica*. notes of the course "Análise Numérica", Instituto Superior Técnico, Feb. 1993.

[59] C. Lourenço, J. Rebola, and J. Oliveira, "Projecto e Simulação de um Sistema de Comunicação Óptica de Muita Alta Velocidade," final degree work in Electrical Engineering and Computers, Instituto Superior Técnico, Portugal, Sep. 1999.

[60] P. Parolari, L. Marazzi, M. Brunero, M. Martinelli, A. Maho, S. Barbet, F. Lelarge, R. Brenot, G. Gavioli, G. Simon, F. Saliou, Q. Deniel, and P. Chanclou, "Operation of a RSOA WDM PON self-seeded transmitter over More than 50 km of SSMF up to 10 Gb/s," *Conference on Optical Fiber Communication, Technical Digest Series (OFC)*, paper W3G.4, San Francisco, CA, USA, Mar. 2014.

[61] A. Marques, J. Rebola, and A. Cartaxo, "Transmission of CPRI signals along weakly-coupled multicore fibers for support of 5G networks," *International Conference on Transparent Optical Networks (ICTON)*, paper We.B2.7, Bucharest, Romania, Jul. 2018.

[62] G. Rademacher, R. S. Luis, B. J. Puttnam, Y. Awaji, and N. Wada, "Crosstalk dynamics in multi-core fibers," *Optics Express*, vol. 25, no. 10, pp. 12020–12028, May 2017.

[63] P. J. Winzer and G. J. Foschini, "MIMO capacities and outage probabilities in spatially multiplexed optical transport systems," *Optics Express*, vol. 19, no. 17, pp. 16680–16696, Aug. 2011.

[64] N. Cvijetic, S. Wilson, and D. Qian, "System outage probability due to PMD in high-speed optical OFDM transmission," *Journal of Lightwave Technology*, vol. 26, no. 14, pp. 2118–2127, Jul. 2008.

[65] J. Rebola, A. Cartaxo, T. Alves, and A. Marques, "Outage Probability due to Intercore Crosstalk in Multicore Fiber Links with Direct - Detection," *submitted to IEEe Photonics Technology Letters*, Oct. 2018.

[66] A. Udalcovs, R. Lin, O. Ozolins, L. Gan, L. Zhang, and X. Pang, "Inter-Core Crosstalk in Multicore Fibers: Impact on 56-Gbaud/λ/Core PAM-4 Transmission," *European Conference on Optical Communications (ECOC)*, Valencia, Spain, Oct. 2015.

[67] J. Perin, A. Shastri, and J. Khan, "Data center links beyond 100 Gbit/s per wavelength," *Optical Fiber Technology*, vol. 44, pp. 69–85, Aug. 2018.